Dissertation zur Erlangung des Doktorgrades
der Fakultät für Chemie und Pharmazie
der Ludwig-Maximilians-Universität München

Glucosylation of the signal molecules salicylic acid and N-hydroxypipecolic acid – A complex switch to regulate stress response and pathogen defense

Ping Xu
aus
Fujian, China

2025

Erklärung

Diese Dissertation wurde im Sinne von § 7 der Promotionsordnung vom 28.November 2011 von Herrn PD. Dr. Anton R. Schäffner betreut.

Eidesstattliche Versicherung

Diese Dissertation wurde eigenständig und ohne unerlaubte Hilfe erarbeitet.

München, den.....03.02.2025.....

.....

(Ping Xu)

Dissertation eingereicht am **03.02.2025**

1. Gutachter: PD. Dr. Anton Rudolf Schäffner
2. Gutachter: Prof. Dr. Jörg Durner

Mündliche Prüfung am **27.03.2025**

Publications and conference contributions related to this thesis:

Ping Xu, Sophia Fundneider, Birgit Lange, Anton R. Schäffner (2024). “Root-derived N-hydroxypipecolic acid manipulates shoot defense.” Botanik-Tagung 2024 International Conference of the German Society for Plant Sciences. Halle, Poster presentation.

Ping Xu, Sophia Fundneider, Anton R. Schäffner (2024). “N-hydroxypipecolic acid mediates root-shoot communication in response to root microbes.” Botanik-Tagung 2024 International Conference of the German Society for Plant Sciences. Halle, Poster presentation.

Ping Xu, Sophia Fundneider, Birgit Lange, Johannes Stuttmann, Anton R. Schäffner, “A standby N-hydroxypipecolic acid circuit fuels root-triggered systemic resistance and growth of shoots.” (Accepted by *Nature Plants*)

Ping Xu[1], Sibylle Bauer[1], Birgit Lange, Rafał P. Maksym, Birgit Geist, Robert Janowski, Elisabeth Georgii[1], Anton R. Schäffner. “An enzymatic triad orchestrates *Arabidopsis* salicylic acid glucosylation.” (in preparation, [1] first authors)

Parts of this thesis will be incorporated into manuscripts for publication in a scientific journal.

Abstract

Salicylic acid (SA) plays a pivotal role in activating plant defense responses against both abiotic and biotic stresses. In *Arabidopsis thaliana*, the glucosyltransferase UGT76B1 inactivates SA alongside other immune modulators, N-hydroxypipecolic acid (NHP) and isoleucic acid (ILA). Soil-borne microbes can trigger systemic shoot resistance through jasmonic acid– and/or SA-dependent pathways, but the identity of root-derived signals remains unclear. UGT76B1 plays a pivotal role in mediating systemic acquired resistance (SAR) in leaves, while the relevance of its constitutive expression in roots remained enigmatic. This study identified a root-triggered systemic resistance (RSR) mechanism that relies on components of the SAR machinery known from leaves. Unlike the inducible nature of SAR, FLAVIN-DEPENDENT MONOOXYGENASE 1 (FMO1) constitutively produces NHP in roots, while UGT76B1 immobilizes NHP via conjugation. Loss of UGT76B1 in roots increases NHP release, activating shoot defenses. This tightly regulated FMO1/UGT76B1 circuit is modulated by root-associated microbes. Notably, endophytic and (hemi)biotrophic fungi induce UGT76B1 degradation and FMO1 expression, leading to variable NHP release, which differentially regulates shoot defense and growth.

Additionally, UGT74F1 and UGT74F2 glucosylate SA, with UGT74F2 being the sole enzyme forming SA glucose esters. UGT76B1, UGT74F1, and UGT74F2 are the principal SA glucosyltransferases (SA-GTs) of *Arabidopsis* since the triple mutant no longer accumulated SA glucosides. A previous study systematically investigated the roles of three SA-GTs by analyzing SA metabolite levels and transcriptomic profiles of combinatorial loss-of-function mutants. However, their collaborative or independent functions remained unclear. By characterizing responses to both abiotic and biotic stresses, this thesis revealed their unique and overlapping roles. The three SA-GTs exhibit differential, partially overlapping expression patterns. The SA-*O*-glucoside-forming UGT74F1 and UGT76B1 cannot compensate each other due to differences in their substrate specificities and cellular expression. Transcriptomic analyses and stress-response phenotypes further distinguish their roles: UGT76B1 is central to immune regulation, whereas UGT74F1 and UGT74F2 are primarily involved in abiotic stress responses. Nevertheless, all three enzymes contribute to defense against bacterial pathogens and to tolerance of drought, salt, osmotic, and cold stress.

Beyond SA, these enzymes may also act on other substrates. An *in silico* modeling pipeline was used to predict additional substrates, and these predictions were experimentally validated. Neither UGT74F1 nor UGT74F2 glucosylates NHP or ILA, while nicotinic acid, another UGT74F2 substrate, is not conjugated by UGT74F1 or UGT76B1. Similarly, UGT76B1 does not glucosylate anthranilic acid, a substrate of UGT74F1 and UGT74F2. These findings highlight the substrate specificity of SA-GTs and their distinct biochemical roles.

Table of content

Figures

Tables

Abbreviations

AA	Anthranilic acid
AAG	Anthraniloyl-*O*-glucose, anthraniloyl glucose ester
ABA	Abscisic acid
Arabidopsis	*Arabidopsis thaliana*
BTH	Benzo (1,2,3) thiadiazole-7-carbothioc acid S-methyl ester
Co	Cortex
dpi	Day post inoculation
En	Endodermis
ET	Ethylene
GO	Gene Ontology
GUS	β-glucuronidase
ILA	Isoleucic acid
ISR	Induced systemic resistance
JA	Jasmonic acid
MS	Murashige and Skoog
NA	Nicotinic acid
NAG	Nicotinoyl-*O*-glucoside, nicotinate glucose ester
NHP	N-hydroxypipecolic acid
NHP-*O*-Gluc	N-hydroxypipecolic acid glucoside
PGPF	Plant-growth-promoting fungi
PGPR	Plant growth-promoting rhizobacteria
Pip	Pipecolic acid
Pst	*Pseudomonas syringae pv. tomato DC3000*
Rh	Rhizodermis
RMSD	Root mean square deviation
RSR	Root-triggered systemic resistance
SA	Salicylic acid
SA-GT	Salicylic acid glucosyltransferase
SAG	SA-*O*-glucoside
SAR	Systemic acquired resistance
SGE	Salicyloyl glucose ester
TSKO	Tissue-specific knockout
UDP-glucose	Uridine diphosphate glucose
UGT	UDP-glycosyltransferase
WT	Wild type

1. Introduction

1.1 History background and roles of SA in plant

Salicylic acid (SA, 2-hydroxybenzoic acid) is a pivotal phenolic compound in plants that regulates various biochemical and physiological processes essential for growth and development (Dempsey *et al.*, 2011). SA is integral to plant life because it participates in numerous signaling pathways. Historically, humans have utilized SA and its related compounds as pain relievers for over 4,000 years (Norn *et al.*, 2009). In the early 19th century, SA and its derivative salicin were first isolated from willow bark and meadowsweet (Norn *et al.*, 2009).

Within plants, basal levels of SA vary widely—up to a hundredfold difference can exist among plants within the same family, and even greater variation is observed between different species (Raskin, 1992). SA was first proposed as an endogenous signaling molecule after it was detected in the phloem and observed to induce flowering in duckweed (Cleland and Ajami, 1974). This finding marked the beginning of understanding SA's role in plant physiology. Over the past decades, extensive research has demonstrated that SA acts as a versatile internal signal, enabling plants to manage a broad range of stresses and developmental changes. It plays a critical role in alleviating abiotic stresses such as heat, cold, drought, UV radiation, heavy metals, salinity, and osmotic shock. Additionally, SA regulates various aspects of plant development, including seed germination, growth, photosynthesis, thermogenesis, flowering, and senescence (Rivas-San Vicente and Plasencia, 2011). However, SA is most renowned for its essential role in coordinating plant immune responses (Ding and Ding, 2020).

1.2 SA biosynthesis and metabolism

1.2.1 Biosynthesis and regulation of SA

Plants synthesize SA primarily through two chorismate-derived pathways: the isochorismate synthase (ICS) pathway and the phenylalanine ammonia-lyase (PAL) pathway (Silverman *et al.*, 1995). The relative importance of each pathway varies among species, and some enzymes involved remain unidentified. In *Arabidopsis thaliana*, the ICS pathway is the main route for SA biosynthesis, whereas in rice, the PAL pathway plays a more significant role in SA accumulation. In species like soybeans, both pathways contribute approximately equally to SA production (Duan *et al.*, 2014).

In *Arabidopsis*, two ICS enzymes are encoded, with ICS1 (SID2, *SA* INDUCTION-DEFICIENT2) being primarily responsible for SA accumulation in leaf tissues, especially under biotic and abiotic stress conditions (Wildermuth *et al.*, 2001; Garcion and Métraux, 2008).

Recent studies have revealed that the conversion of chorismate to isochorismate by ICS1 occurs exclusively within chloroplasts, making it the only step of SA biosynthesis that takes place in this organelle (Rekhter *et al.*, 2019). After its formation, isochorismate is transported from the chloroplast to the cytosol via the MATE transporter protein ENHANCED DISEASE SUSCEPTIBILITY 5 (EDS5). Mutants lacking EDS5 exhibit severely reduced SA levels upon pathogen infection, underscoring EDS5's crucial role in SA transport and the plant's pathogen response (Nawrath and Métraux, 1999; Nawrath *et al.*, 2002). Once in the cytosol, isochorismate is conjugated with glutamate by the aminotransferase AVRPPHB SUSCEPTIBLE 3 (PBS3), yielding isochorismate-9-glutamate. This intermediate is then converted into SA, either through the action of the acyltransferase ENHANCED PSEUDOMONAS SUSCEPTIBILITY 1 (EPS1) or via spontaneous decomposition (Rekhter *et al.*, 2019; Torrens-Spence *et al.*, 2019). Interestingly, small amounts of SA remain detectable even when the ICS pathway is disrupted. Recent evidence suggests that this residual SA is not derived from phenylalanine, indicating the existence of an alternative, yet unidentified, biosynthetic pathway (Wu *et al.*, 2023).

1.2.2 SA metabolism pathway

In addition to its biosynthesis, SA undergoes various metabolic modifications that modulate its activity, distribution, and storage within plants. These modifications include glucosylation, methylation, amino acid conjugation, and hydroxylation. Each process regulates SA's function by inactivating the molecule to prevent potential toxicity and facilitate its transport or storage.

Glucosylation: Glucosylation is a major modification that inactivates SA and facilitates its storage, particularly within vacuoles, allowing plants to accumulate large quantities without toxic effects. In *Arabidopsis thaliana*, three UDP-glucosyltransferases—UGT74F1, UGT74F2, and UGT76B1—are responsible for this modification, forming SA-*O*-glucoside (SAG) (Bauer, 2020; Georgii *et al.*, 2025). Uniquely, UGT74F2 can also glucosylate the carboxyl group of SA, producing salicyloyl glucose ester (SGE) (Lim *et al.*, 2002; Song, 2006; Dean and Delaney, 2008; Noutoshi *et al.*, 2012). While SAG is predominantly stored in vacuoles, SGE remains localized outside the vacuole (Vaca *et al.*, 2017). It has been hypothesized that SAG might release bioactive SA under specific conditions (Fu and Dong, 2013); however, direct evidence for such reactivation is still lacking.

Methylation: Methylation enhances SA's membrane permeability and volatility, serving as another means of inactivation. In *Arabidopsis*, this process is catalyzed by the enzyme BA/SA carboxyl methyltransferase 1. The methylated form, methyl salicylate, can revert to active SA through the action of methylesterases, providing a dynamic mechanism for regulating SA levels (Park *et al.*, 2007; Vlot *et al.*, 2008).

Amino acid conjugation: SA can conjugate with amino acids, forming compounds such as salicyloyl-L-aspartate (SA-Asp), the most abundant amino acid conjugate of SA in plants. This reaction is catalyzed by GH3.5 in *Arabidopsis* and results in an inactive form of SA, although its precise physiological role remains unclear. Overexpression of GH3.5 leads to elevated SA-Asp levels, but GH3.5 mutants do not show significant changes in basal or pathogen-induced SA-Asp levels (Zhang *et al.*, 2013; Westfall *et al.*, 2016). Recent findings have also identified SA conjugation with malate, resulting in SA-malate accumulating in response to bacterial infection. Application of SA-malate has been observed to enhance plant immunity modestly, potentially balancing immune response with overall plant health (Scholten *et al.*, 2024).

Hydroxylation: Hydroxylation of SA leads to the formation of dihydroxybenzoic acids (DHBAs), specifically 2,3-DHBA and 2,5-DHBA. *In vitro*, SA can act as a non-enzymatic scavenger of hydroxyl radicals, forming these DHBAs in readily reversible reactions (Maskos *et al.*, 1990; Chang *et al.*, 2008). In *Arabidopsis*, the SA-5-hydroxylase encoded by the gene DOWNY MILDEW RESISTANT 6 converts SA into 2,5-DHBA (Zhang *et al.*, 2017). Additionally, two homologs, DMR6-LIKE OXYGENASE 1 and *2*, may function as SA-3-hydroxylases, enhancing the production of 2,3-DHBA (Zeilmaker *et al.*, 2015; Torrens-Spence *et al.*, 2019). Both DHBAs can undergo further inactivation through glycosylation mediated by UGT89A2 and UGT76D1 (Chen and Li, 2017; Huang *et al.*, 2018).

Sulfonation: While sulfonation of SA has been demonstrated *in vitro* via the sulfotransferase enzyme family—similar to modifications of other plant compounds such as flavonoids and brassinosteroids—no evidence of sulfonated SA has been found in plant tissues (Klein and Papenbrock, 2008; Baek *et al.*, 2010).

1.3 Glucosyltransferases in *Arabidopsis*

Glycosylation is one of the most prevalent and functionally significant modifications in plant cells, playing a crucial role in the modulation of numerous secondary metabolites (Wang and Hou, 2009; Strasser, 2016). This process is essential for controlling the levels of various hormones—including abscisic acid (ABA), auxin, cytokinin, jasmonic acid (JA), and SA—thus enabling plants to respond effectively to a wide range of biotic and abiotic stressors (Tognetti *et al.*, 2010; von Saint Paul *et al.*, 2011; Wang *et al.*, 2013; Tanaka *et al.*, 2014; Liu *et al.*, 2015; George Thompson *et al.*, 2017; Haroth *et al.*, 2019).

Glycosylation reactions are primarily catalyzed by glycosyltransferases (GTs), enzymes that facilitate the attachment of sugar moieties from activated donors to a diverse array of acceptor molecules—including proteins, nucleic acids, antibiotics, lipids, and small bioactive compounds, resulting in the formation of glycosidic bonds (Lairson *et al.*, 2008; Yonekura-Sakakibara and Hanada, 2011). The most common sugar donor in plant glycosylation is

uridine diphosphate-glucose (UDP-Glc), although other nucleotide sugars such as UDP-arabinose, UDP-galactose, UDP-glucuronic acid, UDP-rhamnose, and UDP-xylose can also serve as glycosyl donors (Bowles *et al.*, 2006; Yin *et al.*, 2014).

Glycosyltransferases are classified according to the types of glycosidic bonds they form, such as *O*-, *S*-, *N*-, and *C*-glycosyltransferases, with *O*-glycosides being the most widely studied and common among these (Liang *et al.*, 2015). In the Carbohydrate-Active enZyme (CAZy) database (http://www.cazy.org/, accessed on 3 September 2023), GTs are grouped into 116 families based on similarities in protein sequence, glycosidic bond stereochemistry, and substrate specificity. In plants, the majority of GTs belong to family 1 (GT1) and are typically referred to as UDP-glycosyltransferases (UGTs) due to their preference for UDP-Glc as a sugar donor (Zhang *et al.*, 2020). In *Arabidopsis*, 122 genes are predicted to encode enzymes within the GT1 family (Rehman *et al.*, 2018).

Deciphering the structural characteristics of GT1s is essential for understanding the mechanisms of glycosylation catalysis. A notable structural feature of plant GT1 enzymes is the plant secondary product glycosyltransferase (PSPG) box, a conserved motif of 44 amino acids located at the C-terminus, which likely aids in glycosyl donor binding (Wang and Hou, 2009). Besides the PSPG box, GTs generally show limited sequence similarity across their structures, with substantial variability observed in the N-terminal regions, suggesting that these regions may contribute to the enzymes' substrate specificity and binding flexibility (Yonekura-Sakakibara and Hanada, 2011).

Three UGTs are involved in SA glucosylation in *Arabidopsis:* UGT74F1, UGT74F2, and UGT76B1 (Dean and Delaney, 2008; von Saint Paul *et al.*, 2011; Bauer, 2020).

1.3.1 UGT74F1 and UGT74F2

UGT74F1 and UGT74F2 share significant sequence similarity, with 77% identity and conserved active site residues. Despite their structural resemblance, they catalyze the formation of different SA conjugates: UGT74F1 primarily produces SAG, while UGT74F2 predominantly forms SGE (George Thompson *et al.*, 2017). Beyond SA, both enzymes have demonstrated activity against a variety of benzoate substrates *in vitro*, including benzoic acid, phenylacetothiohydroximate, 3-hydroxybenzoic acid, and the folate precursor p-aminobenzoate (Lim *et al.*, 2002b; Eudes *et al.*, 2008; Grubb *et al.*, 2014a). Notably, when tested for activity against the flavonoid quercetin, only UGT74F1 exhibited glucosylation ability (Cartwright *et al.*, 2008). Both UGT74F1 and UGT74F2 can metabolize anthranilic acid (AA), but evidence suggests that UGT74F2 is the main catalyst for this reaction *in vivo* (Quiel and Bender, 2003). Additionally, *in vitro* assays and observations of reduced nicotinic acid-*O*-

glucoside formation in specific mutants indicate that UGT74F2 mediates the glucosylation of nicotinic acid (NA) *in vivo* (Li *et al.*, 2015). Among these substrates, only NA and AA are confirmed as physiological substrates within the plant.

The roles of UGT74F1 and UGT74F2 in SA regulation have been investigated through mutant studies, yielding some conflicting results. Noutoshi *et al.* (2012) reported that the *ugt74f1-1* mutant accumulates higher levels of free SA and displays increased resistance to both virulent and avirulent strains of *Pseudomonas syringae pv. tomato* DC3000 (*Pst*) compared to the wild-type ecotype Wassilewskija (Ws). This finding aligns with previous *in vitro* and *in vivo* studies suggesting that UGT74F1 is involved in conjugating SA to form SAG, thereby regulating SA levels (Dean and Delaney, 2008). Conversely, Boachon *et al.* (2014) found that the same *ugt74f1-1* mutant exhibited lower free SA and SAG levels, resulting in increased susceptibility to pathogens. Later research using *ugt* mutants generated in a consistent Col genomic background revealed that the loss of UGT74F1 did not alter SA or SAG levels, nor the defense marker gene PR1, compared to wild-type plants. Interestingly, the mutants exhibited moderately enhanced resistance to *Pst* (Bauer, 2020).

UGT74F2 has been reported to form both SAG and SGE *in vitro* (Song, 2006). Studies involving radiolabeled [7-^{14}C]-SA fed to *ugt74f2-1* knockdown plants revealed that wild-type leaves produce both SAG and SGE, with SGE formation specifically attributed to UGT74F2 (Dean and Delaney, 2008). Similarly, Li *et al.* (2015) observed that wild-type plants showed increased levels of SA, SAG, and SGE after pathogen infection. In contrast, the *ugt74f2-1* knockdown line significantly reduced all three metabolites. Interestingly, Boachon *et al.* (2014) reported higher levels of free SA in *ugt74f2-1* mutants following infection, despite using the same mutant line as other studies. In *Pst* infection assays, overexpression of UGT74F2 led to heightened susceptibility, while the *ugt74f2-1* knockdown mutant exhibited slightly increased resistance three days post-infection (Song *et al.*, 2008; Boachon *et al.*, 2014). Similar to *ugt74f1*, Bauer (2020) reported that *ugt74f2* mutants displayed increased resistance to *Pst*. However, SA and SAG levels remained unaffected, and only marginal amounts of SGE were detectable in the mutants, indicating that UGT74F2 is the principal producer of SGE.

At the transcriptional level, UGT74F1 is not induced by exogenous SA application or *Pst* infection (Song, 2006; Song *et al.*, 2008; Okamoto *et al.*, 2009). This lack of induction was corroborated by GUS staining analyses, where UGT74F1 expression remained unaffected by treatments with *P. syringae*, SA, or the SA analog benzo(1,2,3)-thiadiazole-7-carbothioic acid S-methyl ester (BTH) (Meßner and Schäffner, unpublished data). In contrast, UGT74F2 expression is upregulated in response to pathogen infection as well as SA or BTH treatment (Song, 2006; Song *et al.*, 2008; Okamoto *et al.*, 2009; Meßner and Schäffner, unpublished

data). This induction suggests that UGT74F2 plays a more dynamic role in the plant's defense response and SA metabolism during stress conditions.

1.3.2 UGT76B1

UGT76B1 is one of the most stress-responsive UGTs in *Arabidopsis*, playing a pivotal role in the plant's defense mechanisms. It is significantly upregulated by various abiotic stresses—including UV-B radiation, osmotic stress, oxidative stress, drought, and physical wounding—as well as by both biotrophic and necrotrophic pathogens (von Saint Paul *et al.*, 2011). For instance, during infection by the biotrophic oomycete pathogen *Hyaloperonospora arabidopsidis*, UGT76B1 expression is notably elevated in the early stages of infection and continues to increase as the infection progresses (Hok *et al.*, 2011). Additionally, UGT76B1 ranks among the top ten transcripts highly expressed in response to exogenous SA treatment (Krinke *et al.*, 2007).

Functionally, UGT76B1 has been shown to glucosylate multiple defense-related small molecules, underscoring its role as a versatile hub enzyme in plant immunity. *In vitro* studies reveal that UGT76B1 can glucosylate SA, indicating its involvement in SA metabolism and regulation (von Saint Paul *et al.*, 2011; Noutoshi *et al.*, 2012). Beyond SA, UGT76B1 also glucosylates ILA, a branched-chain amino acid-related 2-hydroxycarboxylic acid. ILA works synergistically with SA to activate SA-responsive genes and enhance plant resistance through a UGT76B1-dependent mechanism. Notably, ILA can also induce an SA-independent stress response, including the formation of superoxide in SA-deficient lines (von Saint Paul *et al.*, 2011; Bauer *et al.*, 2020). Recent research has identified N-hydroxypipecolic acid (NHP) as another substrate of UGT76B1. NHP is recognized as a key mobile signal for systemic acquired resistance (SAR) in plants. UGT76B1 glucosylates NHP, thereby modulating its levels within the plant. Loss of UGT76B1 leads to elevated levels of SA and NHP, resulting in the autonomous activation of SAR. This activation is dependent on the NHP biosynthesis gene *FLAVIN-DEPENDENT MONOOXYGENASE 1* (*FMO1*), highlighting the interconnected roles of UGT76B1 and NHP in plant immunity (Bauer *et al.*, 2021; Cai *et al.*, 2021; Holmes *et al.*, 2021; Mohnike *et al.*, 2021). *In vitro* enzyme assays also indicate that UGT76B1 glucosylates scopoletin (Mohnike, 2022), a coumarin with antimicrobial activity that is essential for root-beneficial microbial interactions (Stassen *et al.*, 2020). Combined with the fact that UGT76B1 is constitutively expressed in roots (von Saint Paul *et al.*, 2011), this suggests that UGT76B1 also likely plays an important role in root-microbe interactions.

1.4 Roles of SA in plant

1.4.1 SA in abiotic stresses

While SA is primarily recognized for its role as a defense hormone against biotic stressors, increasing evidence highlights its significance in plant responses to various abiotic stresses—including cold, drought, thermogenesis, osmotic stress, and metal toxicity (Guo *et al.*, 2019; Ignatenko *et al.*, 2019; Wassie *et al.*, 2020; Mohi-Ud-Din *et al.*, 2021; Kumar *et al.*, 2022). Treatment with optimal levels of SA can induce acclimation effects, enhancing tolerance to a range of abiotic stressors (Horváth *et al.*, 2007; Nazar *et al.*, 2015).

Drought Stress: In addition to ABA, SA contributes to the regulation of drought responses. Drought conditions lead to elevated endogenous SA levels in plants such as *Phillyrea angustifolia* and barley roots (Munne-Bosch and Penuelas, 2003; Bandurska and Stroiński, 2005). In *Arabidopsis*, SA biosynthetic genes like *EDS5*, *PBS3*, and *SID2* are upregulated following prolonged water deficit, with SA-inducible genes *PR1* and *PR2* being activated after extended drought periods (Miura *et al.*, 2013; Xu *et al.*, 2023). This accumulation of SA appears to play a protective role, as mutants accumulating higher SA levels—such as *coi1*, *siz2*, *acd6*, and *cpr5*—demonstrate enhanced drought tolerance (Miura *et al.*, 2013; Okuma *et al.*, 2014a; Venegas-Molina *et al.*, 2020). Moreover, exogenous applications of SA have proven effective in boosting drought resilience in various crops. For instance, foliar application of SA at 1.0 μM significantly strengthens antioxidant defenses in drought-tolerant maize (Saruhan *et al.*, 2012). Similarly, treatments with acetyl SA (0.1–1 mM) have improved drought tolerance in muskmelon seedlings (Korkmaz *et al.*, 2007), and SA-imbibed seeds in tomato and bean have shown increased resistance to heat, cold, and drought (Senaratna *et al.*, 2000).

Salinity and Osmotic Stress: Salinity stress affects plants through both sodium-induced toxicity, which disrupts ionic balance, and osmotic stress. SA has shown substantial promise in enhancing plant tolerance to salinity and osmotic stresses across various crops, including *Vicia faba* (Azooz, 2009), *Brassica juncea* (Nazar *et al.*, 2011a, 2015), *Medicago sativa* (Palma *et al.*, 2013), and *Vigna radiata* (Nazar *et al.*, 2011b). In rice seedlings, salinity induces both endogenous SA levels and the activity of SA biosynthetic enzymes (Sawada *et al.*, 2006). In *Arabidopsis* seeds, high salinity inhibits germination; however, low concentrations of SA (<50 μM) reduce this inhibition (Lee *et al.*, 2010). Exogenous SA also elevates reactive oxygen species (ROS) and the expression of antioxidant enzymes, thereby improving salt tolerance in *Arabidopsis* (Horváth *et al.*, 2015). Conversely, SA-deficient NahG transgenic *Arabidopsis* plants exhibit heightened salinity-induced damage and diminished antioxidant enzyme activity (Cao *et al.*, 2009). Additionally, the *wrky54 wrky70* double mutant, which accumulates high

levels of endogenous SA, shows increased resilience to osmotic stress, demonstrated by better water retention and enhanced stomatal closure (Li *et al.*, 2013).

Cold Stress: Cold stress promotes the buildup of free SA and SAG in plants such as *Arabidopsis*, wheat, and grape berries (Scott *et al.*, 2004; Wan *et al.*, 2009; Kosová *et al.*, 2012), suggesting SA's involvement in cold stress responses. Treatment with 0.5 mM SA has been shown to improve cold tolerance in maize, cucumber, and rice (Kang and Saltveit, 2002). However, prolonged or high-dose applications of SA can be detrimental, leading to decreased cold tolerance. For example, while foliar application of SA enhances freezing tolerance in winter wheat (Taşgın *et al.*, 2006), continuous hydroponic application causes severe damage in both winter and spring wheat under freezing conditions (Horváth *et al.*, 2007). Endogenous accumulation of SA due to mutations can mimic these adverse effects. *Arabidopsis* mutants such as *acd6* and *siz1*, which accumulate high levels of SA, show increased cold sensitivity—a phenotype reversible upon the introduction of the NahG gene (Miura and Ohta, 2010). Additionally, the *ice1* mutant, initially identified as cold-sensitive (Chinnusamy *et al.*, 2003), exhibits upregulation of SA-responsive genes and enhanced pathogen resistance (Zhu *et al.*, 2011). Overexpression of *DEAR1*, which increases SA levels, also heightens freezing sensitivity (Tsutsui *et al.*, 2009). These findings suggest an intricate relationship between cold stress and SA signaling pathways, where SA's effects on cold tolerance are dose- and duration-dependent.

1.5 Plant immune system

In natural ecosystems, most plants exhibit resistance to the majority of pathogens. Understanding and harnessing the mechanisms behind this phenomenon is considered one of the holy grails in plant pathology (Staskawicz, 2001). To effectively respond to and defend against biotic threats, plants have evolved highly complex pathogen defense systems or surveillance networks, functioning similarly to the innate immune systems of humans. These networks enable plants to recognize a broad range of biotic threats, including pathogens, pests, viruses, and beneficial microorganisms (Sanabria *et al.*, 2008).

The plant immune system comprises both local and systemic immunity. Local immunity is primarily divided into two major branches: the recognition of pathogen-associated molecular patterns (PAMPs) leading to PAMP-triggered immunity (PTI) and effector-triggered immunity (ETI). Systemic immunity involves SAR and induced systemic resistance (ISR) (Thomma *et al.*, 2011; Vlot *et al.*, 2021). Systemic immunity refers to signals that spread from the site of infection to unaffected tissues, thereby enhancing resistance to subsequent secondary stresses (De Kesel *et al.*, 2021).

PAMPs are highly conserved microbial motifs essential for a microbe's survival and lifestyle—for example, flagellin and chitin (Jones and Dangl, 2006). When PAMPs are recognized, plants mount a basal defense known as PTI. However, many pathogens have evolved strategies to evade or suppress PTI, such as injecting effector proteins into plant cells, effectively hijacking the plant's immune system. In response, plants have developed an additional surveillance platform, ETI (Cui *et al.*, 2015). ETI is a robust and sustained immune response activated upon recognizing pathogen-secreted effector proteins. As an added layer of immune surveillance, ETI shares many downstream mechanisms with PTI, including calcium signaling, phytohormone signaling, reactive oxygen species production, and mitogen-activated protein kinase cascades (Yuan *et al.*, 2021).

1.5.1 Systemic acquired resistance

Upon primary infection of a plant leaf (locally associated with PTI and/or ETI), distant leaves can induce SAR—a heightened immune state that counteracts subsequent infections and limits the spread of otherwise compatible pathogens throughout the foliage (Shah and Zeier, 2013; Vlot *et al.*, 2021). SAR establishment is controlled by two key immune-active small molecules: SA and the recently discovered NHP. NHP accumulates in infected *Arabidopsis* tissues and can move systemically through the entire rosette (Chen *et al.*, 2018; Hartmann *et al.*, 2018). NHP plays a critical role in SAR across various plant species, including both monocots and dicots (Holmes *et al.*, 2019; Schnake *et al.*, 2020).

Conversely, SA has long been recognized as an indispensable signal for SAR (Gaffney *et al.*, 1993; Nawrath and Métraux, 1999). Nonetheless, grafting experiments with tobacco wild-type plants onto rootstocks deficient in SA ruled it out as the sole mobile signal triggering SAR from rootstock leaves to scion leaves (Vernooij *et al.*, 1994). Several other mobile signals have also been proposed (Wendehenne *et al.*, 2014; Singh *et al.*, 2017; Hartmann *et al.*, 2018). Strong evidence suggests that NHP functions as a mobile defense signal, traveling from locally inoculated leaves to distant leaves during SAR induction. Detailed time-course analyses of *Pseudomonas*-inoculated *Arabidopsis* revealed that NHP levels in distant leaves begin to rise at the onset of SAR, whereas systemic levels of its precursor pipecolic acid (Pip) and SA remain unchanged (Hartmann *et al.*, 2018). Moreover, local application of NHP or deuterium-labeled NHP to *Arabidopsis* leaves via pressure infiltration leads to detectable translocation of NHP to distant tissues (Chen *et al.*, 2018; Cai *et al.*, 2021; Mohnike *et al.*, 2021; Yildiz *et al.*, 2021).

SA-triggered defense responses rely on the transcriptional co-activator NON-EXPRESSOR OF PR GENES1 (NPR1). Upon pathogen inoculation, SA levels accumulate, causing NPR1 to relocate from the cytosol to the nucleus (Mou *et al.*, 2003); SA then binds to NPR1,

prompting increased expression of pathogenesis-related genes and immune activation (Wu *et al.*, 2012; Ding *et al.*, 2018). NPR1 is also required for pathogen-induced SAR, as it is essential for NHP-responsive gene expression (Ding and Ding, 2020; Nair *et al.*, 2021). Thus, the cooperative interplay between NHP and SA is crucial for the establishment of SAR (Hartmann and Zeier, 2019).

Both SA and NHP accumulate in local and distal tissues following pathogen attack, reprogramming the plant at the transcriptional level and priming it for enhanced defensive capacity. However, excessive levels of SA and NHP can cause stunted growth and premature senescence. To mitigate these effects, the glucosyltransferase UGT76B1 is induced to inactivate both molecules (Ding and Ding, 2020; Bauer *et al.*, 2021; Cai *et al.*, 2021; Holmes *et al.*, 2021; Mohnike *et al.*, 2021). Notably, *FMO1*, a key gene in NHP biosynthesis, is required for SAR; its loss impairs SAR, whereas mutation of UGT76B1 leads to an overaccumulation of endogenous SA and NHP, resulting in an autonomous activation of SAR (Mishina and Zeier, 2007; Bauer *et al.*, 2021; Cai *et al.*, 2021; Holmes *et al.*, 2021; Mohnike *et al.*, 2021).

1.5.2 Induced systemic resistance and SA

Beneficial microbes in the root microbiome play a significant role in enhancing plant health. ISR is a key mechanism by which specific plant growth–promoting bacteria and fungi in the rhizosphere “prime” the entire plant for heightened defense against a wide range of pathogens and insect herbivores (Pieterse *et al.*, 2014). In the early 1990s, the plant growth-promoting rhizobacterium (PGPR) *Pseudomonas fluorescens* WCS417r was shown to colonize roots and enhance resistance in the plant’s aboveground parts against the fungal pathogen *Fusarium oxysporum* (Van Peer *et al.*, 1991). Later studies demonstrated that this PGPR-mediated ISR is not dependent on SA but instead relies on intact JA and ET signaling pathways (Pieterse *et al.*, 1998; Knoester *et al.*, 1999). Genetic evidence in *Arabidopsis* has indicated that JA and/or ET are involved in ISR regulation for other PGPR, such as *Serratia marcescens* 90–166, *Pseudomonas protegens* CHA0, *P. fluorescens* Q2-87, and for plant growth-promoting fungi (PGPF) like *Penicillium* sp. GP16-2, *Trichoderma harzianum* T39, and *Piriformospora indica* (Iavicoli *et al.*, 2003; Ryu *et al.*, 2004; Hossain *et al.*, 2008; Korolev *et al.*, 2008; Stein *et al.*, 2008; Weller *et al.*, 2012).

Although ISR triggered by beneficial microbes is often mediated by SA-independent mechanisms, some PGPRs have been found to activate an SA-dependent type of ISR that resembles pathogen-induced SAR (Pieterse *et al.*, 2014). For instance, PGPR such as *Paenibacillus alvei* K165 (Tjamos *et al.*, 2005), *P. fluorescens* SS101, and Ps14 (van de Mortel *et al.*, 2012a; Alizadeh *et al.*, 2013), and *Fusarium equiseti* GF19-1 (Kojima *et al.*, 2013) induce SA-dependent ISR. Similarly, *Trichoderma* PGPFs like *T. asperellum* SKT-1, *T. harzianum*

Tr6, and *T. hamatum* T382 enhance resistance against *Botrytis cinerea*, *Pst*, and *F. oxysporum*, respectively, in an SA-dependent manner (Yoshioka *et al.*, 2012; Alizadeh *et al.*, 2013). Furthermore, some *Trichoderma* species have been shown to activate both SA and JA signaling. For example, root inoculation with *T. virens* Gv.29-8 and *T. atroviride* IMI206040 can induce the JA marker gene *LOX1* in the shoot when low doses of conidia are applied, and the SA marker *PR1* at higher doses (Contreras-Cornejo *et al.*, 2011).

These findings challenge the conventional view that ISR triggered by root-beneficial microbes is solely mediated by JA and ET. While ISR is commonly described this way in current literature, recent discussions suggest that ISR should not be limited to responses triggered by PGPR or PGPF, as phytohormones other than JA and ET may also mediate ISR (De Kesel *et al.*, 2021). Despite these advances, the nature of the mobile signal involved in SA-dependent ISR remains unclear, and whether it shares pathways with SAR is yet to be determined.

1.5.3 Microbe-mediated root-shoot communication in plant immunity

Root-shoot communication in plants is essential for integrating responses to environmental changes and balancing growth and defense, which optimizes plant survival. Root-derived signals modulate shoot growth, while shoot-derived signals regulate nutrient uptake activity in the root (Notaguchi and Okamoto, 2015; Ko and Helariutta, 2017). Several molecules, including RNAs, microRNAs, small peptides, and phytohormones, have been identified as systemic signals that play essential roles in root-shoot communication under various biotic and abiotic stresses (García *et al.*, 2023).

Soil microbe colonization of plant roots has been widely shown to promote plant growth and enhance shoot resistance against pathogens via SA and/or JA/ET pathways (Pieterse *et al.*, 2014). However, the identity of mobile signals mediating these pathways remains unclear. For conventional JA/ET-dependent ISR ($ISR_{sensu\ stricto}$), the mobile signals generated in the roots that are translocated to systemic tissues have not yet been identified (Pieterse *et al.*, 2014; Yu *et al.*, 2021; De Kesel *et al.*, 2021). A key regulator of ISR initiation is the root-specific transcription factor MYB72, which also regulates the biosynthesis and secretion of coumarins in roots interacting with the ISR-inducing microbe *P. simiae* WCS417 (Segarra *et al.*, 2009; Stringlis *et al.*, 2017). Interestingly, coumarin β-glucosidase BGLU42 is required for ISR activation, as mutants lacking this enzyme are impaired in ISR (Zamioudis *et al.*, 2014). Given that coumarins are mobile between roots and shoots, they are hypothesized to travel from roots to shoots to facilitate ISR activation (Stassen *et al.*, 2020).

Classic SAR is an inducible defense mechanism systemically activated through foliage in response to localized pathogen infection (Sticher *et al.*, 1997; Spoel and Dong, 2012; Shah and Zeier, 2013). The concept of SAR being triggered by root infection with soil-borne

pathogens remains less understood. However, root dipping in BTH and NHP feeding experiments suggest that SAR-like responses can originate in the root and establish in the shoot (Amzalek and Cohen, 2006; Schnake *et al.*, 2020). Conversely, leaf treatment with BTH in *Nicotiana benthamiana* not only enhances root resistance against the soil-borne pathogen *Ralstonia solanacearum* but also transmits BTH-induced SAR to neighboring plants via roots, eventually reaching their shoots (Song *et al.*, 2016). However, whether NHP is essential for transmitting SAR between roots and shoots remains unclear.

Aim of this work

Despite UGT76B1 being known to attenuate SAR by modulating the levels of the signaling molecules NHP and SA (Bauer *et al.*, 2021; Cai *et al.*, 2021; Mohnike *et al.*, 2021; Holmes *et al.*, 2021), an intriguing observation remains unexplained: its constitutive expression in roots (von Saint Paul *et al.*, 2011). Root uptake of NHP has been suggested to potentially trigger defense responses in shoots (Schnake *et al.*, 2020; Yildiz *et al.*, 2021), and the NHP biosynthesis gene FMO1 also appears to be constitutively expressed in roots (Joglekar, 2014). Furthermore, grafting experiments reveal that the loss of UGT76B1 in shoots has only a minor impact, whereas its loss in roots significantly enhances the expression of SA signaling genes in shoots (Rafał, 2017; Bauer, 2020). Interestingly, many upregulated genes in *ugt76b1* mutants have been identified as mobile RNAs traveling between roots and shoots (Bauer, 2020). These findings suggest that the FMO1/UGT76B1-controlled NHP pathway may play a critical role in mediating root-shoot communication. Therefore, the primary aim of this work is to investigate the function of UGT76B1 in roots and its potential involvement in root-to-shoot signaling and interactions with the soil microbiome.

In contrast to UGT76B1, the functions of UGT74F1 and UGT74F2 remain ambiguous, with contradictory reports concerning their roles in defense. This inconsistency may arise from differences in the genetic backgrounds of the mutants used in previous studies. Recently, a complete set of combinatorial mutants for all three SA-GTs in a uniform genetic background has been generated in our laboratory. A comprehensive analysis, including RNA sequencing and SA metabolite profiling, has been performed (Georgii *et al.*, unpublished). However, the specific roles of these three SA-GTs in biotic and abiotic stress responses remain unclear. Thus, the second aim of this work is to investigate their individual and combined roles in mediating responses to both biotic and abiotic stresses.

Given that these SA-GTs are known to glucosylate multiple substrates, it is interesting to explore how various ligands can be incorporated into the enzymes' binding pockets for a successful catalytic conjugation or whether catalysis of certain ligands is hampered. With the advent of the groundbreaking protein modeling tool AlphaFold2 (Jumper *et al.*, 2021), resolving protein structures has become significantly more accessible. By combining advanced tools for protein-ligand docking and molecular dynamics simulations, it is now possible to predict enzyme activities and substrate specificities. Therefore, the third aim of this work is to obtain predicted structures of the three SA-GTs, perform docking studies with different substrates, and investigate their substrate specificities. Establishing such a pipeline would accelerate and simplify the process of screening UGTs for specific molecules.

2 Results

2.1 The unique role of UGT76B1 in root-shoot communication

Previous study shows UGT76B1 is constitutively expressed in the roots of naïve plants(von Saint Paul *et al.*, 2011), and given that root uptake of NHP can potentially trigger shoot defense(Schnake *et al.*, 2020; Yildiz *et al.*, 2021; Löwe *et al.*, 2023), it is hypothesized that NHP plays a key role in mediating root-shoot communication in defense responses.

2.1.1 NHP is constitutively synthesized and glucosylated in roots

UGT76B1 is known to be induced in the shoot under stress conditions, where it glucosylates three defense-related compounds: ILA, SA, and NHP (von Saint Paul *et al.*, 2011; Noutoshi *et al.*, 2012; Bauer *et al.*, 2021). However, its role in roots remains unexplored despite its constitutive expression in the root endodermis and cortex of naïve plants (von Saint Paul *et al.*, 2011). To better understand this expression pattern, co-regulation between *UGT76B1* and the biosynthesis genes of its substrates was analyzed. As the biosynthesis process of ILA remains unclear, the analysis focused on genes involved in SA and NHP biosynthesis. Despite *UGT76B1* catalyzing the glucosylation of SA, its co-expression coefficient with SA biosynthesis genes is generally lower than with NHP biosynthesis genes. Among NHP biosynthesis genes, *FMO1* shows the highest level of co-expression with *UGT76B1* (Fig. 1). Additionally, the root single-cell expression database indicates that *FMO1* is constitutively expressed in the cortex and differentiating endodermis/cortex cells (Fig. S1A, B). GUS staining experiments reveal that both *FMO1* and *UGT76B1* are constitutively expressed in the root, with *UGT76B1* showing a much stronger expression than *FMO1* (Fig. 2A).

Gene name	AGI Code	Pathway	Gene name	AGI Code	coex z
UGT76B1	AT3G11340	NHP biosynthesis	*FMO1*	AT1G19250	4.1
			ALD1	AT2G13810	4.0
			SARD4	AT5G52810	3.5
		SA biosynthesis	*SID2*	AT1G74710	2.8
			EDS5	AT4G39030	2.5
			PBS3	AT5G13320	1.4
			EPS1	AT5G67160	0.6
			ICS2	AT1G18870	-0.7

Fig. 1: Co-expression coefficient between UGT76B1 and NHP, SA biosynthesis genes. *ALD1*, *AGD2-LIKE DEFENSE RESPONSE PROTEIN1*; *SARD4*, *SAR-DEFICIENT4*; *SID2*, *SA INDUCTION-DEFICIENT2*; *EDS5*, *ENHANCED DISEASE SUSCEPTIBILITY5*; *PBS3*, *AVRPPHB SUSCEPTIBLE3*; *EPS1*, *ENHANCED PSEUDOMONAS SUSCEPTIBILITY*; *ICS2*, *ISOCHORISMATE SYNTHASE2*. Data obtained from ATTED-II, Platform: ath-m.c9-0 ath-r.c5-0. (https://atted.jp/top_draw/#CoexViewer)

For a more detailed examination, fluorescent protein-labeled transgenic lines were used for confocal microscopy. mTFP-UGT76B1 was observed in both the endodermis and cortex, whereas FMO1-YFP was only detectable in the cortex under high detection sensitivity (Fig.

2A). To analyze the metabolites produced by both enzymes, extracts from root and shoot were analyzed using LC-MS. Consistent with the expression patterns, NHP and NHP-*O*-Gluc levels were significantly higher in the root than in the shoot (Fig. 2B). In line with the low expression of *FMO1*, free NHP in the root was also at a relatively low level compared to levels observed in plants induced by *Pst* (0.08 vs. 10 ng mg^{-1}; Bauer *et al.*, 2021).

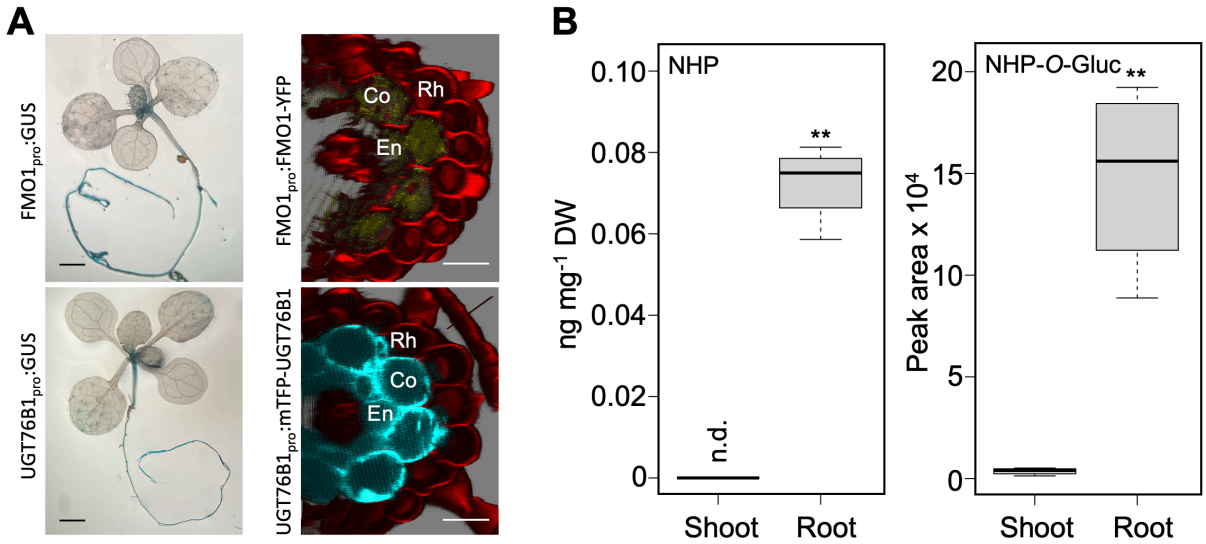

Fig. 2: Expression pattern of *FMO1* and *UGT76B1* involved in NHP biosynthesis and glucosylation. A. Transgenic plant carrying *UGT76B1*$_{pro}$:GFP-GUS and *FMO1*$_{pro}$:GUS construct illustrate the expression patterns of *UGT76B1* and *FMO1* in 12-day-old naive plants grow on soil. 30 min of GUS staining for UGT76B1 GUS line, 12 hours for FMO1 GUS line. Confocal laser scanning microscopy of main roots from 2-week-old *ugt76b1* mutant complemented with UGT76B1$_{pro}$:mTFP-UGT76B1, *fmo1* mutant complemented with FMO1pro:FMO1-YFP grown on half MS plate. Red, propidium iodide; Yellow, FMO1-YFP; Cyan, mTFP-UGT76B1. Black bar, 3 mm; white bar, 30 µm. En, endodermis; Co, cortex; Ep. Epidermis. B. Distribution of NHP and NHP-*O*-Gluc in root and shoot tissues of 2-week-old plant grown on half-strength MS petri-dishes determined by LC-MS analysis. bars are means ± SD; $n = 4$. Differences between root and shoot were analyzed by Welch two-sample t test; $^*P < 0.05$.

2.1.2 NHP but not NHP-*O*-Gluc is bidirectionally mobile

Although NHP is known to move systemically between leaves (Mohnike *et al.*, 2021b=; Yildiz *et al.*, 2021), its mobility between roots and shoots, as well as that of NHP-*O*-Gluc, remains unclear. To investigate this, reciprocal micro-grafting was performed between *ugt76b1* and *fmo1* plants. In *ugt76b1*$_{shoot}$/*fmo1*$_{root}$ grafts, NHP synthesis occurs only in the shoot, with *O*-glucosylation limited to the root, and vice versa in *fmo1*$_{shoot}$/*ugt76b1*$_{root}$ plants. Grafted plants were treated with BTH to induce NHP biosynthesis, after which roots and shoots were separately collected for metabolic analysis, with the graft junction removed to prevent ambiguity in genotypes. Results indicated that NHP-*O*-Gluc was detectable only in tissues expressing *UGT76B1*, confirming its lack of mobility. In contrast, NHP was found in both roots and shoots even in the absence of *FMO1*, strongly suggesting that NHP moves bidirectionally between root and shoot (Fig. 3).

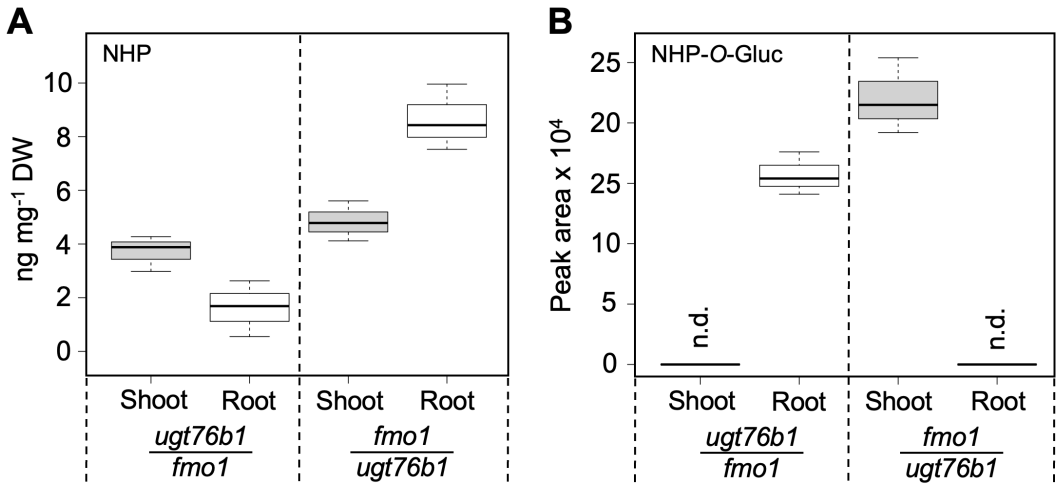

Fig. 3: Mobility of NHP and NHP-*O*-Gluc. NHP-deficient shoots *fmo1* grafted onto *ugt76b1* roots which is incapable of NHP glucosylation, and vice versa. Roots and shoots of 3-week-old grafted plants were sprayed with 1mM BTH, then harvested separately for LC-MS analysis in two days. Distribution of NHP in rosettes and roots in both grafting combinations highlights NHP's bidirectional mobility. In contrast, NHP-*O*-Gluc was exclusively detected in tissues containing a functional UGT76B1 enzyme, demonstrating its immobility.

2.1.3 Root expression of UGT76B1 affects shoot defense via NHP

To investigate the role of *UGT76B1* in the root, knockouts in roots or shoots were achieved via micro-grafting by combining wild-type plants with *ugt76b1* mutants. To ensure comparability, homo-grafts of both wild type and *ugt76b1* were used as controls. After a 16-day recovery period, shoots from 3-week-old plants were harvested for expression analysis. Compared to wild-type homo-grafts, *ugt76b1* homo-grafts exhibited a strong upregulation of *PR1*, *PR2*, and *PR5 SA marker genes*. Notably, the loss of *UGT76B1* in the roots also promoted the expression of these PR genes in wild-type shoots, whereas the loss of *UGT76B1* in shoots alone had no effect on their expression (Fig. 4). This finding aligns with previous observations (Maksym, 2018; Bauer, 2020) that the presence of *UGT76B1* in the root influences gene expression in the shoot.

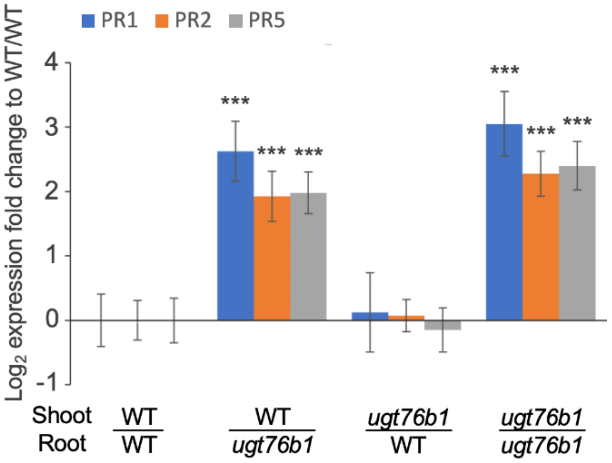

Fig. 4: Impact of *UGT76B1* in root and shoot on SA markers expression. The absence of *UGT76B1* in roots is associated with the upregulation of SA marker genes in shoot, an effect not observed with *ugt76b1* knockout in shoot only. Bars show means ± SD, $n = 5$; significant differences between genotypes were analyzed by two-way ANOVA with Welch two-sample t test, $^{***}P < 0.001$.

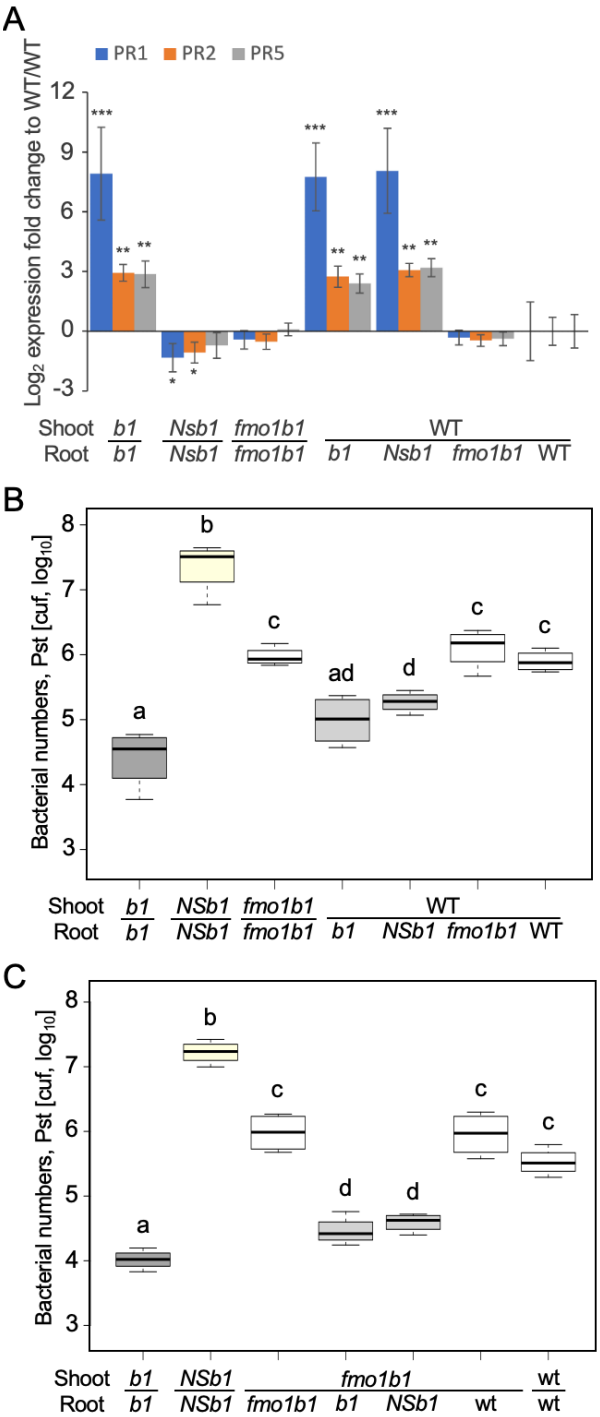

To assess whether *UGT76B1* substrates in the root affect shoot phenotypes, SA- and NHP-defective mutations were introgressed into *ugt76b1* roots. In homo-grafts, induction of SA marker genes was abolished when *fmo1* was introgressed into *ugt76b1*. When SA was depleted in *ugt76b1* roots by introgression of NahG *sid2*, PR gene expression was even lower than in the wild type. In hetero-grafts, *ugt76b1* root-induced PR gene expression in wild-type shoots was unaffected by SA depletion in the root but was abolished if NHP was depleted by introducing *fmo1* into the *ugt76b1* root (Fig. 5A).

Similarly, *ugt76b1* roots enhanced the resistance of wild-type shoots against *Pst*, almost reaching the level observed in *ugt76b1* knockout plants. In WT_{shoot}/NahG *sid2* $ugt76b1_{root}$ plants, SA depletion in the roots did not alter the enhanced shoot resistance caused by the absence of *UGT76B1* in roots, suggesting that root-derived SA does not influence shoot defense in this context. However, when *FMO1* was additionally absent in *ugt76b1* roots, shoot resistance reverted to wild-type levels (Fig. 5B).

Fig. 5: Impact of *FMO1* and *UGT76B1* root expression on shoot defense responses. Expression of SA marker genes *PR1*, *PR2* and *PR5* in shoot of grafted plants. **A.** Root *ugt76b1*-dependent enhanced SA signaling marker expression in shoots is abolished by the additional loss-of-*FMO1* function in roots, but not affected when SA depletion in roots by introducing bacterial SA hydroxylase NahG and knockout *sid2* and. *b1*, *ugt76b1*; *Nsb1*, NahG *sid2 ugt76b1*. Bars indicate means ± SD; $n = 4$. **B.** Enhanced defense against *Pst* DC3000 is observed in scenarios where *UGT76B1* is absent in roots. However, this enhancement is lost when *FMO1* is also absent in roots, whereas the absence of root-expressed *SID2* does not impact this defense enhancement. C. used *fmo1 ugt76b1* as a shoot for different grafting combinations. Bars show means ± SD, $n = 5$; significant differences between genotypes were analyzed by two-way ANOVA with Welch two-sample t-test, $^*P < 0.05$ (a) or post hoc Lincon test (b, c) as indicated by letters (*P.adj.* < 0.05).

Due to the positive feedback loop of NHP biosynthesis, root-derived NHP may amplify its biosynthesis in the shoot. Additional grafting combinations using *fmo1 ugt76b1* shoots were tested for *Pst* resistance (Fig. 5C). Since these shoots cannot synthesize or O-glucosylate NHP, their defense relies entirely on root-derived NHP. Consistently, root SA depletion did not impact the enhanced shoot defense induced by *ugt76b1* roots, whereas NHP depletion in roots abolished this effect. In conclusion, the enhanced defense in *ugt76b1* knockout plants results from the absence of *UGT76B1* in roots, where NHP is constitutively synthesized and possibly transported to the shoot in the absence of glucosylation capacity.

2.1.4 UGT76B1 endodermal expression is critical for root-controlled shoot phenotypes

To investigate the role of *UGT76B1* at the cell-layer level, tissue-specific knockout (TSKO) was employed to achieve "genetic grafting." For confirmation of targeted knockouts, a fluorescently labeled complementation line, *ugt76b1* $UGT76B1_{pro}$*:mTFP-UGT76B1* (*Compl.mTFP-B1*), was used as the parental line for TSKO. A mCherry-labeled Cas9 protein, driven by tissue-specific promoters *CO* and *CASP1*, was used to target *UGT76B1* in the cortex and endodermis cells, respectively. In the endodermis-specific knockout line (*ugt76b1*$_{endo}$), the mTFP-UGT76B1 signal was absent in endodermis cells. In the cortex-specific knockout line (*ugt76b1*$_{cortex}$), the mTFP-UGT76B1 signal was eliminated in cortex cells. Both knockouts were stable, with no mTFP signal—and thus no *UGT76B1* expression—detected in the targeted cell layers (Fig. 6; Fig. S2).

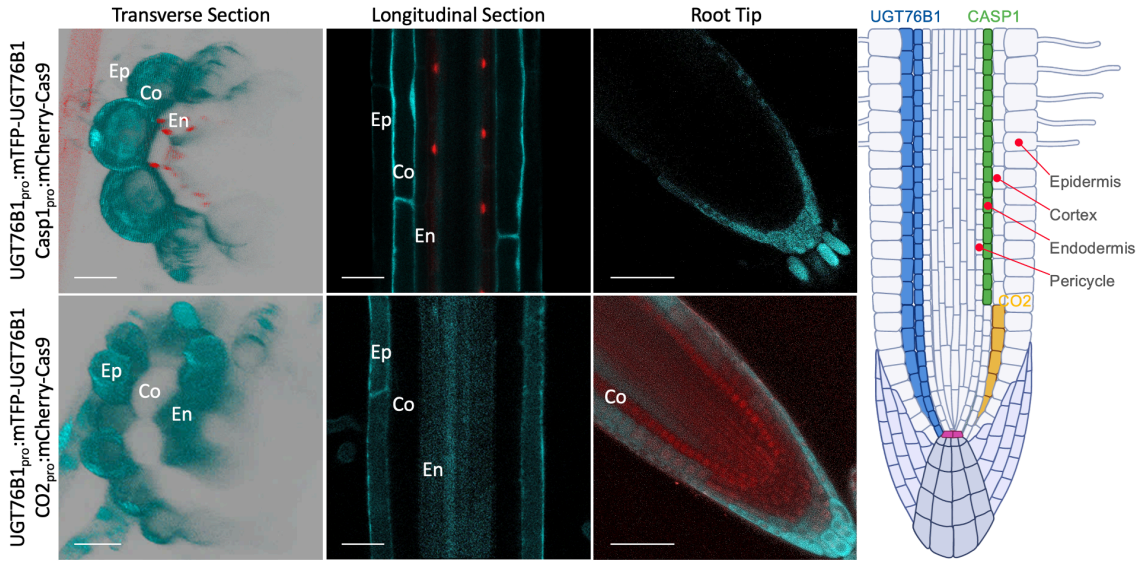

Fig. 6: Verification of tissue-specific knockout. Confocal microscopy visualization of tissue-specific knockout in 12-day-old plants grown on half-strength MS medium. The mTFP-UGT76B1 signal is shown in cyan, while the mCherry-Cas9 (red) is driven by the *CASP1* and *CO2* promoters in cortex and endodermis initial cells, respectively. The mTFP-UGT76B1 signal is absent in tissues where mCherry-Cas9 is expressed (By $CASP1_{pro}$*:mCherry-Cas9* and $CO2_{pro}$*:mCherry-Cas9* constructs). In the cortex knockout line, mCherry-Cas9 is expressed specifically in

cortex initial cells, efficiently knocking out the gene and resulting in the absence of the mTFP-UGT76B1 signal in differentiated cortex cells. Bar, 30 µm.

Upon *Pst* infection, *Compl.mTFP-B1* exhibits similar resistance to wild-type, indicating successful complementation and that the fluorescent tag does not impair protein function. Notably, the enhanced resistance of *ugt76b1*$_{cortex}$ against *Pst* matched that of the full knockout mutant, while *ugt76b1*$_{endo}$ exhibited intermediate resistance between wild-type and *ugt76b1* (Fig. 7). Additionally, *ugt76b1* plants exhibited growth retardation, early senescence compared to wild-type (von Saint Paul *et al.*, 2011), and reduced anthocyanin accumulation upon day-length alterations (Fig. S3A, B).

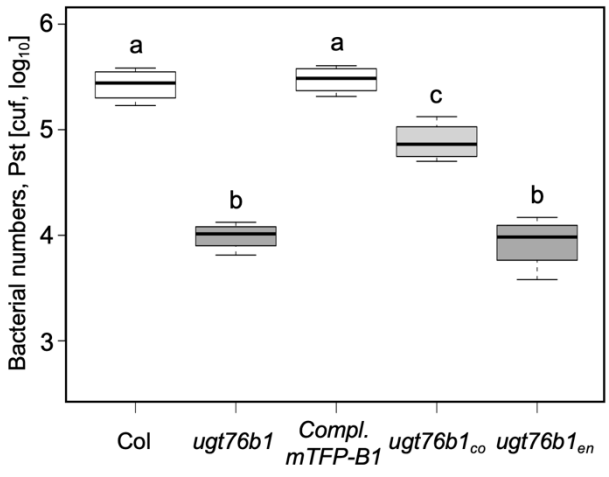

ugt76b1$_{endo}$ mirrored the phenotypes to *ugt76b1*, whereas *ugt76b1*$_{cortex}$ presented phenotypes intermediate between WT and *ugt76b1*. These results suggest that endodermal expression of UGT76B1 is critical, as its absence in a single cell layer replicates the full knockout phenotype.

Fig. 7: Differential impact of tissue-specific knockout of *UGT76B1* in root cell layers on shoot defense response. Infection assays of TSKO lines and controls with *Pst* DC3000. The absence of UGT76B1 in the endodermis replicates the defense response observed in whole-plant knockouts, whereas its removal from the cortex layer results in a moderately enhanced defense against the pathogen. Bars show means ± SD, $n = 5$; significant differences between genotypes were analyzed by one-way ANOVA with post hoc Lincon test as indicated by letters ($P.adj. < 0.05$).

2.1.5 UGT76B1 and FMO1 distinctly and specifically react to different types of soil-microbes

To understand the biological significance of the constitutive expression of *UGT76B1* and *FMO1* in roots, their responses to various soil-borne microbes were examined. Roots inoculated with microbes were collected for confocal microscopy. In mock-treated plants, mTFP-UGT76B1 was present in the cortex and endodermis, while FMO1-YFP was barely detectable without enhanced camera sensitivity (Fig. 2A). Upon interaction with endophytic fungi, including three *Trichoderma* species and *Serendipita indica*, mTFP-UGT76B1 signals disappeared following root colonization by hyphae, whereas FMO1-YFP was induced in the pericycle with varying intensities (Fig. 8). Similarly, inoculation with (hemi)biotrophic fungi, including three *Fusarium* species, *Phytophthora parasitica*, and *Sclerotinia sclerotiorum*, resulted in enhanced FMO1-YFP alongside the degradation of mTFP-UGT76B1. In contrast, necrotrophic pathogens such as *Botrytis cinerea* and two *Alternaria* species led to UGT76B1

degradation without FMO1 induction. This pattern was also observed upon inoculation with three non-host pathogens, including tree pathogens *Heterobasidion annosum*, *V. albo-atrum*, and the wheat pathogen *Ustilago nuda*. Inoculation with non-host mycorrhizal fungi, including *Laccaria bicolor*, *Purpureocillium lilacinum*, and *Meliniomyces bicolor*, had no significant effect, though UGT76B1 levels appeared reduced compared to the mock (Fig. 8).

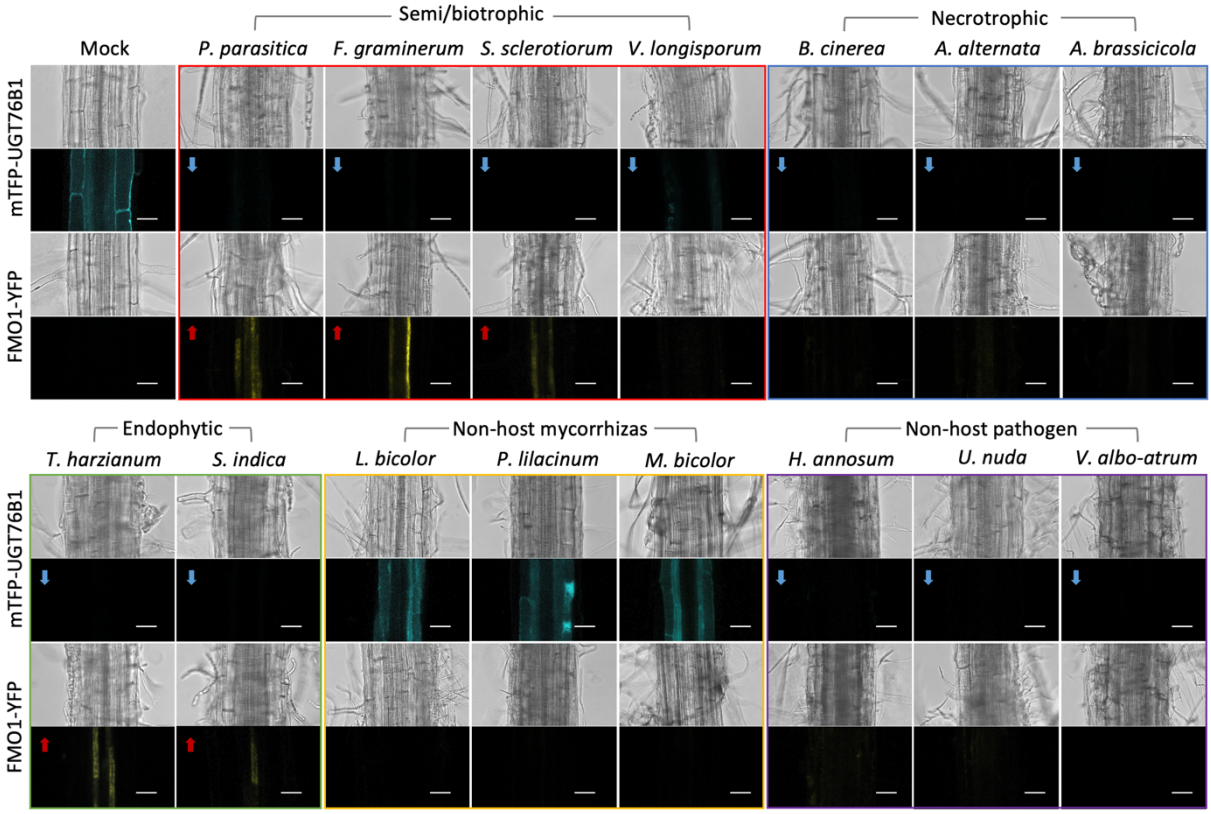

Fig. 8: Differential response of root UGT76B1 and FMO1 to fungal interactions. Fluorescent labeled UGT76B1 and FMO1 protein response to the inoculation of different types of fungi. Two-week-old plants grown on half MS plates were inoculated with fungi plugs next to the root. 1 or 2 days after inoculation, roots colonized with fungal mycelium were taken for confocal microscopy. The blue arrow indicates the down-regulation of UGT76B1 compared to the mock, and the red arrow indicates the up-regulation of FMO1. Bar, 30 µm.

To confirm the spatial expression of FMO1, optical sectioning was performed on roots infected with *F. graminearum*. Similar to inoculations with other (hemi)biotrophic pathogens, mTFP-UGT76B1 signals were absent from the cortex and endodermis, while FMO1-YFP was induced and restricted to the pericycle, as shown in root cross-sections (Fig. 9).

Since both endophytes and (hemi)biotrophs elicit a similar response, two pairs of functionally divergent fungi from representative genera and species were selected: the *Arabidopsis* beneficial root endophyte *Colletotrichum tofieldiae* (Ct) and its pathogenic relative *C. incanum* (Ci, Hacquard *et al.*, 2016). Upon inoculation, both local sites of hyphae-colonized roots and distal parts of the roots, where hyphae had not yet reached, were examined. Interestingly, Ct altered *UGT76B1* and *FMO1* expression only locally, whereas Ci inoculation led to

degradation of mTFP-UGT76B1 and induction of FMO1 even in the distal root regions. A similar pattern was observed with the beneficial *Fusarium oxysporum* strain Fo47 and the pathogenic strain Fo5176 (Fig. 10).

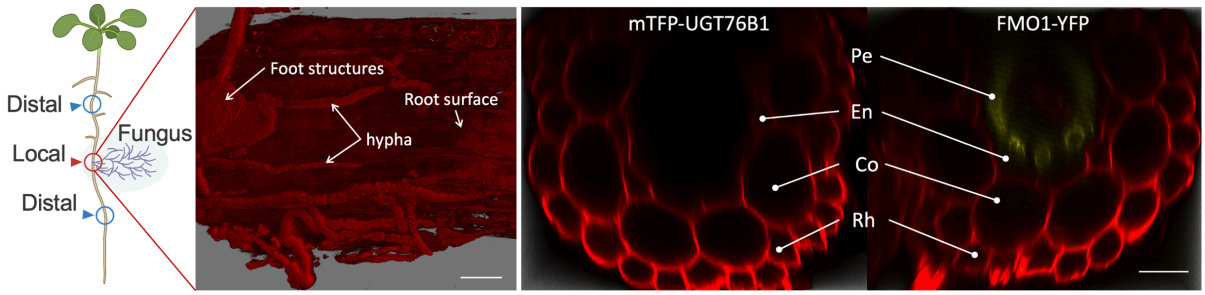

Fig. 9: Illustration of fungal inoculation and spatial expression of FMO1/UGT76B1. Surface and cross section of root infected with *F. graminerum*. The hypha of fungi and root cells are visualized with PI staining. Cortex and endodermis expression of UGT76B1 is absent, while FMO1 is strongly induced in Pericycle. Pe, pericycle; En, endodermis; Co, cortex; Ep, epidermis. Bar, 20 µm.

To investigate the dynamics of *UGT76B1* and *FMO1* regulation, root samples were monitored at multiple time points following inoculation with the fast-growing endophyte *T. harzianum*. mTFP-UGT76B1 degraded rapidly, becoming completely undetectable within three hours, whereas FMO1-YFP induction was significantly slower, with signals visible only after 18 hours (Fig. 11A). To confirm that the loss of mTFP-UGT76B1 during microbial interaction was due to active degradation rather than reduced protein translation, protein synthesis was inhibited using cycloheximide. Under these conditions, mTFP-UGT76B1 remained stable for over three days, with strong signals persisting even after seven days of treatment (Fig. 11B). These findings suggest that the rapid response to microbes within two days is due to active degradation. Overall, both FMO1 and UGT76B1 are actively and specifically regulated upon interaction with different soil microbes.

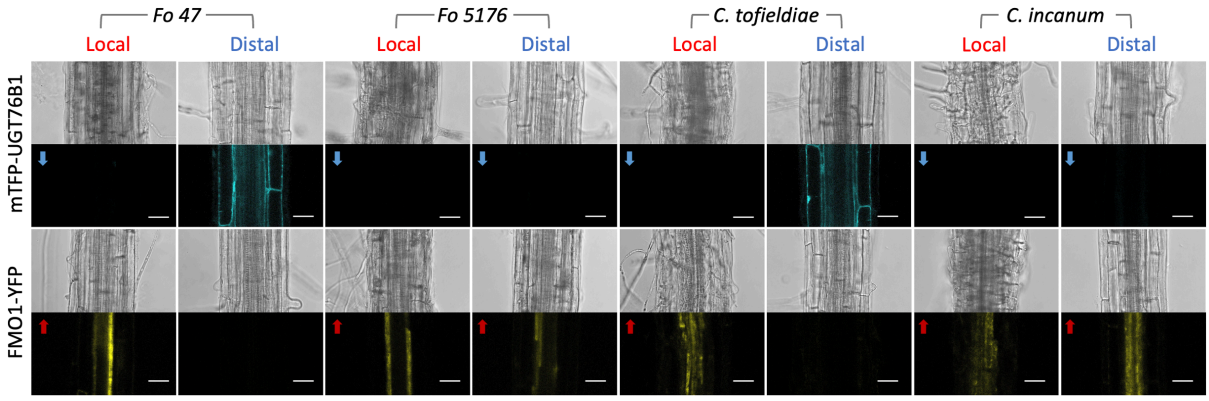

Fig. 10: Regulation of FMO1/UGT76B1 in different root regions upon exposure to various fungi. By confocal microscopy, UGT76B1 and FMO1 signal in local and distal roots inoculated with beneficial or pathogenic fungus. Distal regions are taken from uninfected roots around 1 cm up/downstream of the fungi inoculation, as shown in Fig. 28. Bar, 30 µm.

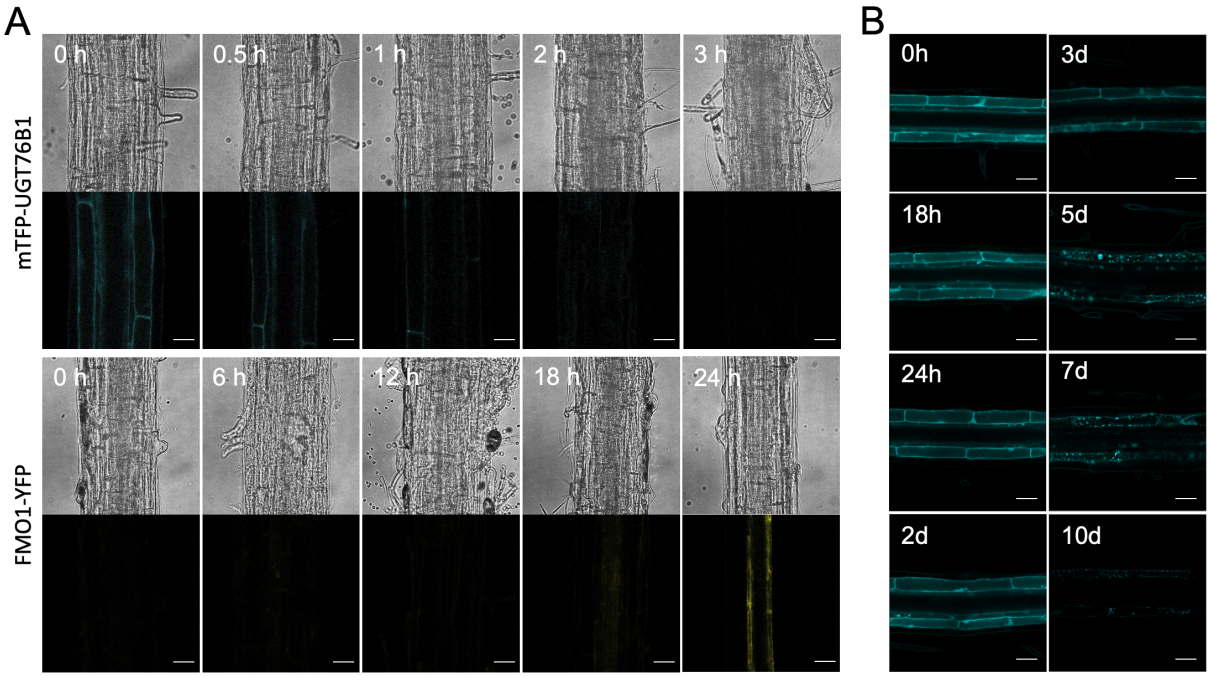

Fig. 11: Time course observation of UGT76B1 and FMO1 degradation and induction. A. The roots of mTFP-UGT76B1 fluorescent lines were observed in response to *T. harzianum*. An agar plug with mycelium was placed directly next to the root, allowing newly emerged hyphae to reach the root immediately. The mTFP-UGT76B1 signal began to fade within 1 hour post-inoculation and was completely lost by 3 hours. In contrast, FMO1-YFP was induced and became visible after 18 hours. Bar, 30 µm. **B.** The Longitudinal section of a root from a 2-week-old plant grown in hydroponic culture, with 100 µM cycloheximide added to the medium to prevent protein synthesis. The mTFP-UGT76B1 signal remained strong in the root after 3 days of treatment. After 5 days, cell collapse began, though the mTFP signal was still visible, eventually fading away by day 10. Scale bar: 50 µm

Since *UGT76B1* acts as a negative regulator of NHP in leaves (Bauer *et al.*, 2021; Cai *et al.*, 2021; Holmes *et al.*, 2021; Mohnike *et al.*, 2021), the degradation of root *UGT76B1* upon microbial interaction results in an unregulated accumulation of NHP produced by induced *FMO1*. To illustrate the dynamics of *UGT76B1* and *FMO1* regulation under long-term *Ci* infection, expression patterns were monitored (Fig. 12). At two days post-inoculation, both the local and distal root regions exhibited degraded *UGT76B1* and induced *FMO1* in the pericycle (Fig. 12C, D), whereas plants in the same Petri dish without inoculation showed only *UGT76B1* degradation (Fig. 12A). By four days post-inoculation, *UGT76B1* expression was re-induced, though not in the original tissues, but in the stele. Meanwhile, *FMO1* was downregulated at the local infection site but remained expressed in distal areas where fungal hyphae had already spread (Fig. 12E, F). This observation suggests that *UGT76B1* is eventually re-induced to function as a negative regulator in the later stages of infection.

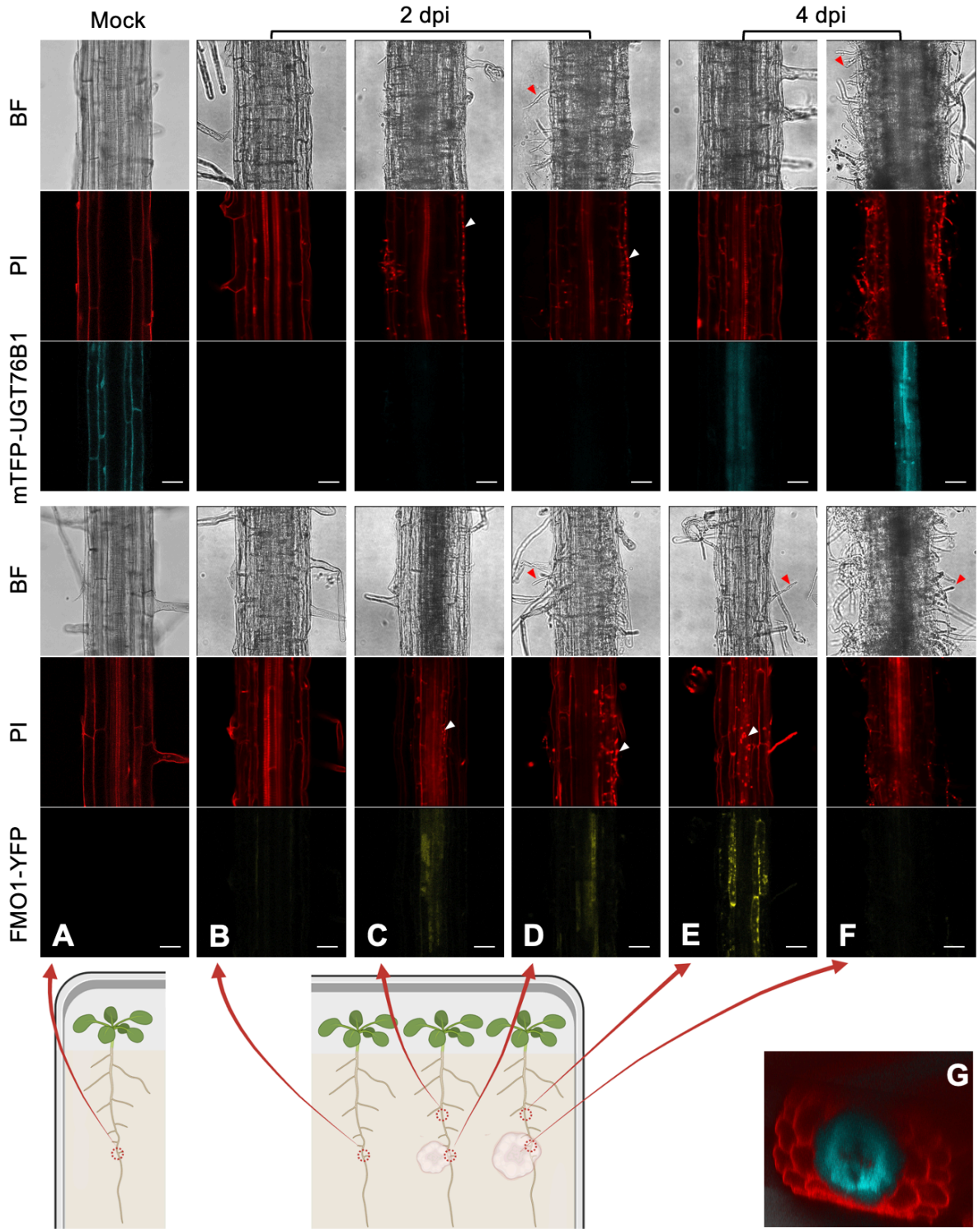

Fig. 12: Long-term infection of *C. incanum*. A, Mock-treated plants: mTFP-UGT76B1 is expressed in the cortex and endodermis, while FMO1-YFP is too weak to be detected. **B,** Plants grown on plates inoculated with Ci for 2 days show complete loss of mTFP-UGT76B1 expression, even without direct contact with the fungus. **C-D,** Roots at distal and local sites of inoculation, 2 days post-inoculation (dpi). White arrows indicate fungal nuclei stained by propidium iodide. Ci penetrates the root, inducing FMO1 expression in the pericycle while keeping UGT76B1 expression suppressed. **E-F,** Roots at distal and local sites of inoculation, 4 dpi. **G**, mTFP-UGT76B1 expression in the stele. UGT76B1 is induced in the stele, while FMO1 expression in the pericycle disappears in severely infected roots and appears in the cortex and endodermis at regions distal to the inoculation site.

2.1.6 Dosage effect of NHP on plant growth and defense

Since both endophytes and (hemi)biotrophs likely manipulate root NHP levels by modulating *FMO1* and *UGT76B1* expression, and given that the endophytes used in this study have been shown to promote plant growth while high endogenous NHP levels lead to growth retardation (Kleifeld and Chet, 1992; Sherameti *et al.*, 2005; Salas-Marina *et al.*, 2011; Mathys *et al.*, 2012; Bauer *et al.*, 2021; Cai *et al.*, 2021), it was hypothesized that NHP may have a dosage-dependent effect on plant growth and defense. Additionally, NHP feeding has been shown to have a dosage effect on shoot defense levels (Schnake *et al.*, 2020).

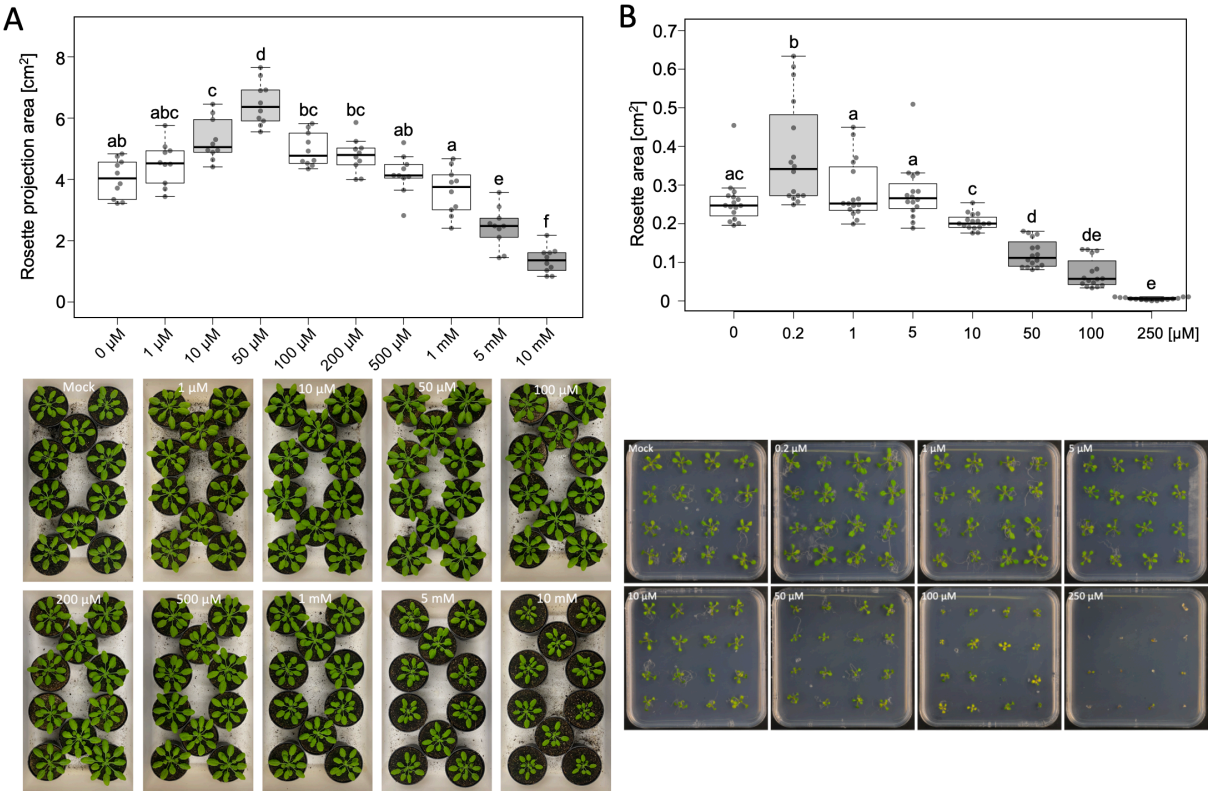

Fig. 13: Dosage dependent effect of NHP. A. Plants were cultivated in soil supplemented with varying concentrations of NHP, and rosette projection area was recorded three weeks post-treatment. The results indicate that low concentrations of NHP stimulate plant growth, whereas high concentrations inhibit it. Bars show means ± SD, *n* = 10. **B.** Plants were grown on half-strength MS plates supplemented with different concentrations of NHP. The rosette projection area was recorded for three-week-old plants. The results indicate that low concentrations of NHP stimulate plant growth, while high concentrations inhibit it, with 250 µM NHP being lethal. Bars represent means ± SD, n = 16. All leaf projection areas were measured using ImageJ.

To test this hypothesis, different concentrations of NHP were supplied to soil-grown plants. Low concentrations of NHP were observed to significantly promote plant growth, whereas high concentrations suppressed it (Fig. 13A). A similar trend was observed in plants grown on agar plates with an additional observation that 250 µM NHP is lethal (Fig. 13B).

To determine if endophyte-induced growth promotion depends on NHP, wild-type, *fmo1*, *ugt76b1*, and NahG *sid2* plants were inoculated with the PGPF *T. harzianum,* and their growth was monitored. After 16 days, wild-type plants exhibited a significantly larger rosette area compared to mock-treated controls, while no growth promotion was observed in *fmo1* and *ugt76b1* mutants. Interestingly, NahG *sid2* plants showed suppressed growth 10 days after *T. harzianum* inoculation, consistent with previous reports that endophytic *Trichoderma* species can become pathogenic in plants deficient in SA biosynthesis (Fig. 14).

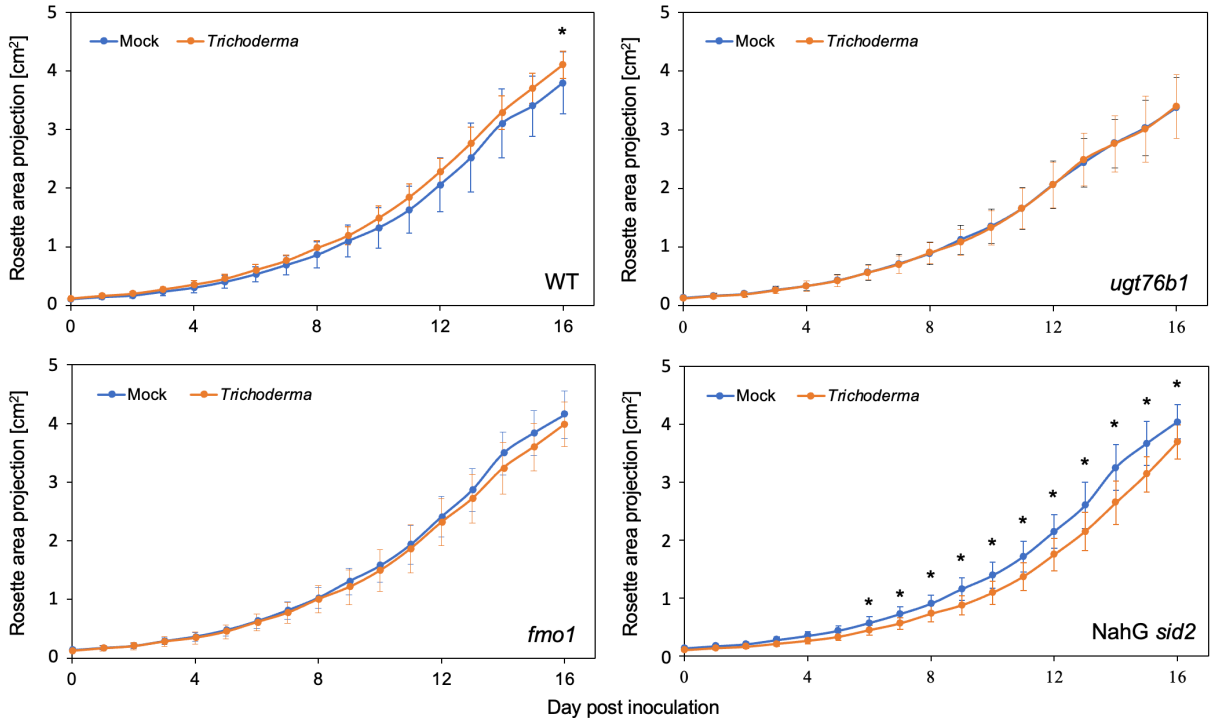

Fig. 14: Growth promotion by *T. harzianum* is NHP- and SA-dependent. One-week-old plants were inoculated with 5 mL of a solution containing 10^6 conidia per mL. Leaf projection area was determined based on regions with active chlorophyll fluorescence using the PSI system, measured daily at 6 a.m. Compared to mock treatment, inoculation with Trichoderma significantly enhanced growth in Col-0 plants, an effect not observed in the *fmo1* and *ugt76b1* mutants. In SA-depleted plants (NahG *sid2*), the growth response to *Trichoderma* inoculation was reduced. n = 20, error bars represent standard deviation. Differences between mock and *Trichoderma* inoculation in time point were analyzed by Welch two-sample t-test; *$P < 0.05$.

To evaluate the early response to root-associated microbes, one-week-old seedlings were inoculated with conidia from four different fungi, and their growth was monitored. One week post-inoculation, before the pathogens entered the necrotrophic phase and caused visible disease symptoms, *WT* plants inoculated with the pathogen *Fo5176* exhibited a significant reduction in growth. Inoculation with *Ci* also resulted in a numerically lower rosette area, whereas endophytic fungi *Ct* and *Fo47* did not affect growth. This growth reduction was diminished in *fmo1* plants, with only *Fo5176* inoculation showing a trend of slowed growth that was not significantly different from the mock treatment (Fig. 15A).

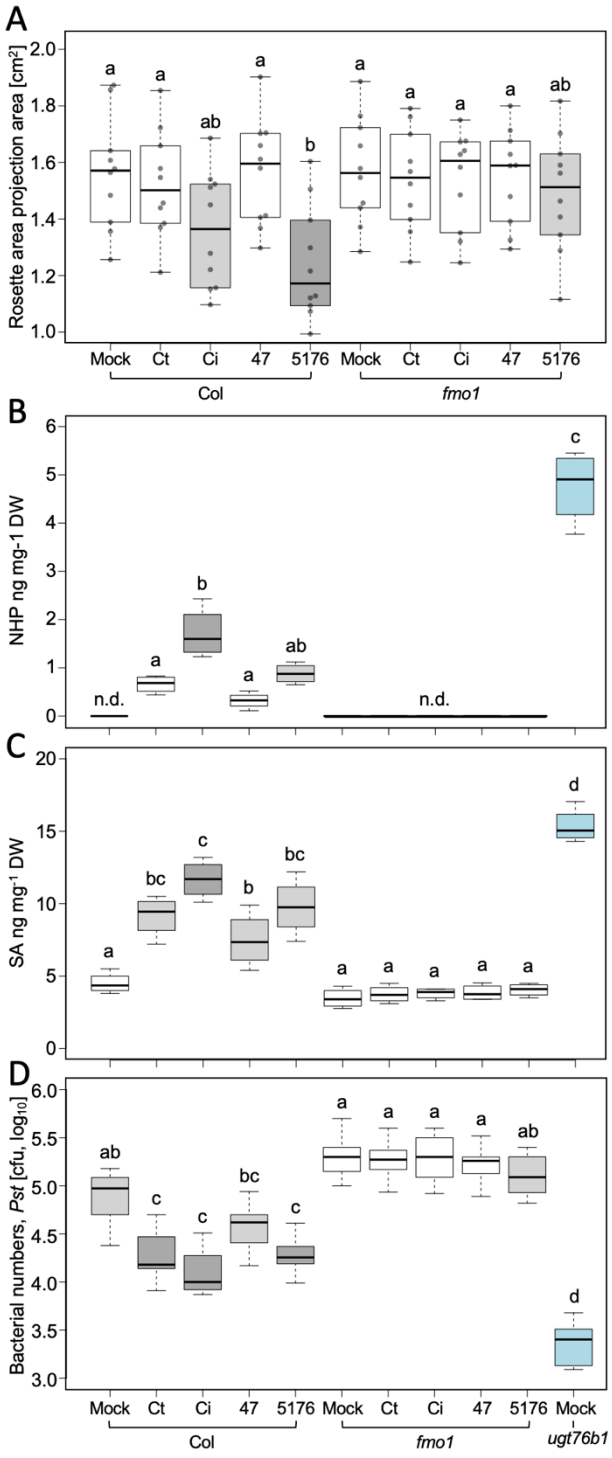

To confirm that NHP mediates root microbe-triggered defense, *WT* and *fmo1* plants were inoculated with *Ct*, *Ci*, *Fo47*, and *Fo5176*. Rosettes were harvested for metabolic analysis three days post-inoculation. NHP was detected in *WT* shoots following root inoculation with fungi but was undetectable in mock-treated and *fmo1* plants (Fig. 15B). Similarly, endogenous SA levels were elevated only in *WT* plants inoculated with all four fungi (Fig. 15C). Following *Pst* infection after fungal inoculation, *WT* plants exhibited enhanced resistance, which was abolished in *fmo1*, consistent with previously described SAR deficiency (Mishina and Zeier, 2006; Bauer *et al.*, 2021) (Fig. 15D). In summary, certain root endophytes trigger shoot immunity and promote growth via NHP, whereas (hemi)biotrophs may lead to elevated NHP levels, stronger immunity, and stunted growth.

Fig. 15: Fungal inoculation effects on immunity mediated by NHP. A. One-week-old plants subjected to fungal inoculations display differential growth responses; rosette projection area at day 7 post-inoculation is shown. Col exhibits suppressed growth when inoculated with pathogenic fungi, whereas *fmo1* is not responsive to fungal inoculation. Means ± SD, $n = 10$; **B-D,** 4-week-old Col and *fmo1* plant inoculated 4 different fungi in the root (see methods), *ugt76b1* is used as reference. The shoot of plants was harvested for analysis. **B**, Col inoculated with different fungi leads to accumulated NHP level, which is not detectable in mock-treated Col and *fmo1* plants; *ugt76b1* shows a very high level of NHP. **C**, root inoculation triggered SA accumulation is only found in Col but not *fmo1*. **D.** 4 day-post-inoculation, plant challenged with *Pst* DC3000. Col plant inoculated with Ci exhibits stronger resistance compared to mock; inoculation of the other three fungi also leads to stronger resistance numerically, while such induction is abolished in *fmo1* plants. Bars show means ± SD, $n = 4$. Significant differences between genotypes were analyzed by two-way ANOVA with posthoc Lincon test as indicated by letters (*P.adj.* < 0.05).

To confirm that NHP mediates root microbe-triggered defense, *WT* and *fmo1* plants were inoculated with *Ct*, *Ci*, *Fo47*, and *Fo5176*. Rosettes were harvested for metabolic analysis three days post-inoculation. NHP was detected in *WT* shoots following root inoculation with fungi but was undetectable in mock-treated and *fmo1* plants (Fig. 15B). Similarly, endogenous SA levels were elevated only in *WT* plants inoculated with all four fungi (Fig. 15C). Following *Pst* infection after fungal inoculation, *WT* plants exhibited enhanced resistance, which was abolished in *fmo1*, consistent with previously described SAR deficiency (Mishina and Zeier, 2006; Bauer *et al.*, 2021; Fig. 15D). In summary, certain root endophytes trigger shoot immunity and promote growth via NHP, whereas (hemi)biotrophs may lead to elevated NHP levels, stronger immunity, and stunted growth.

2.2 The physiological role of SA-GT in *Arabidopsis*

2.2.1 Background

This project was initiated by Wei Zhang and Sibylle Bauer, who developed the full set of combinatorial mutants for the three SA-GTs. Sibylle Bauer and Elisabeth Georgii carried out RNA sequencing and metabolic profiling of SA-related metabolites to explore the expression and interactions among these SA-GTs. The RNA-seq data (Bauer, 2020) serve as the foundation for the expression analyses and interaction studies of the three SA-GTs in this thesis. Under non-stressed conditions, the *ugt74f1*, *ugt74f2*, and *ugt74f1 ugt74f2* mutants displayed SA levels comparable to those of the wild type. In contrast, all mutants containing the *ugt76b1* allele exhibited significantly elevated SA levels, highlighting a distinct and crucial role for UGT76B1 in moderating free SA accumulation. UGT74F2 appears to mitigate SA accumulation when UGT76B1 is absent, as *ugt76b1 ugt74f2* and *ugt76b1 ugt74f1 ugt74f2* mutants showed markedly higher SA levels than the *ugt76b1* single mutant (Fig. 16).

In terms of glucosylated SA derivatives, the highest SAG levels relative to both the wild type and other mutants were observed in *ugt76b1* and *ugt76b1 ugt74f2*. Conversely, SGE levels were significantly elevated in the *ugt76b1* and *ugt76b1 ugt74f1* mutants. Enhanced SAG and SGE production were evident only in the absence of UGT76B1, with SAG formation relying on UGT74F1 and SGE formation depending exclusively on UGT74F2 (Fig. 16).

In summary, these three SA-GTs serve as the primary glucosyltransferases for SA in *Arabidopsis*, as the triple mutant no longer accumulated any SA glucosides. Notably, UGT74F2 is the sole enzyme capable of producing SGE (Bauer, 2020).

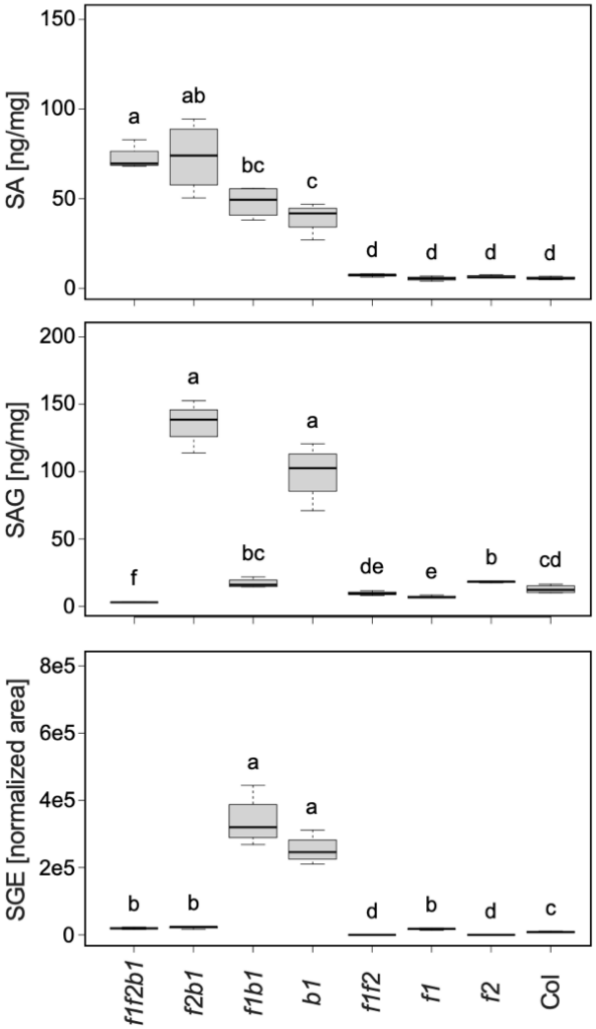

Fig. 16: SA, SAG, and SGE content of *ugt* mutants (Bauer, 2020; Fig. 10). Quantification is based on LC-MS measurement. Plants were cultivated under short-day conditions for 15 days. Distinct lettering indicates groups with significant differences, as determined by an ANOVA with Tukey's posthoc test ($p<0.05$). The normality was confirmed using the Shapiro-Wilk test. Groups differentiated by unique letters exhibit significant

2.2.2 Spatial expression patterns of SA glucosyltransferases

The three SA glucosyltransferases' spatial expression patterns and regulation will be decisive for their function. To investigate this, transgenic lines harboring UGT promoter GFP-GUS reporter fusions were analyzed. *UGT74F1* was predominantly expressed in roots and in leaf vascular tissue, whereas *UGT74F2* was localized in roots and patchy but uniformly in rosette leaves. *UGT76B1* was expressed in cotyledons, weakly and in a patchy manner in leaves, yet enhanced in roots and at the root tips (Fig. 17D-F; von Saint Paul *et al.*, 2011). The ePlant database (Waese *et al.*, 2017) corroborates the root expression of all three UGTs, with UGT76B1 displaying a much more pronounced root expression than UGT74F1. Importantly, the GUS expression patterns of both UGT74F1 and UGT74F2 did not strongly change when the reporter lines were introgressed into the respective other single mutant backgrounds, and only UGT76B1 is in the rosette of *ugt74f1* and *ugt74f2* mutant backgrounds (Fig. S4). The induction of UGT76B1 possibly compensates for the absence of the other two enzymes regarding SA glucosylation.

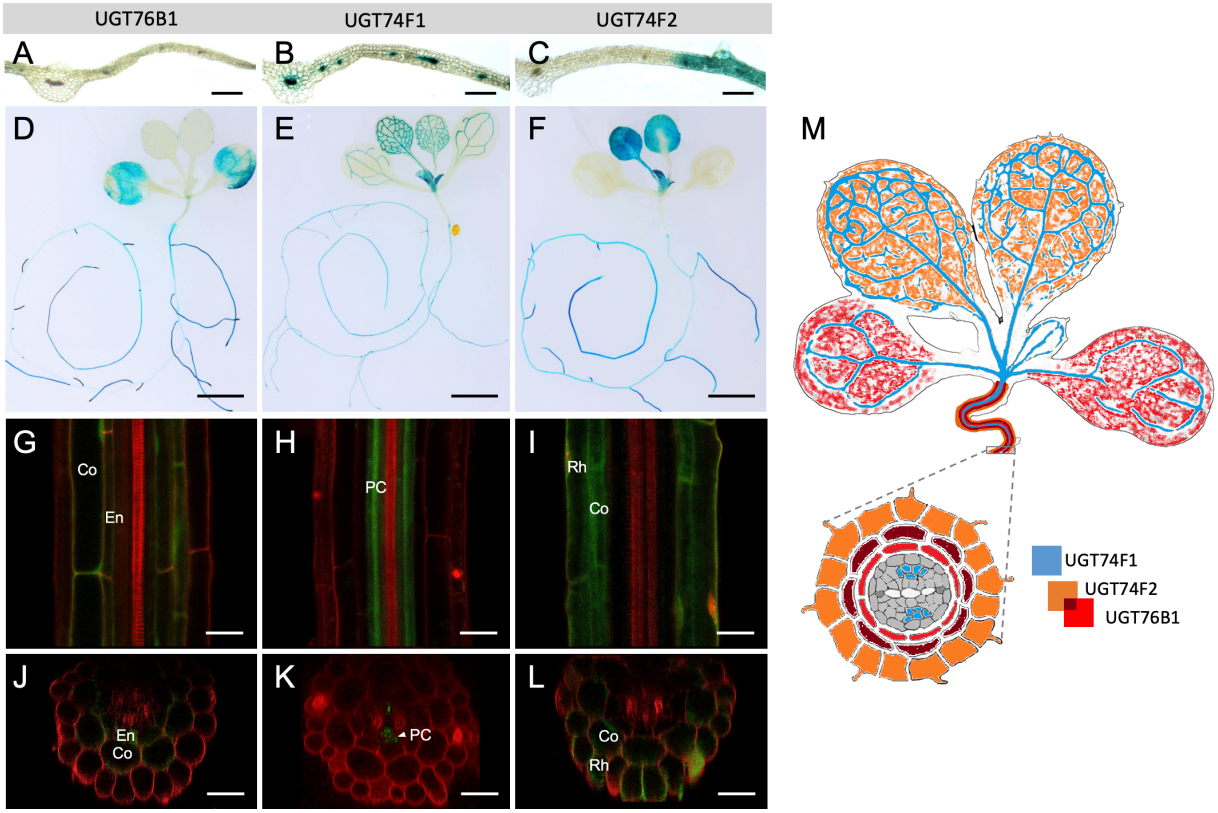

Fig. 17: Localization of the expression of the SA glucosyltransferases using transgenic promoter:GFP-GUS lines. From left to right, the three columns represent *UGT76B1*, *UGT74F1*, and *UGT74F2*. (A-C) Cross-sections of true leaves. Scale bars: 500 µm. (provided by Burkhard Messner and Anton Schäffner) (D-F) Overview of GUS staining patterns. Scale bars: 2 mm. (G-I) Longitudinal sections of roots, showing Co (cortex), En (endodermis), PC (phloem cells), and Rh (rhizodermis). Scale bars: 50 µm. (J-L) Cross-sections of roots. Scale bars: 500 µm. All samples were derived from two-week-old plants grown on ½ MS plates. For GUS staining, plants

were vacuum infiltrated in GUS staining solution for 10 minutes and then incubated at 37°C (*UGT76B1* for 30 min, *UGT74F1* for 120 min, *UGT74F2* for 60 min). (M) Illustration depicting the spatial expression patterns of the three SA glucosyltransferases throughout the plant.

For a detailed view of the expression in roots, the GFP reporter was monitored by confocal microscopy. Matching the ePlant root single-cell database (Ryu *et al.*, 2019), UGT74F1 was confined to proto/meta-phloem cells and phloem companion cells, UGT74F2 was found in both epidermis and cortex cells, and UGT76B1 was mainly present in the cortex and endodermis (Fig. 17A-C; G-L; von Saint Paul *et al.*, 2011). Together, three SA-GTs additively cover the whole rosette and root (Fig. 17M).

2.2.3 Biological processes affected by single and combined *ugt* mutations

Previously, RNA sequencing was conducted on *ugt* mutants grown under unstressed conditions, and gene expression profiling as well as functional enrichment analyses were performed by former colleagues (Bauer, 2020). In this study, additional bioinformatic analyses were carried out to further investigate the specific regulatory mechanisms associated with distinct gene categories.

To differentiate and relate the enriched GO terms to specific biological processes, topical clusters addressing response to *hormones, biological stimuli, abiotic stimuli,* and *physiological responses* were combined (Fig. 18; 19). Using the expression levels of wild type as a baseline, the *ugt74f2* single mutant did not exhibit significant gene regulation revealing specific effects of the loss of UGT74F2 (Fig. 19). Similarly, further specific impacts of the loss of UGT74F1 and UGT76B1 may remain obscured. To address more subtle roles and interactions among the three SA glucosyltransferases, a multi-way comparison was employed. The concurrent absence of SA glucosyltransferases markedly altered gene expression profiles compared to single mutant backgrounds, with additional (gain) or abrogated (loss) deregulated genes surpassing the aggregate of individual impacts (Fig. 18).

The combined absence of UGT74F1 and UGT74F2 resulted in complex expression patterns of the genes related to the selected GO terms, often displaying concurrent up- and downregulation, suggesting a dynamic interplay when both genes are missing. *ugt74f2* introgression attenuated many hormone-responsive genes upregulated in *ugt74f1* (Fig. 18; 19). This was concomitant with the attenuation of biotic stress-responsive genes involved in *response to fungi, bacteria,* and *oomycetes*, as well as various abiotic stress-related genes, including *responses to water deprivation, to salt* or *to osmotic, hypoxic,* and *oxidative stresses*. In contrast, genes implicated in *temperature responses* were significantly regulated by combining *ugt74f1* and *ugt74f2*, with pronounced upregulation of genes associated with heat

and cold acclimation. Furthermore, altered transcription of genes associated with *circadian rhythm* and *light response* was strongly promoted by the loss of either *UGT74F1* or *UGT74F2* in the *ugt76b1* background (Fig. 18; 19).

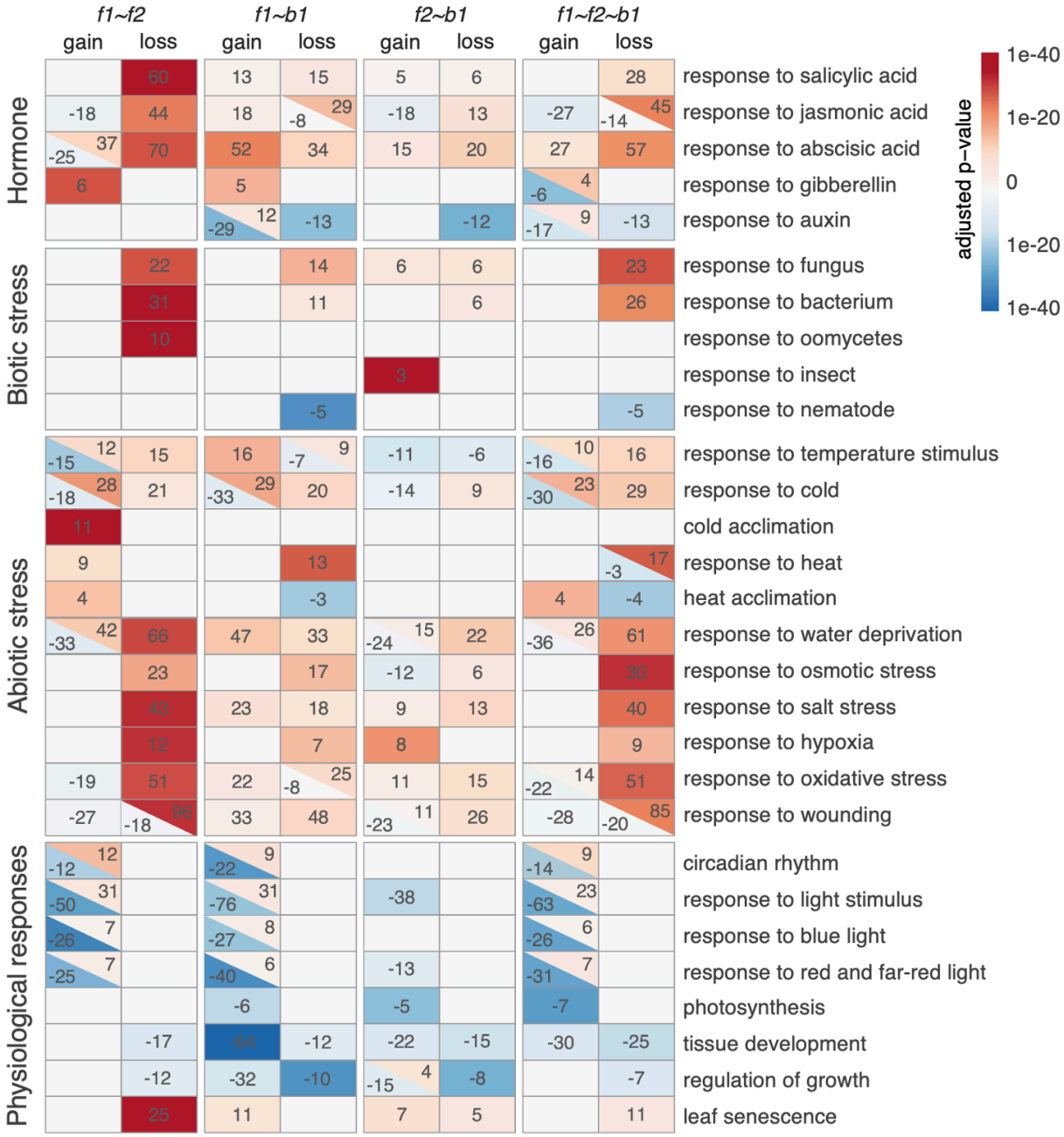

Fig. 18: The interplay of the SA glucosyltransferase mutations through functional annotation based on multi-way comparison in relation to the changes observed for single *ugt* mutants. The heatmap depicts functionally categorized GO terms. The upper section designates the interaction of mutations, *gain* and *loss* indicate the additional gain or loss of gene regulation compared to the changes attributed to respective single mutants. Color gradients, ranging from red to blue, indicate the p-value of the GO assignment of up- and downregulated genes, respectively, with intensifying shades indicating a lowered adjusted p-value. Only genes with an adjusted p-value less than 0.05 and an absolute log_2-fold change exceeding 1 are considered.

Genes related to response to SA, to JA, and to ABA were significantly modulated in mutants including *ugt74f1* or *ugt76b1*, with a consistently stronger impact of *ugt76b1* (Fig. 19). The *ugt74f1* and *ugt76b1* interaction revealed simultaneous loss of and gain in deregulated genes responsive to SA, JA, auxin, and ABA, suggesting specific adjustments in the respective signaling pathways. However, this was not reflected for genes related to *biotic stimuli* (Fig. 18). In terms of abiotic stress responses, the individual loss of UGT76B1 or UGT74F1 triggered a robust regulation of genes responding to *temperature changes,* to *water deprivation,* to *osmotic stress,* to *salt stress,* to *oxidative stress,* and to *wounding*. The simultaneous loss of both genes had an additive influence on these GO categories (Fig. 19), which included a significant reprogramming of gene expression, aligning with the hormonal response alterations (Fig. 18). Moreover, *ugt74f1 ugt76b1* exhibited a substantial shift in genes linked to *physiological responses*, which remained unaltered in the single mutants and additional downregulation of *photosynthesis, tissue development,* and *growth regulation,* and upregulation of *leaf senescence*. Finally, the expression profile of the ultimate, triple mutant, i.e., introgression *ugt74f2* to *ugt74f1 ugt76b1* vastly reflects the changes of *ugt74f1 ugt76b1* with a weaker, ameliorating effect of the *ugt742* introgression (Fig. 19).

The gene expression changes induced by *ugt74f2 ugt76b1* and *ugt76b1* were similar as well, again denoting a minor influence of UGT74F2 (Fig. 19). Nevertheless, *ugt74f2 ugt76b1* led to the gain and loss of deregulated genes among all four topical categories suggesting specific interactions dependent on the combined loss of both genes (Fig. 18).

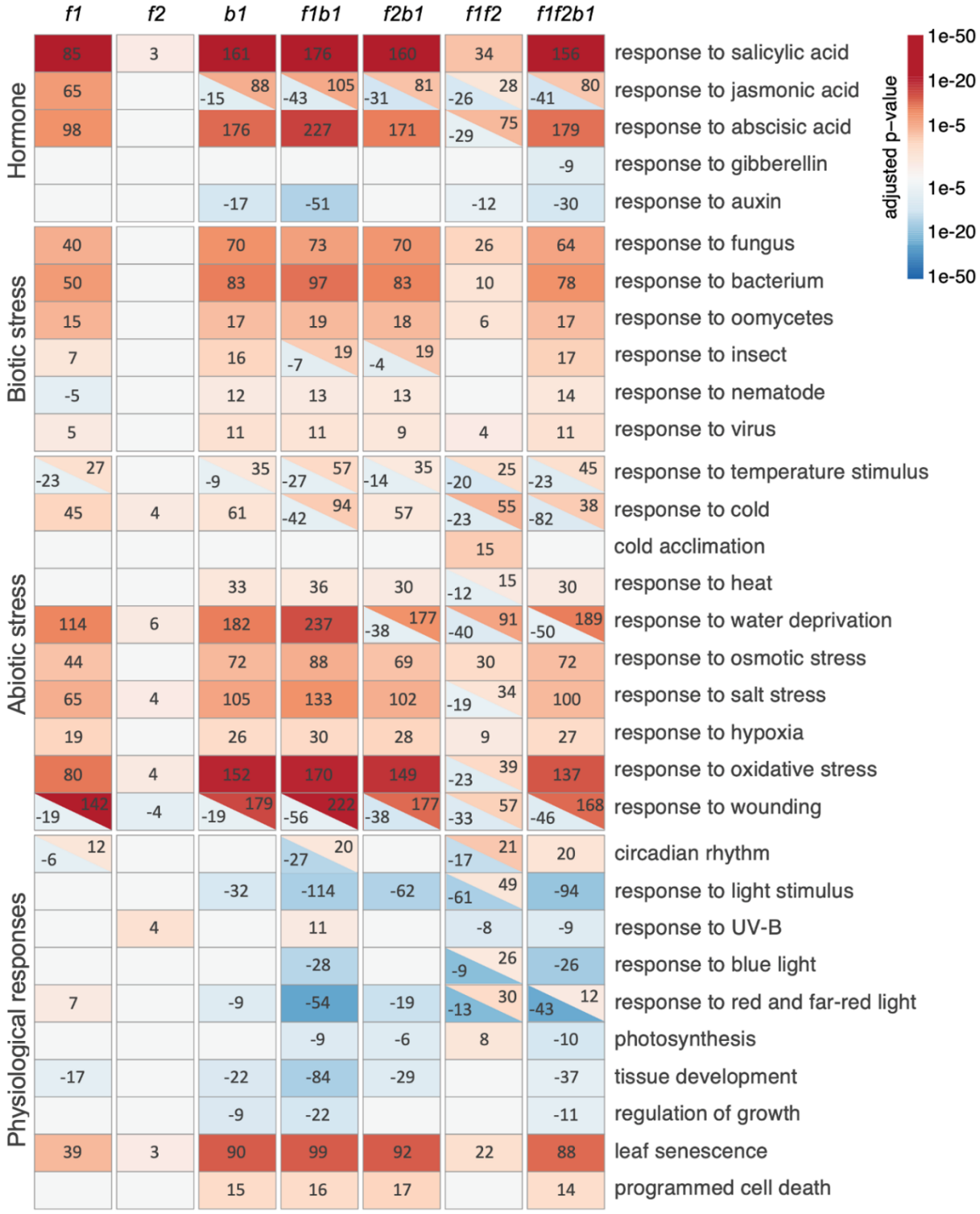

Fig. 19: Detailed heatmap of GO terms for targeted biological processes. Blue blocks indicate downregulation, whereas red blocks signify upregulation. The numbers within each block denote the count of regulated genes corresponding to the particular GO term. The intensity of the color codes correlates inversely with the p-value, i.e., deeper shades indicate more significant changes. Blocks split by a diagonal line represent instances where both upregulation and downregulation occur within the same GO terms, reflecting the complex nature of the regulatory mechanisms at play.

2.2.4 UGT74F1 and UGT74F2 are not involved in disease resistance

Enhanced endogenous SA plays a pivotal role in boosting plant immunity. The loss of UGT76B1 leads to an accumulation of SA concomitant with an enhanced resistance against *Pst* DC3000 and early senescence (von Saint Paul *et al.*, 2011). However, mutants harboring UGT76B1 do not significantly raise unconjugated SA, irrespective of whether UGT74F1 and UGT74F2 are absent individually or in tandem (Fig. 16).

Mutants containing the *ugt76b1* allele induced SA- and defense-related gene expression, including *PR* genes and regulatory factors *NPR1*, *PAD4*, *EDS1*, and *WRKY70*. Conversely, the expression of *PDF1.2* indicative of jasmonic acid and ethylene signaling was downregulated in these mutants. In contrast, there was no significant variation in the expression of SA marker genes by the *ugt74f1*, *ugt74f2*, and *ugt74f1 ugt74f2* mutants (Fig. 20A). We then explored whether these differences were also reflected in response to bacterial infection. All genotypes including the *ugt76b1* allele exhibited a similarly enhanced resistance against *Pst* infection compared to wild type, *i.e.*, introducing mutations of *UGT74F1* and *UGT74F2* to *ugt76b1* did not intensify its resistance. Single or combined loss of *UGT74F1* and *UGT74F2* did not affect the susceptibility towards *Pst* either (Fig. 20B).

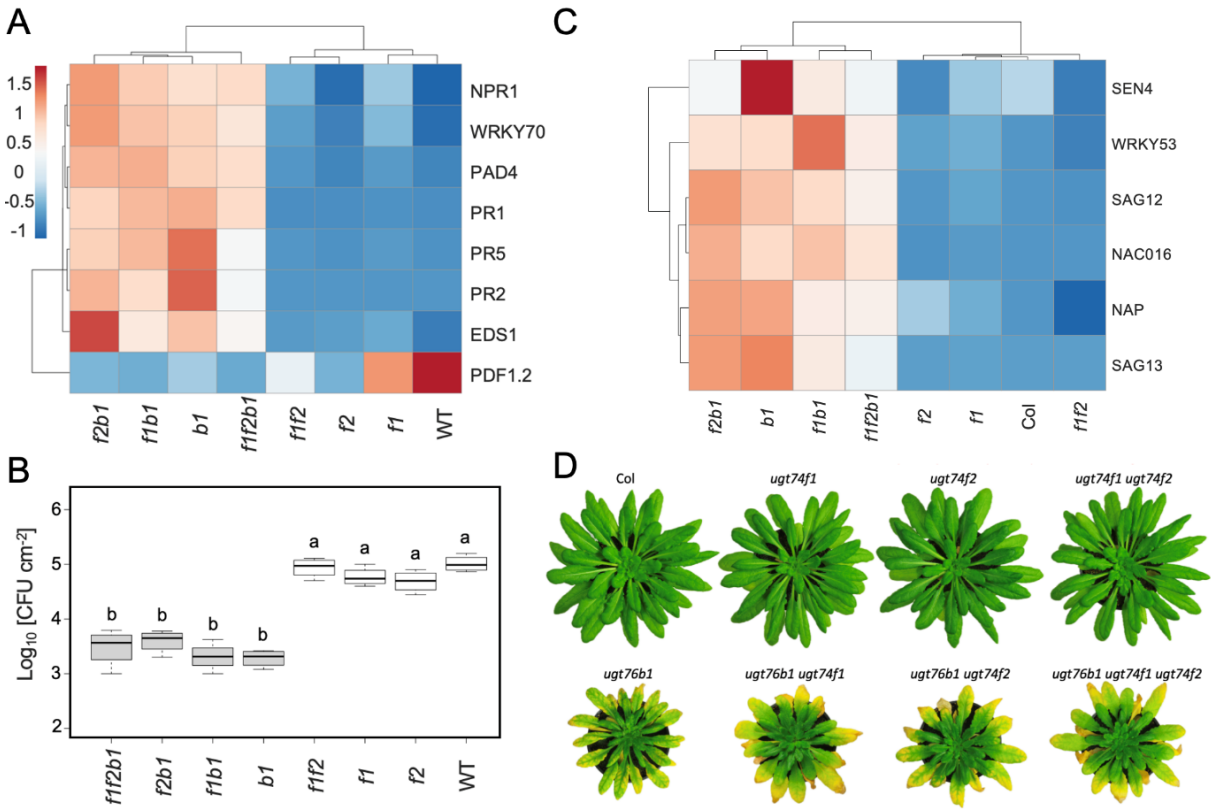

Fig. 20: UGT74F1 and UGT74F2 do not impact senescence and resistance to *Pst*. **A.** SA signaling marker genes *PR1/2/5, NPR1, PAD4, EDS1* and JA signaling marker gene *PDF1.2*, the color of each block represents the log_2-fold difference compared to means value of all eight genotypes. **B.** Bacterial counts of all eight genotypes two

days after infection with *Pst*. Means ± SE from four independent experiments; different letters denote significant group differences as determined by one-way ANOVA followed by Tukey's posthoc tests (p<0.05). **C.** Analysis of senescence-associated marker genes from RNA-seq data reveals a dichotomy among the eight genotypes tested, with one cluster comprising those with an active UGT76B1 and another without UGT76B1. Mutants lacking functional UGT76B1 exhibited increased expression of senescence markers. The further removal of either UGT74F1 or UGT74F2 did not enhance this upregulation. **D.** Visual comparison of 7-week-old plants highlights those mutants deficient in UGT76B1 exhibited retarded growth with yellowing at the leaf margins, symptomatic of accelerated senescence. In contrast, *ugt74f1*, *ugt74f2*, and the double mutant *ugt74f1 ugt74f2* grew like Col, showing no signs of senescence.

Besides, double and triple mutants carrying the *ugt76b1* allele exhibit an early senescence phenotype, as previously described for the ugt76b1 mutant (Fig. 20D; von Saint Paul *et al.*, 2011). In contrast, plants lacking UGT74F1 and/or UGT74F2 display rosette morphology similar to that of wild-type plants, which is consistent with the expression of senescence marker genes. Specifically, the levels of *SEN4*, *WRKY53*, *SAG12*, *SAG13*, *NAP*, and *NAC016* are higher in mutants containing the *ugt76b1* allele (Fig. 20C).

2.2.5 UGT76B1 cannot be substituted by the second SAG-forming enzyme UGT74F1

UGT74F1 and UGT76B1 overlap in their ability to conjugate SA to SAG (Noutoshi *et al.*, 2012). However, they have distinct impacts on defense against bacterial pathogens, which are attributed to their differential spatial expression patterns and enzymatic properties (Fig. 17; 20B). Bauer (2020) demonstrated that the coding sequence of *UGT74F1* could not complement the *ugt76b1* mutant when placed under the control of the 5' and 3' regulatory regions of *UGT76B1*.

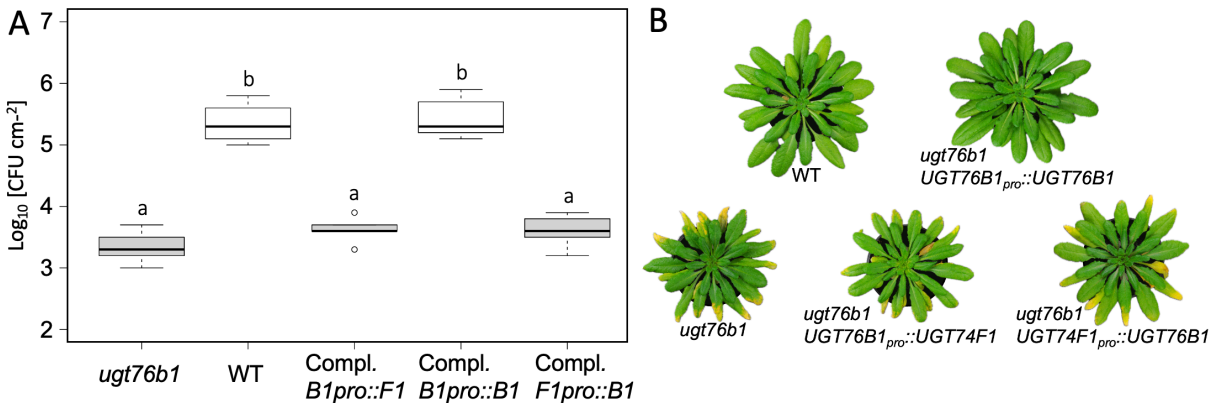

Fig. 21: UGT76B1 cannot be substituted by UGT76B1. A. Bacterial counts in different complementation lines of *ugt76b1* two days post-infection with *Pst*. **B**. early senescence phenotype of ugt76b1 and different complementation lines. Means ± SE from four independent experiments; different letters denote significant group differences as determined by one-way ANOVA followed by Tukey's posthoc tests (p<0.05).

In this study, another hybrid gene construct was generated, in which the *UGT76B1* coding sequence was driven by the 5' and 3' regulatory regions of *UGT74F1* (Methods). Both hybrid constructs failed to rescue the defense phenotype of the *ugt76b1* mutant (Fig. 21A). Additionally, the senescence phenotype observed in *ugt76b1* was not complemented by either construct. In contrast, reintroducing the full-length *UGT76B1* gene, including its native regulatory regions, restored the wild-type phenotypes (Fig. 21B).

2.2.6 Impact of SA levels on plant growth and drought tolerance

SA is also involved in response to abiotic stress scenarios. To study the interplay between SA and its glucosyltransferases under drought we compared the growth of the complete mutant set under progressively reduced water availability to well-watered controls. Growth rates deduced from rosette sizes and photosynthetic parameters were monitored over a period of 40 days. Finally, rosettes were harvested to analyze SA metabolites. Under well-watered conditions, wild type, *ugt74f1*, *ugt74f2*, and the combined *ugt74f1 ugt74f2* mutant grouped according to similar rosette size and SA content. However, mutants harboring *ugt76b1* showed diminished leaf sizes but enhanced SA levels (Fig. 22), as previously observed for the single mutant *ugt76b1* (Bauer *et al.*, 2021; Cai *et al.*, 2021). Thus, *UGT76B1*-dependent SA levels and plant growth are inversely related under control conditions.

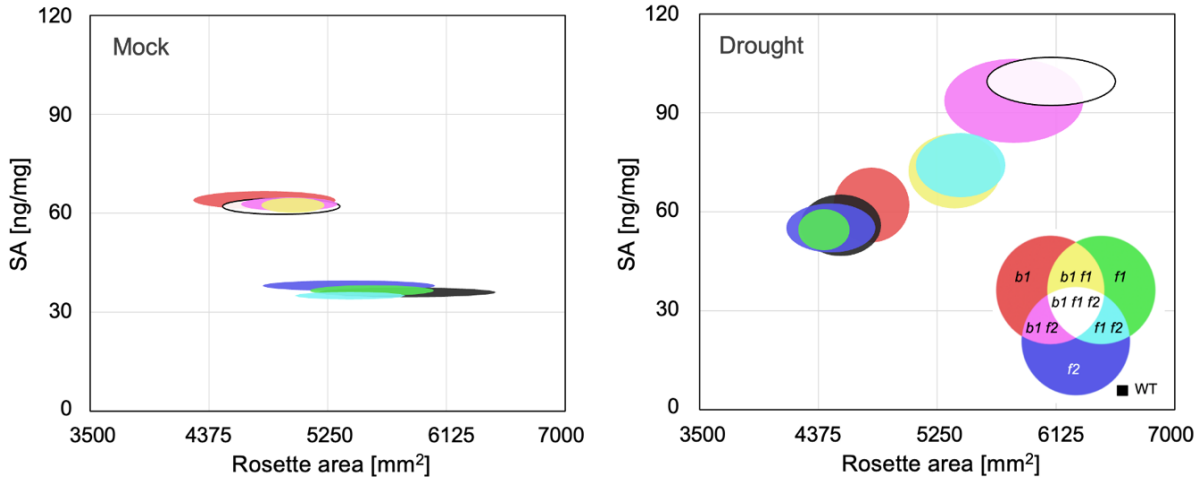

Fig. 22: Distinct correlation between free SA level and rosette projection area under control and drought conditions. The width of ovals represents the mean value ± standard deviation of the rosette area of 15 plants. Three plants each were bulked for metabolic analysis. The height of the ovals represents the mean value ± standard deviation of the free SA level. The color codes represent different mutants.

Progressive drought led to a general decline in rosette size across all genotypes (Fig. 22; 23A, B). The *ugt* mutants provided a series of plants exhibiting increasingly higher free SA levels. In contrast to well-watered conditions, the SA content positively correlated with rosette sizes, *i.e.*, with resilience towards progressive drought. In addition, the three SA glucosyltransferases' impact on SA levels differed from control conditions. All single *ugt*

mutants and the wild type had similar, relatively low SA levels (Fig. 22). Thus, *UGT76B1* lost its dominant role in suppressing free SA. Instead, *UGT74F1* and *UGT74F2* gained a more crucial role. A key finding was the pronounced increase in SA levels and, thus, drought resistance, when *UGT74F2* was missing along with *UGT76B1* (Fig. 22). This indicates a synergistic role of the two genes in SA glucosylation and a negative impact during drought, with the additional removal of *UGT74F1* yielding only a slight further benefit.

Thus, the adverse effect of SA on growth under regular, well-watered conditions is reverted to a beneficial factor upon drought. In parallel, the contribution of the SA glucosyltransferase triad is changed. While *UGT74F1* and *UGT74F2* do not impact SA levels in control conditions, in particular, *UGT74F2* exhibits a major, suppressive role in attenuating free SA during drought in contrast to its non-responsive role during biotic stress.

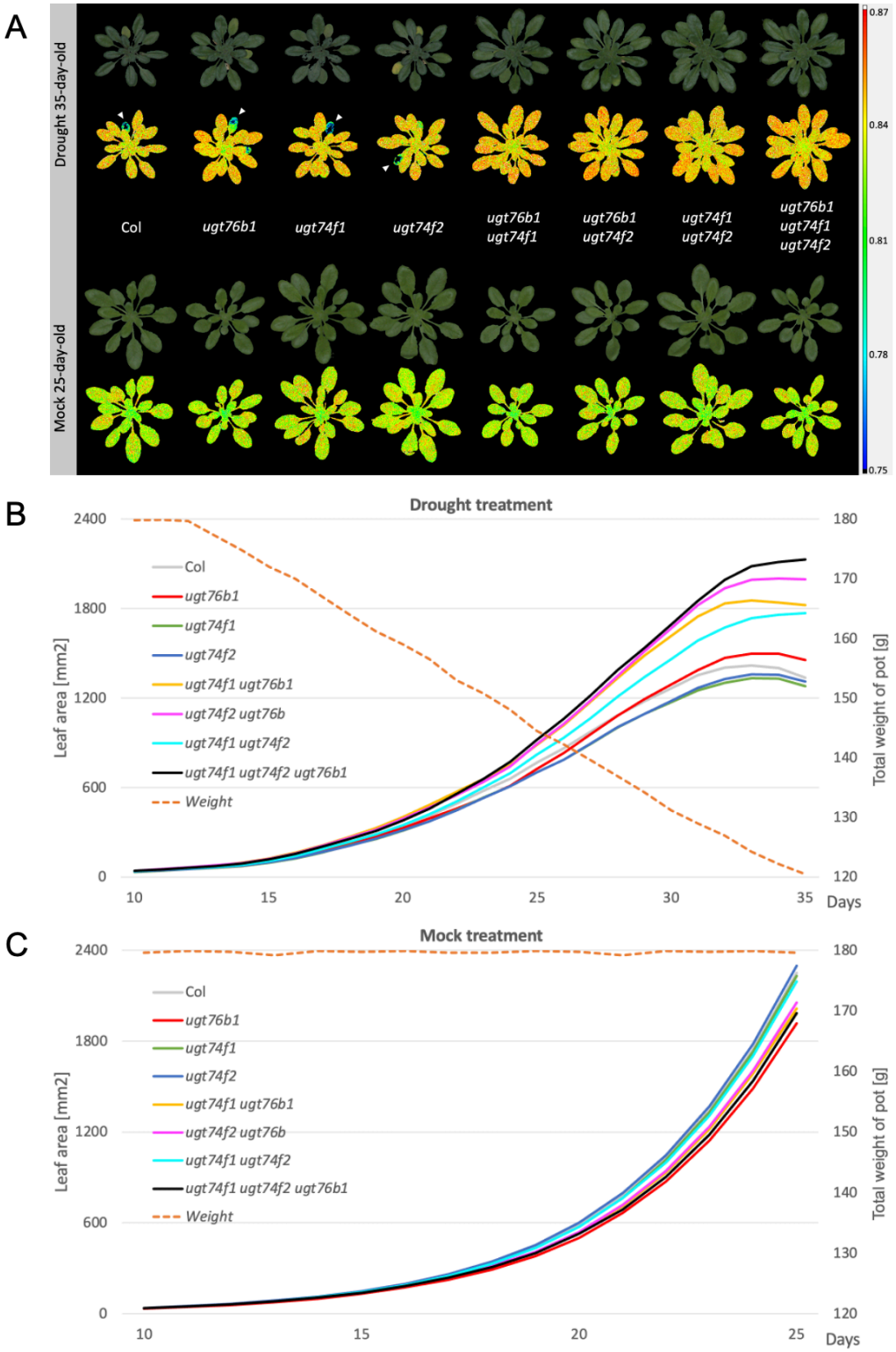

Fig. 23: Variable drought tolerance of *ugt* mutants. A. Under severe water scarcity, Col and single mutants exhibited stunted growth with leaves beginning to yellow and to decline in photosynthetic capacity. In contrast, double and triple mutants maintained a significantly rosette leaf area. **B.** With ongoing water depletion, Col and single mutants ceased growth indicated by reduced growth of the rosette area, whereas double and triple mutants continued to expand their leaves, even under conditions of critically low soil moisture. **C.** In the absence of stress (mock condition), mutants carrying the *ugt76b1* loss-of-function allele demonstrated reduced leaf size compared to their counterparts.

2.2.7 Comprehensive abiotic phenotyping of *ugt* mutants

Apart from the role of UGT74F2 in drought response, the transcriptome analyses of the *ugt* mutant series suggested further links of SA glucosylation to abiotic stress responses, in line with the role of SA in such scenarios. Therefore, the impact of the SA glucosyltransferases on abiotic stress responses was further addressed. The relative expression level of curated lists of stress-specific marker genes specific for salt stress, osmotic stress, and cold was deduced from the transcriptome analyses of wild type and all seven *ugt* mutants to predict differential responses (Fig. 24-26).

Transcript levels of genes involved in salt stress resilience, *SALT OVERLY SENSITIVE (SOS) 1*, encoding a plasma membrane Na^+/H^+ antiporter, and *SOS2* increased upon loss of *UGT76B1* (Fig. 24A). *UGT74F2* deletion on its own led to a robust induction of *NHX1* encoding the vacuolar Na^+/H^+ ANTIPORTER 1; however, this induction was suppressed with the concurrent absence of *UGT74F1* or *UGT76B1*. Conversely, *FERONIA (FER)*, encoding a receptor-like kinase, is downregulated when *UGT74F2* is missing, whereas the loss of *UGT76B1* and *UGT74F1* leads to a cumulative upregulation. About one-third of the wild-type plants survived when plants were subjected to a 100 mM NaCl regime in hydroponic culture for two weeks. Depletion of any SA glucosyltransferase leads to enhanced survival rates, however, combined mutations further improved resistance. After three weeks with NaCl, only double mutants and the triple mutant initiated bolting, with *ugt74f1 ugt74f2* demonstrating the lowest flowering propensity (Fig. 24B).

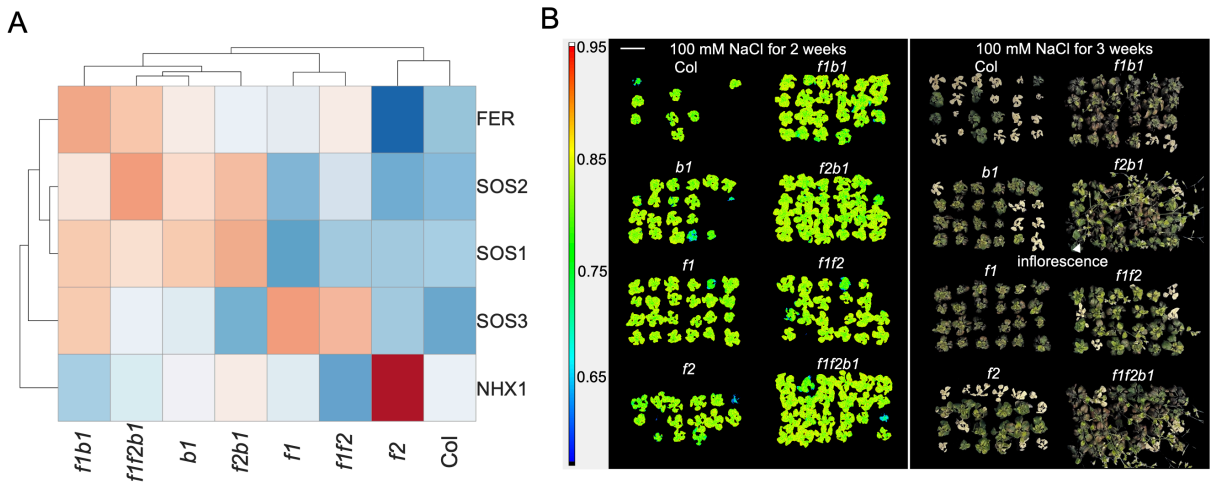

Fig. 24: Salt tolerance and marker gene expression in *ugt* mutants. A. Expression pattern of salt stress marker genes *SOS1/2/3*, *FER,* and *NHX1*. The color of each block represents the log_2-fold difference compared to mean expression value of all eight genotypes. **B.** Hydroponically grown plants treated with 100 mM NaCl. Salt stress was applied to seven-day-old seedlings, the images (left panel) were taken one week later using a fluorescent photo station, the color code depicts the maximum quantum yield (Fv/Fm). The images (right panel) were taken two weeks after the shift to salt stress by an RGB top camera. The numbers represent the Fv/Fm value.

ABA-dependent genes *ABRE BINDING FACTORS (ABF) 1/2/3/4* and ABA-independent markers genes *DEHYDRATION RESPONSIVE ELEMENT-BINDING (DREB) 1a/2a* exhibited a differential expression pattern among *ugt* mutants (Fig. 25A). Single loss of *UGT76B1* or *UGT74F1* caused subtle shifts of the transcript levels of these markers, with both mutants displaying survival rates like wild type under osmotic challenge. Interestingly, the absence of *UGT74F2* led to enhanced expression of *ABF2* and *ABF3*. This correlated with increased survival rates of *ugt74f2* compared to other single mutants under osmotic stress (Fig. 25B). Combined deletion of *UGT76B1* and *UGT74F1* led to upregulation of *ABF1/4* and *DREB2a*, and to augmented growth during osmotic stress. Remarkably, *ugt74f1 ugt74f2* plants were the most robust under these conditions, paralleled by the unique upregulation of *DREB1a*.

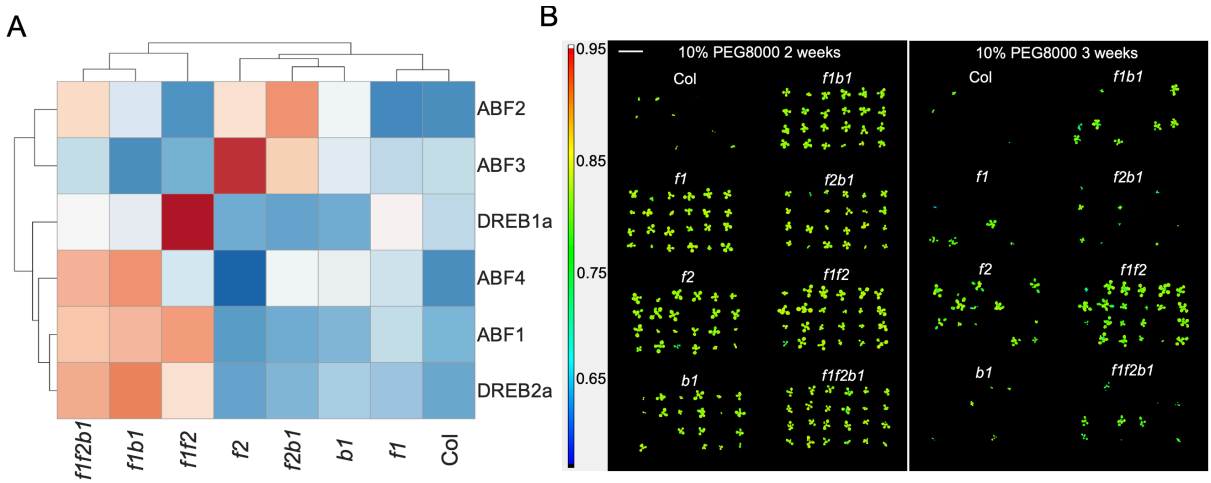

Fig. 25: Osmotic stress tolerance and marker gene expression in *ugt* mutants. A. Expression pattern of osmotic stress marker genes *ABF1/2/3/4*, *DREB1a/2a*. The color of each block represents the $\log_2$-fold difference compared to mean expression value of all eight genotypes. **B.** One-week-old hydroponically grown plants were treated with 10% PEG8000, fluorescent images were taken two and three weeks after PEG8000 application. Bars, 2 cm. The numbers represent the Fv/Fm value.

C-REPEAT/DRE BINDING FACTOR (CBF) 1/2/3, *INDUCER OF CBF EXPRESSION (ICE) 1/2*, and *COLD-RESPONSIVE (COR) 15A* were chosen as markers for cold stress. Slower greening, a beneficial trait offering protection against cold stress, was measured using maximum quantum yield (Fv/Fm) and correlated with greening of seedlings germinating at 4 °C (Fig. 26B). *ugt74f2 ugt76b1* was the most cold-sensitive genotype next to the *ugt74f2* and *ugt76b1* single mutants. This correlated with a unique downregulation of *CBF1/2/3* and relative upregulation of *ICE1/2* (Fig. 26A). In contrast, *ugt74f1 ugt74f2* and, less pronounced, *ugt74f1* exhibited a reversed expression pattern paralleled by the most cold-resistant phenotype. Thus, *UGT74F2* exhibits opposing roles: it counteracts the cold sensitivity of *ugt76b1*, whereas it enhances the sensitivity of *ugt74f1*.

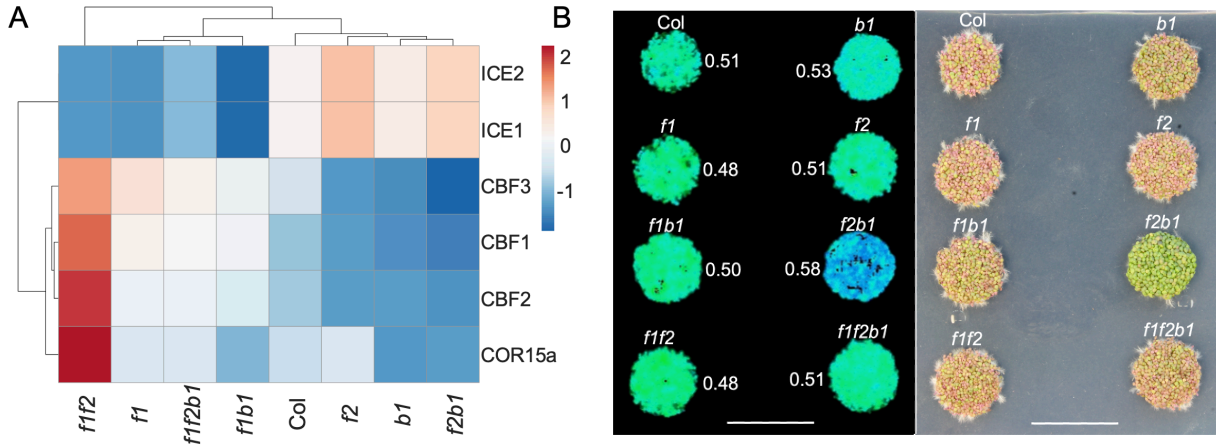

Fig. 26: Cold resilience and marker gene expression in *ugt* mutants. A. Expression pattern cold acclimation/resilience marker genes *ICE1/2*, *CBF1/2/3*, and *COR15A*. The color of each block represents the log_2-fold difference compared to the mean expression value of all eight genotypes. **B.** Seeds of *ugt* mutants and wild type germinating on ½ MS agar plates at 4 ˚C, 16-hour light, long day condition. Both RBG (left panel) and fluorescent (right panel) images were taken four weeks after cold treatment. The numbers represent the Fv/Fm value.

2.3 In vitro activity and specificity of three UGT enzymes

This part was initiated together with former master student Sophia Fundneider, the substrate binding pocket analysis, ligand docking, and protein-ligand interaction were partially performed by her under my guidance.

UGTs are organized as two-domain GT-B proteins, with ligand-binding sites located in the cleft between these domains. While UDP-glucose binds to a conserved site, the glucose acceptor binds to a variable site composed of residues from the N-terminal domain (Fig. 27A). In this region, conserved residues—including histidine and two aspartates—are involved in catalysis (Fig. 27B, C; George-Thompson *et al.*, 2017).

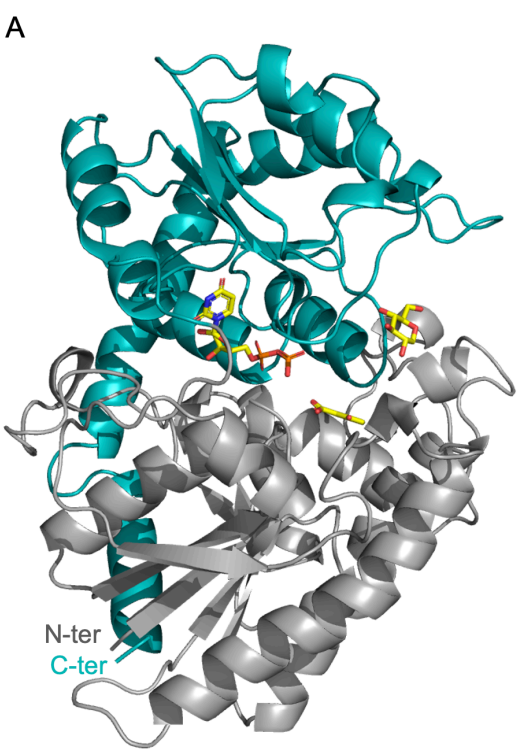

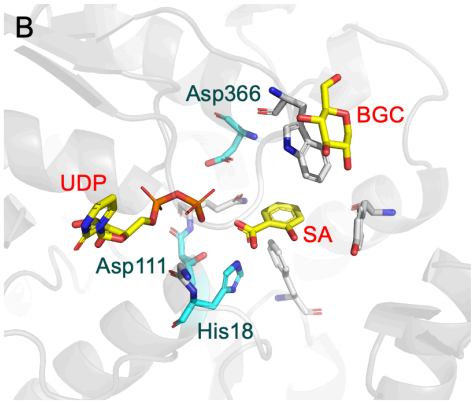

C

UGT74F2	UGT74F1	UGT76B1
His18	His18	His20
Asp111	Asp111	Asp109
Asp366	Asp366	Asp369
Trp364	Trp364	Phe367
Phe113	Phe113	Leu111
Tyr180	Tyr180	Gly185
Gln134	Gln134	Val132
Phe131	Phe132	Arg130

Fig. 27: Overview of UGT74F2 crystal structure and active center. A. UGT74F2 in complex with SA and UDP-Glc (yellow), cleaved into UDP and β-D-Glucose (BG) during crystallization. The N-terminal domain (residues 4 to 245) is colored cyan, and the C-terminal domain (residues 246 to 449) is gray. **B.** Representation of the active center with the catalytic triad His18, Asp111, and Asp369 highlighted in cyan, visualized in PyMOL. **C.** Comparison of important amino acid residues lining the binding pockets of the glucosyltransferases UGT74F2, UGT74F1, and UGT76B1 from *Arabidopsis thaliana*. The catalytic triad (His-Asp-Asp) is conserved among all three UGTs.

Previous structural studies on UGT74F2 (George-Thompson *et al.*, 2017) and UGT76B1 (R. Jankowski and A.R. Schäffner, unpublished) have used crystal structures to explain differences in substrate specificity, showing that UGT76B1 has a wider substrate-binding pocket compared to UGT74F1 and UGT74F2 (Bauer, 2020b). Key amino acids lining the binding pockets of these three UGTs were identified and compared (Fig. 27C). However, the

exact mechanisms of pocket-ligand interactions, and whether these differences can be used to predict substrate specificity, remain unclear. Although the co-crystallization structure of UGT74F2 with its substrates SA and UDP-glucose is available, the sugar moiety of UDP-glucose was cleaved within the binding pocket and did not attach to the recipient SA, likely due to hydrolysis during crystallization (George-Thompson *et al.*, 2017). As a result, it is difficult to deduce the precise interaction model between SA, UDP-glucose, and the residues surrounding the binding pockets. To address these challenges, we first used AlphaFold2 for protein structure prediction, followed by ligand docking into the binding pockets using Maestro Schrödinger to predict enzyme activity based on protein-ligand interactions. Finally, we validated these predictions by testing the *in vitro* activity of each enzyme with different substrates.

2.3.1 AlphaFold prediction and crystal structure

The experimental structure of UGT74F2, determined by X-ray crystallography, is publicly available in the Protein Data Bank (PDB ID: 5U6M; George-Thompson *et al.*, 2017). Similarly, the crystal structure of UGT76B1 has been determined (R. Jankowski and A.R. Schäffner, unpublished). To compare the structures of all three SA-GTs and to simulate mutations, AlphaFold2 was used to predict both wild-type and mutated protein structures.

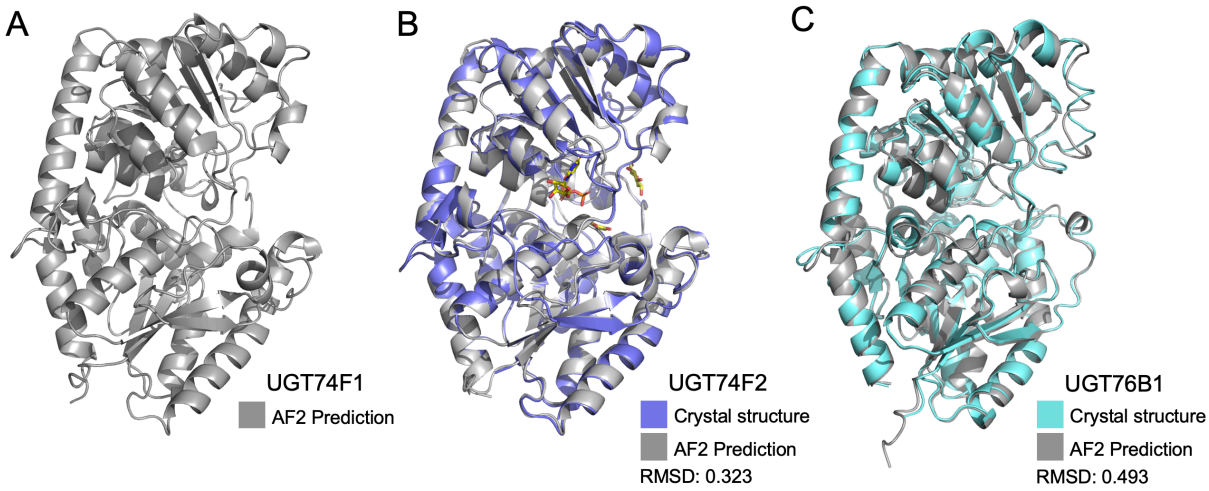

Fig. 28: Structures of the three SA-GTs. Proteins in gray are predicted by AlphaFold2. The predicted structures of UGT74F2 and UGT76B1 are superimposed with their respective crystal structures. UGT74F2 was co-crystallized with its substrates, SA and UDP-glucose, while UGT76B1 was crystallized without ligands. The RMSD of atomic positions was calculated using PyMOL.

To assess the reliability of the AlphaFold2 predictions, the predicted structures were superimposed onto the experimental crystal structures. The root mean square deviation (RMSD) of atomic positions was calculated using PyMOL and is presented below the models (Fig. 28). The predicted structure of UGT74F2 showed a high degree of similarity to the

experimental structure, with an RMSD of only 0.323 Å (RMSD values below 1 Å are considered highly similar, with 0 Å indicating identical structures; Carugo and Pongor, 2001). For UGT76B1, the RMSD was slightly higher at 0.493 Å. However, considering the more flexible regions of UGT76B1, the main structural core remains highly similar. Therefore, the AlphaFold2-predicted models are reliable for SA-GTs and can be confidently used in subsequent analyses.

2.3.2 *In silico* modeling of ligands

Due to the highly conserved binding pockets of UGTs (Hans *et al.*, 2004; Zhang et al, 2020; George Thompson *et al.*, 2017), the regions accommodating UDP-glucose and aglycons are similar among the three SA-GTs. The crystal structure of UGT74F2 with ligands served as a reference for the study (George-Thompson *et al.*, 2017). Using the defined regions for UDP-glucose and aglycons, ligands were docked into their corresponding positions using Maestro Schrödinger.

To account for the flexibility of ligands and amino acid residues, the induced fit docking (IFD) function was applied, allowing optimal fitting of both components. This approach generated multiple poses for each ligand (Fig. 29). To identify the most probable pose, the binding pose molecular dynamics (BPMD) function was used to evaluate the stability of each pose. Six poses underwent 10 ns of molecular dynamics simulation (Fig. 29). Pose 5 exhibited a relatively low RMSD value, suggesting that it remained stable in its spatial position and had a higher likelihood of interacting effectively with other ligands and amino acid residues.

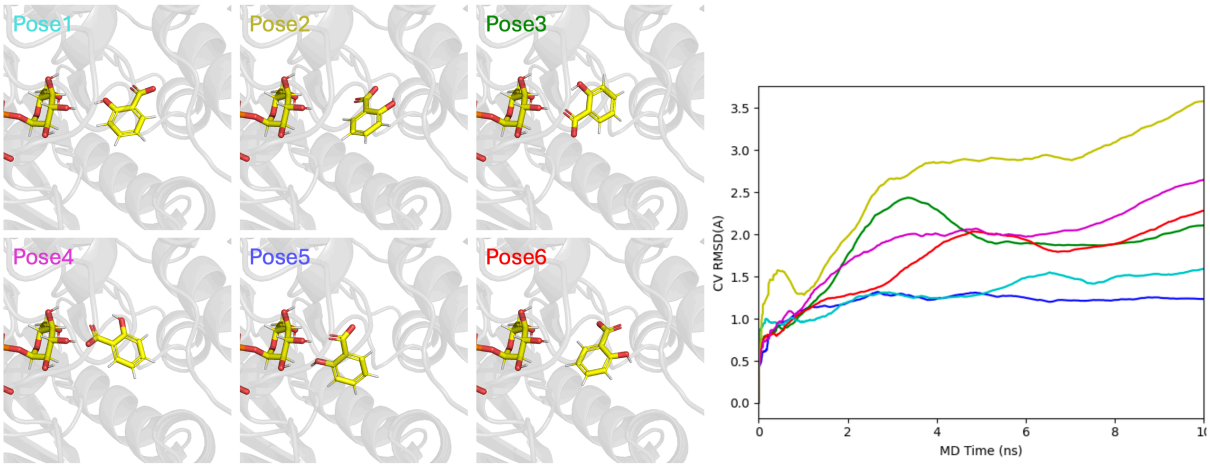

Fig. 29: Different binding poses of ligands and molecular dynamics simulations. For each ligand, 50 poses were generated using the IFD function. These poses were clustered based on their spatial positions and orientations; in the case of SA in UGT74F1, six groups of poses were formed. Within each group, poses were ranked according to their interaction assessments, which quantify the stability of binding by evaluating interactions such as hydrogen bonds, hydrophobic interactions, and π-π stacking using energy scoring functions. The top-

ranked pose in each group was then subjected to molecular dynamics simulations, with each pose undergoing 10 ns of simulation, repeated a total of 10 times.

UGT74F2 forms both SAG and SGE, leading to the hypothesis that SA binds in two different poses within the binding pocket, depending on the pH (George-Thompson *et al.*, 2017). The active triad of UGTs, particularly the catalytic Asp-His dyad, is essential for their activity, with significant evidence supporting the role of this interaction (Wang, 2009). Physical modeling of the Asp-His catalytic dyad under different pH conditions supports the existence of two forms of the imidazole group of His18 (Fig. 30). Due to their spatial proximity, the amino group of His18 can form hydrogen bonds with the carboxyl group of Asp111.

At neutral pH, the imidazole group of His18 acts as a base; its nitrogen atom can deprotonate the substrate, facilitating nucleophilic attack on UDP-glucose. The negative charge of Asp111 enhances His18's ability to accept protons, increasing its catalytic effectiveness. However, at acidic pH levels (below neutral), the imidazole group of His18 becomes protonated, enabling it to form a hydrogen bond with the carboxyl group of Asp111. This interaction orients the ligand toward the sugar moiety of UDP-glucose. Although both forms of the catalytic dyad coexist, molecular simulations can only represent one form at a time. Therefore, in the subsequent modeling, the protonated form of His18 was used to model glucose–ester–forming ligands, while the neutral form was used for O-glucoside–forming ligands.

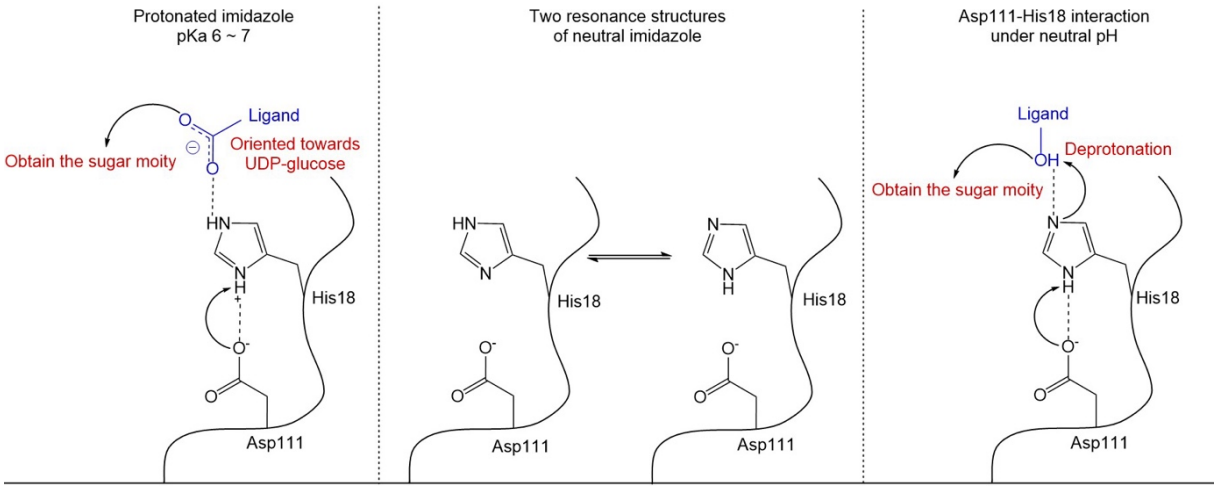

Fig. 30: Two forms of the His18-Asp111 catalytic dyad. The interactions between the amino acid residues were simulated using Maestro Schrödinger and illustrated with ChemDraw. At neutral pH, the imidazole group of His18 exists in two resonance structures and forms a hydrogen bond with the carboxyl group of Asp111. When simulated at pH 5.8, the imidazole group becomes protonated and adopts another resonance form.

2.3.3 Ligand-binding pocket interaction and activity prediction

Following ligand docking and molecular dynamics simulations of binding poses, we selected the most stable models to illustrate binding pocket–ligand interactions and predict substrate

activity. All SA-GTs were modeled with UDP-glucose and five different substrates: SA, NA, AA, ILA, and NHP. Across all three SA-GTs, the interactions between key amino acid residues and UDP-glucose were highly similar. For UGT74F1 and UGT74F2 (Fig. 31-33), Asn364 and Ser347 form hydrogen bonds with the phosphoryl group adjacent to the glucosyl moiety, along with other residues in the UDP-glucose binding tunnel, anchoring the UDP portion. The glucosyl unit resides in the central binding pocket near the ligands, interacting with one of the catalytic triad residues, Asp366. This interaction lifts the glucosyl group, allowing the ligand to access the anomeric carbon. In UGT76B1 (Fig. 34), the interaction model is comparable, but the amino acid residues involved are the positionally equivalent Asn369, Ser350, and Asp369.

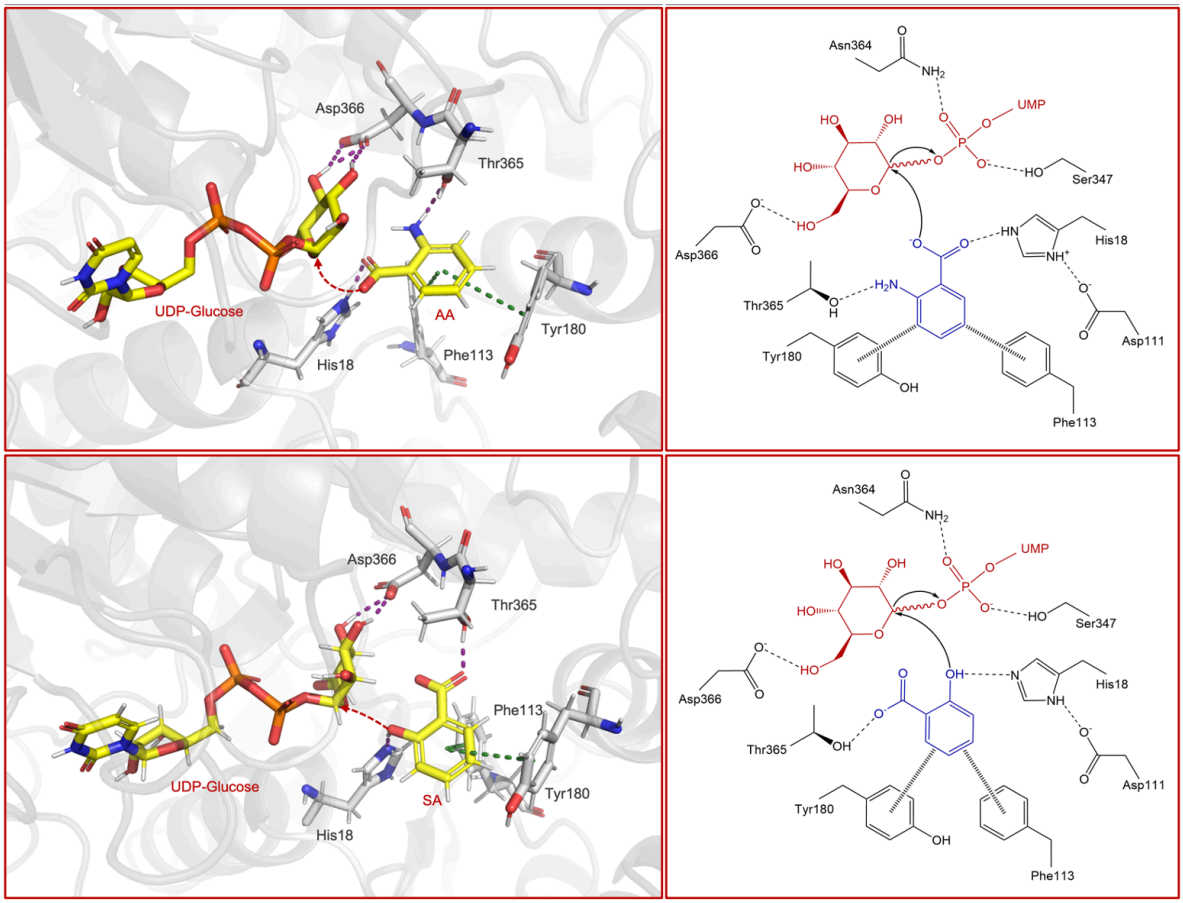

Fig. 31: Interaction of UGT74F1 binding pocket with SA and AA. Left: Visualized using PyMOL. Purple dashed lines represent hydrogen bonds; green dashed lines represent π–π interactions. Right: Visualized using ChemDraw. Dashed lines represent hydrogen bonds; thick dashed lines represent π–π interactions.

When interacting with different ligands, UGT74F1 exhibits a similar binding model toward NA, AA, and SA, as these compounds possess aromatic structures. Phe113 and Tyr180 engage in π–π interactions with all three ligands, stabilizing their positions within the binding pocket (Fig. 31). For SA and AA, Thr365 forms hydrogen bonds with the carboxyl and amino groups, helping to orient the hydroxy and carboxyl groups of the substrates toward UDP-glucose. In

the case of AA, protonated His18 forms a hydrogen bond with one of the oxygens in the carboxyl group, polarizing the other oxygen and facilitating the transfer of the sugar moiety. For SA, neutral His18 deprotonates the hydroxyl group, enabling it to attack the anomeric carbon of UDP-glucose. Theoretically, His18 of UGT74F1 can also be protonated under acidic conditions to form SGE, as marginal SGE production has been observed under such conditions (George-Thompson *et al.*, 2017).

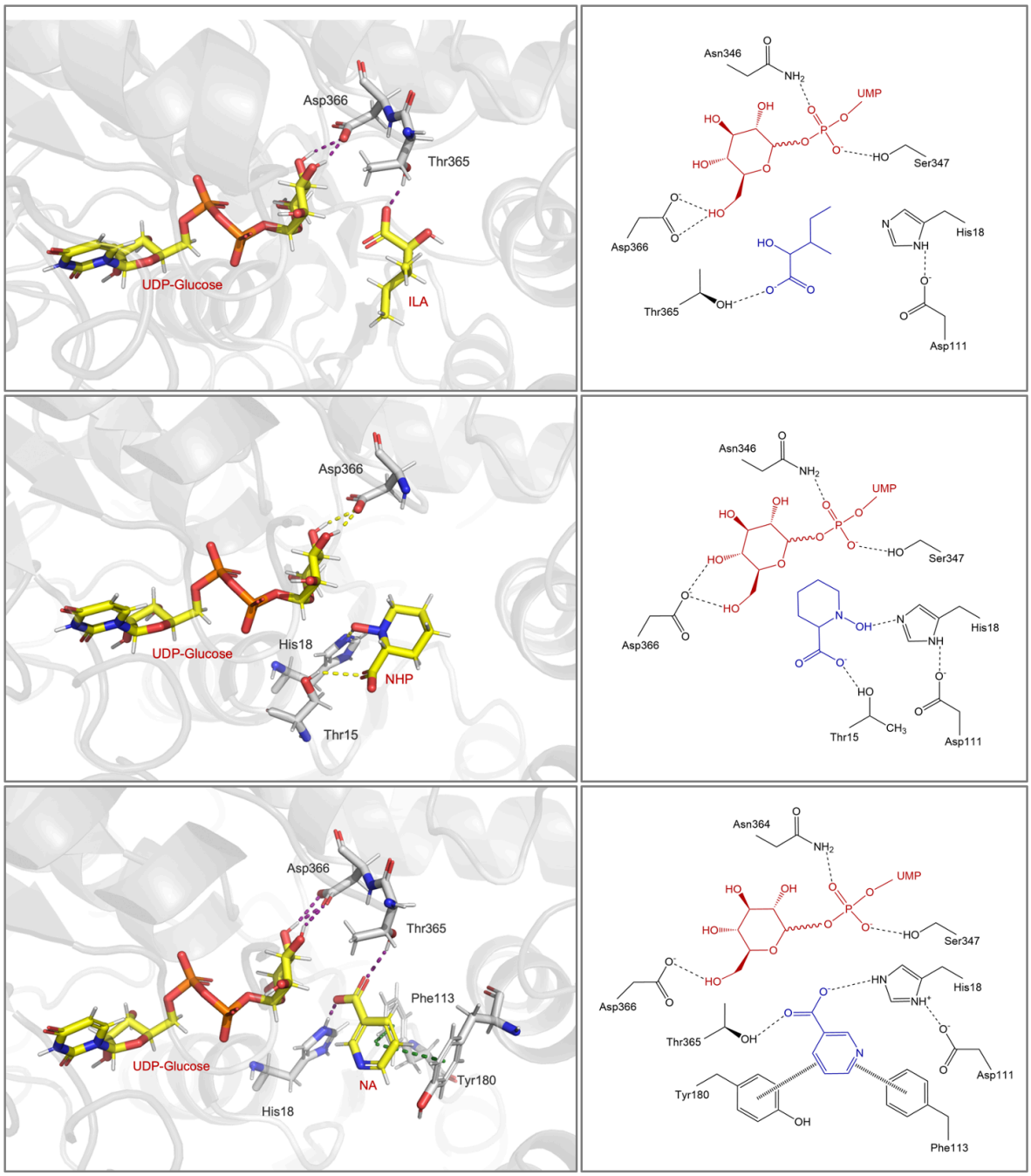

Fig. 32: Interaction of UGT74F1 binding pocket with ILA, NHP and NA. Left: Visualized using PyMOL. Purple dashed lines represent hydrogen bonds; green dashed lines represent π–π interactions. Right: Visualized using ChemDraw. Dashed lines represent hydrogen bonds; thick dashed lines represent π–π interactions.

Although NA also forms π–π interactions, its single substituent means that both oxygens of the carboxyl group are engaged in hydrogen bonds with Thr365 and His18, respectively (Fig. 32). This arrangement hinders access to the sugar moiety. In the case of ILA and NHP, lacking aromatic structures prevents these compounds from being properly guided into the binding pocket. Despite interactions with key amino acids such as Thr365 and His18, both substrates adopt orientations incapable of glucosylating the substrate (Fig. 32).

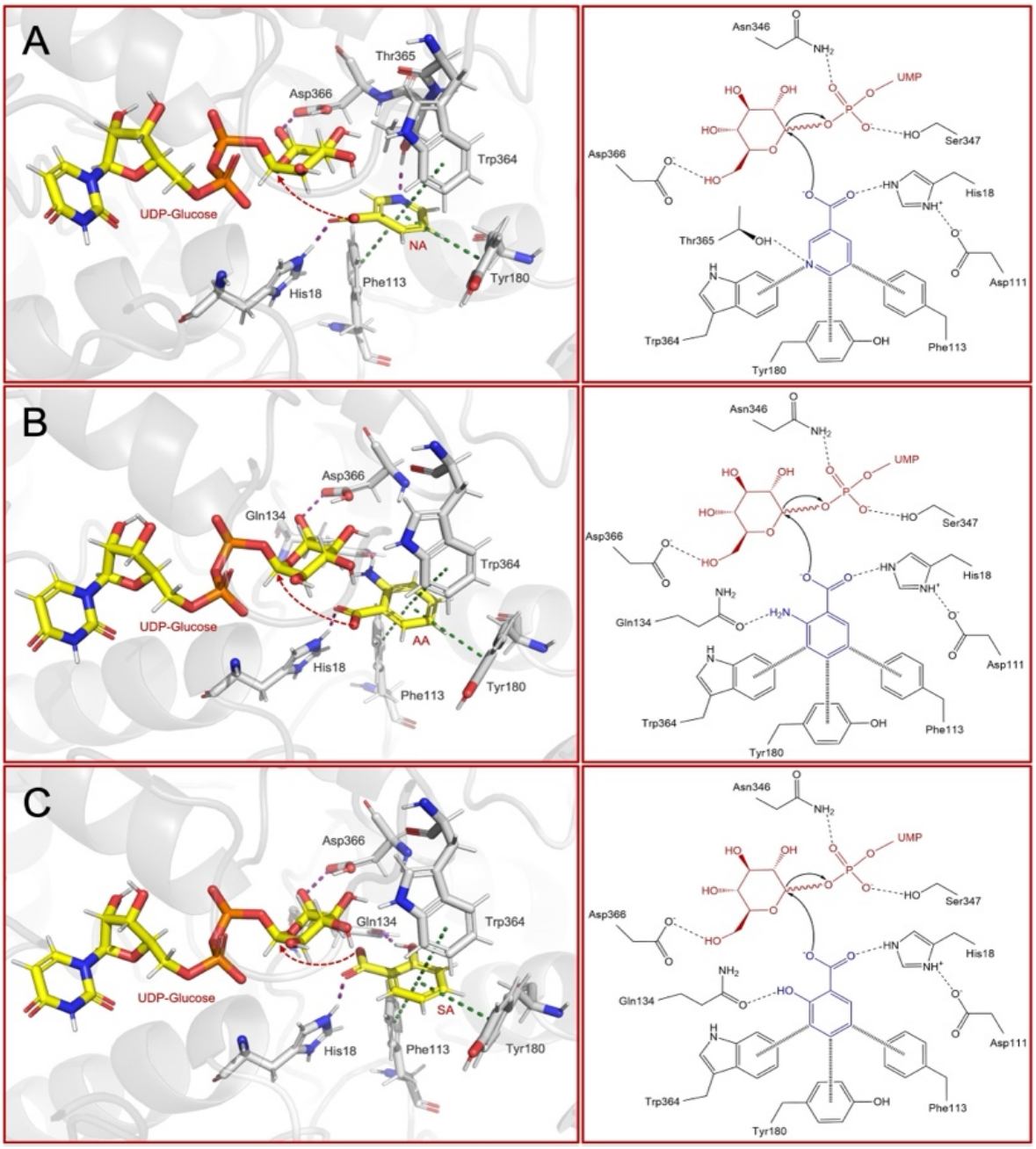

Fig. 33 continue in next page.

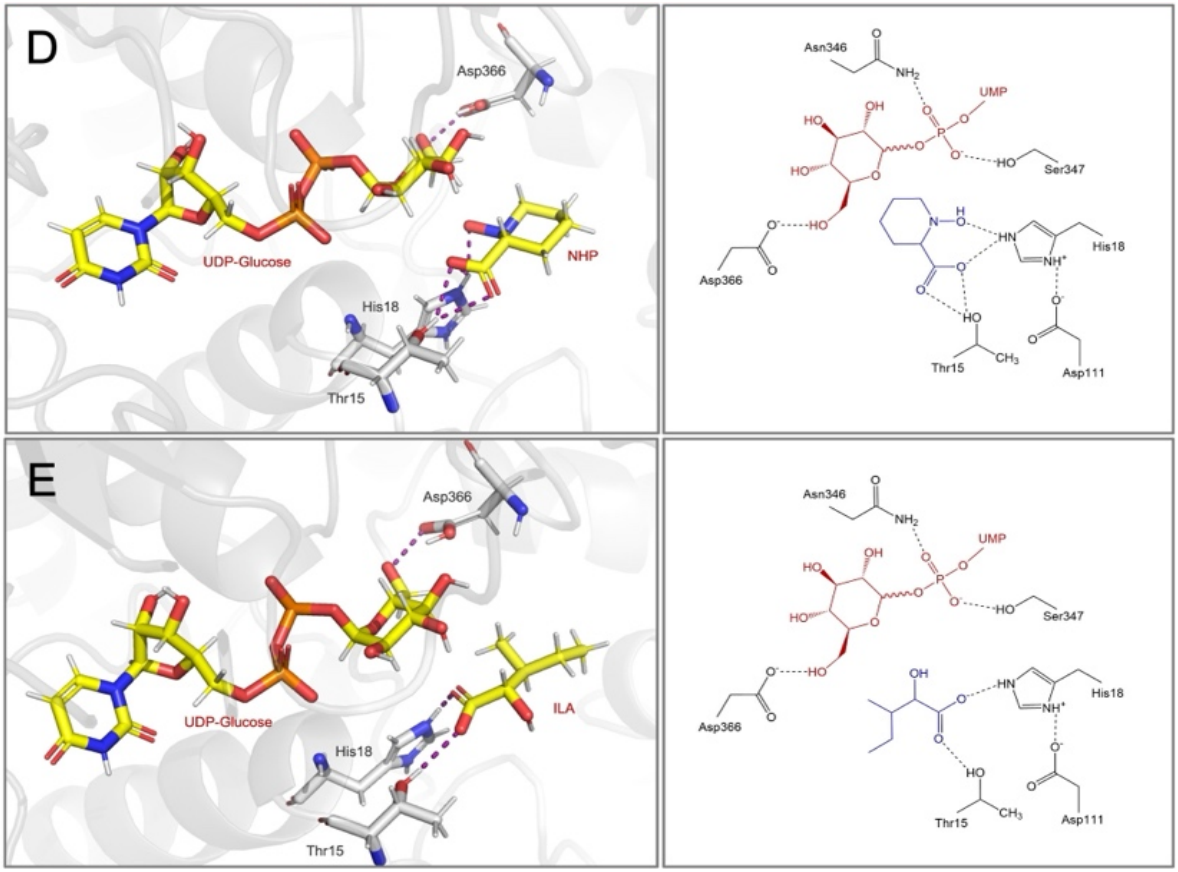

Fig. 33: Interaction of UGT74F2 binding pocket with AA, NA, SA, NHP and ILA. Left: Visualized using PyMOL. Purple dashed lines represent hydrogen bonds; green dashed lines represent π–π interactions. Right: Visualized using ChemDraw. Dashed lines represent hydrogen bonds; thick dashed lines represent π–π interactions.

Compared to UGT74F1, UGT74F2 possesses three aromatic residues in the binding pocket that interact with aromatic ligands. This strong interaction results in NA, AA, and SA being incorporated in nearly identical positions (Fig. 33). For AA and SA, Gln134 forms hydrogen bonds with the second substituent other than the carboxyl group. In the case of NA, lacking a second substituent, another amino acid residue, Thr365, near the aromatic ring forms a hydrogen bond with the nitrogen atom in the ring. For all three substrates, His18 forms a hydrogen bond with one of the oxygen atoms in the carboxyl group, orienting the substrate properly so that the oxygen can access the anomeric carbon of the sugar moiety. Similarly to UGT74F1, without interactions with aromatic amino acid residues, hydroxy acid substrates NHP and ILA cannot be correctly oriented in the binding pocket of UGT74F2. Although both substrates maintain stable poses interacting with His18 and Thr15, the hydroxy groups cannot be deprotonated. Additionally, both oxygens of the carboxyl groups interact with His18 and Thr15, reducing the likelihood of attacking the anomeric carbon of UDP-glucose.

In the binding pocket of UGT76B1, fewer aromatic amino acid residues are available to interact with substrates; Phe177 is the only one oriented toward the inside of the pocket (Fig. 34). For the hydroxy acid ligands, Arg130 plays a critical role by interacting with the carboxyl group, positioning the ligand closer to UDP-glucose. Subsequently, His20 forms a hydrogen bond with the hydroxy group, allowing deprotonation and enabling an attack on UDP-glucose. For AA and NA, similar to SA, Phe177 and Arg130 stabilize the aromatic structures and hydroxy groups of the ligands. However, due to the absence of a hydroxy group, His20 does not interact with any substituent, resulting in a low probability of reaction occurring.

In summary, the protein–ligand docking results suggest that UGT74F1 and UGT74F2 are unlikely to catalyze compounds like ILA and NHP due to the lack of aromatic structures. Compared to UGT74F2, UGT74F1 may not effectively catalyze NA because it lacks a second substituent. UGT76B1, which is structurally more distinct from UGT74F1 and UGT74F2, appears to require substrates containing both hydroxy and carboxyl groups, indicating that AA and NA are less likely to react.

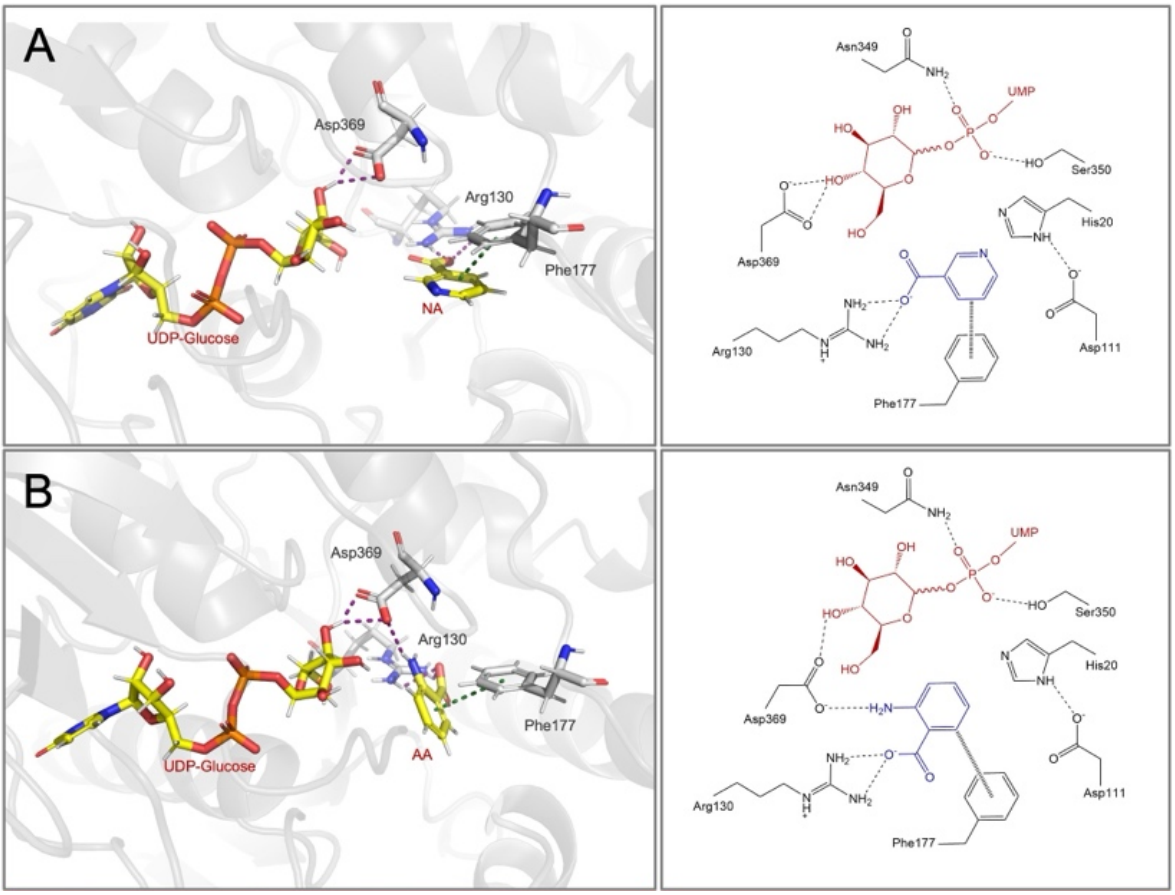

Fig. 34 continue in next page.

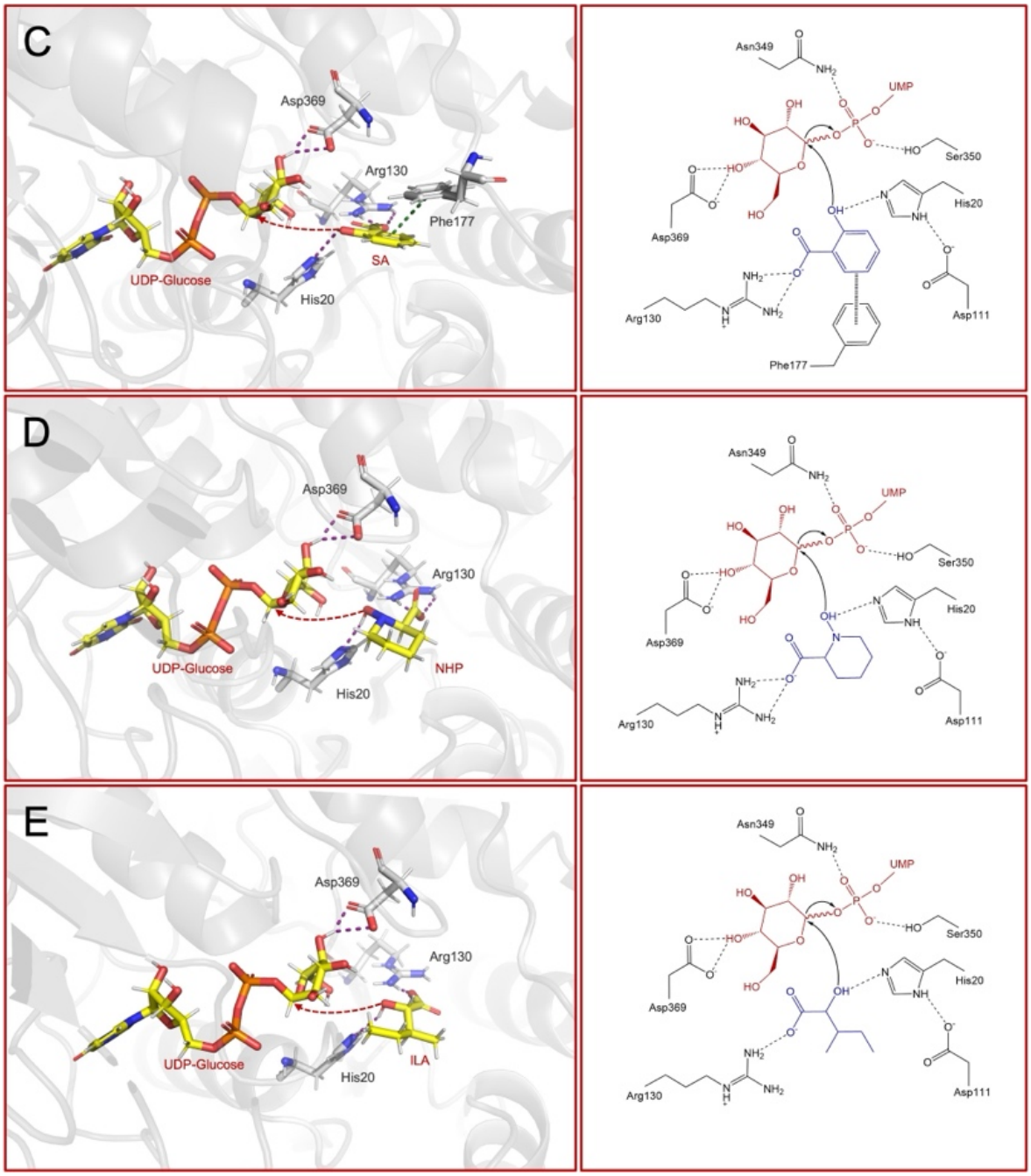

Fig. 34: Interaction of UGT6B1 binding pocket with NA and AA. Left: Visualized using PyMOL. Purple dashed lines represent hydrogen bonds; green dashed lines represent π–π interactions. Right: Visualized using ChemDraw. Dashed lines represent hydrogen bonds; thick dashed lines represent π–π interactions.

2.3.4 *In vitro* activity testing of three enzymes

Then, the recombinant SA-GT proteins were produced to explore their enzymatic specificity by collectively confirming the catalytic activities *in vitro*. Identical to literature and *in silico* modeling, UGT76B1 and UGT74F1 exclusively catalyze the production of SAG. In contrast, UGT74F2 can catalyze the formation of both SAG and SGE. Both UGT74F1 and UGT74F2 are able to produce Anthraniloyl-*O*-glucose (AAG), whereas UGT76B1 does not exhibit this

activity (Fig. 35A). Consistent with previous reports, UGT74F2 is active against NA to form Nicotinoyl-*O*-glucoside (NAG), while neither UGT76B1 nor UGT74F1 has this activity (Fig. 35B; Li *et al.*, 2015). Neither UGT74F1 nor UGT74F2 possesses the ability to conjugate ILA or NHP, which are additional substrates of UGT76B1 (Bauer *et al.*, 2021; Fig. 35C). In summary, the ligand-protein modeling and catalytic site analysis suggested enzyme activity is surely predictive for SA-GTs and these five substrates.

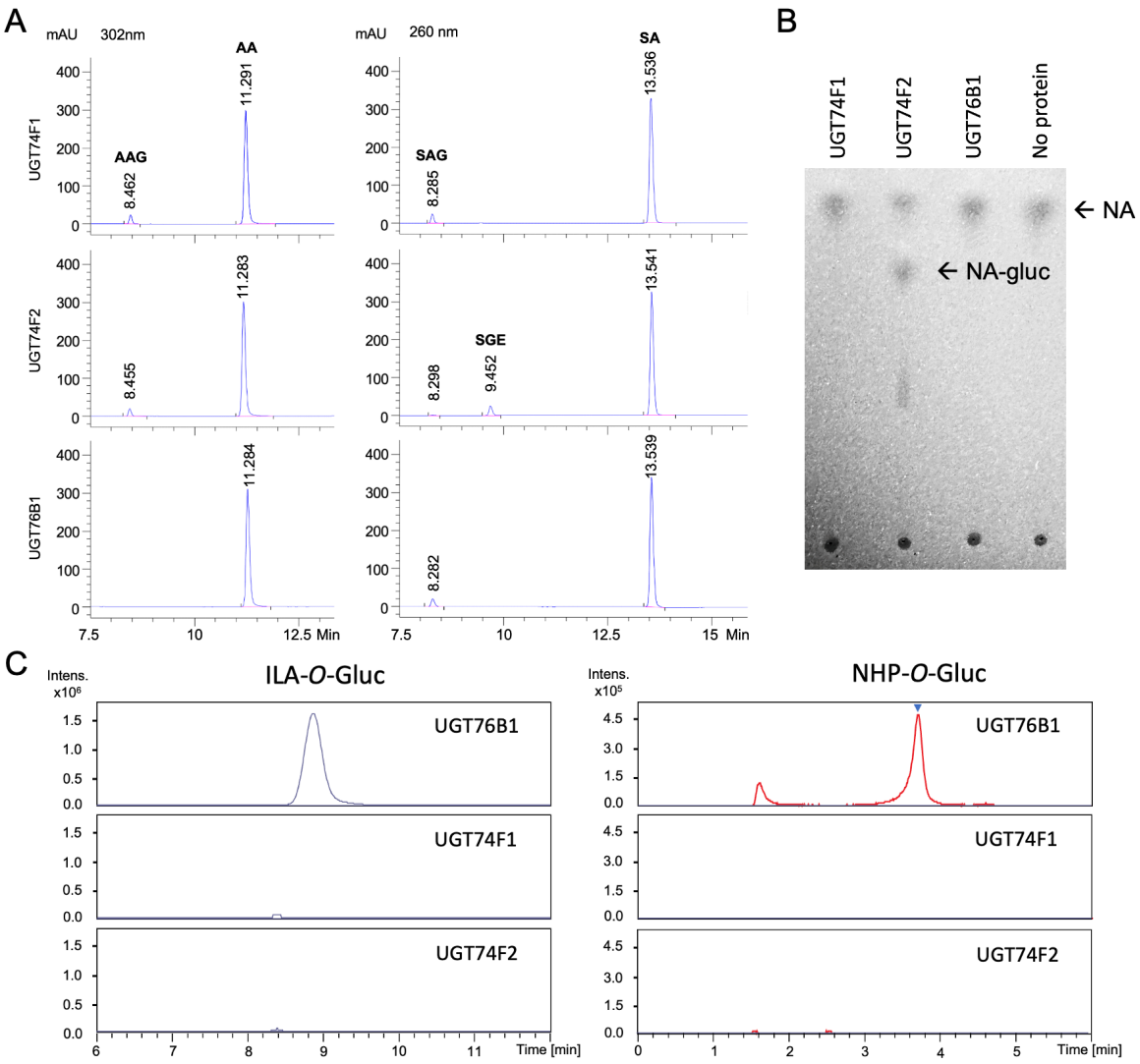

Fig. 35: *In vitro* enzymatic profiling of UGT74F1, UGT74F2, and UGT76B1 with SA, NHP, ILA, NA, and AA. **A.** HPLC analyses of enzymatic reactions with AA and SA. All three enzymes are active toward SA. UGT76B1 and UGT74F1 catalyze the formation of SAG, whereas UGT74F2 is unique in producing both SAG and SGE. AA was the substrate of UGT74F1 and UGT74F2 (compare Quiel and Bender, 2003), but not of UGT76B1. **B.** Thin-layer chromatographic analysis and fluorescent quenching after thin-layer chromatography on Silica gel 60 F_{254} plates indicate that only UGT74F2 is capable of glucosylating NA (compared to Li *et al.*, 2015b) **C.** LC-MS analyses reveal that only UGT76B1 is capable of glucosylating ILA and NHP to yield ILA-*O*-glucoside and NHP-*O*-glucoside, respectively. Enzymatic reactions were conducted with 1 µg of recombinant GST-UGT fusion proteins in a total volume of 20 µl, 0.5 mM aglycon, and 2 mM UDP-glucose. Reactions were incubated at 30 °C for 30 minutes (Maksym, 2018).

3 Discussion

3.1 Root UGT76B1 and FMO1 mediated root-shoot communication

Roots are essential for land plants, providing physical support and enabling the acquisition of nutrients and water. Additionally, roots engage in reciprocal information exchange with shoot tissues. Among these root-shoot interactions, ISR is a well-studied mechanism by which root-associated plant growth-promoting microbes establish JA- and ET-dependent, *PR* gene-independent resistance against pathogens and herbivores in shoots (Pieterse *et al.*, 1996, 2014). However, in some cases—even within the same microbial genus—root-induced shoot resistance deviates from this model and instead relies on SA (Pieterse *et al.*, 1998; van de Mortel *et al.*, 2012). In both cases, the specific triggers originating from roots remain largely unknown.

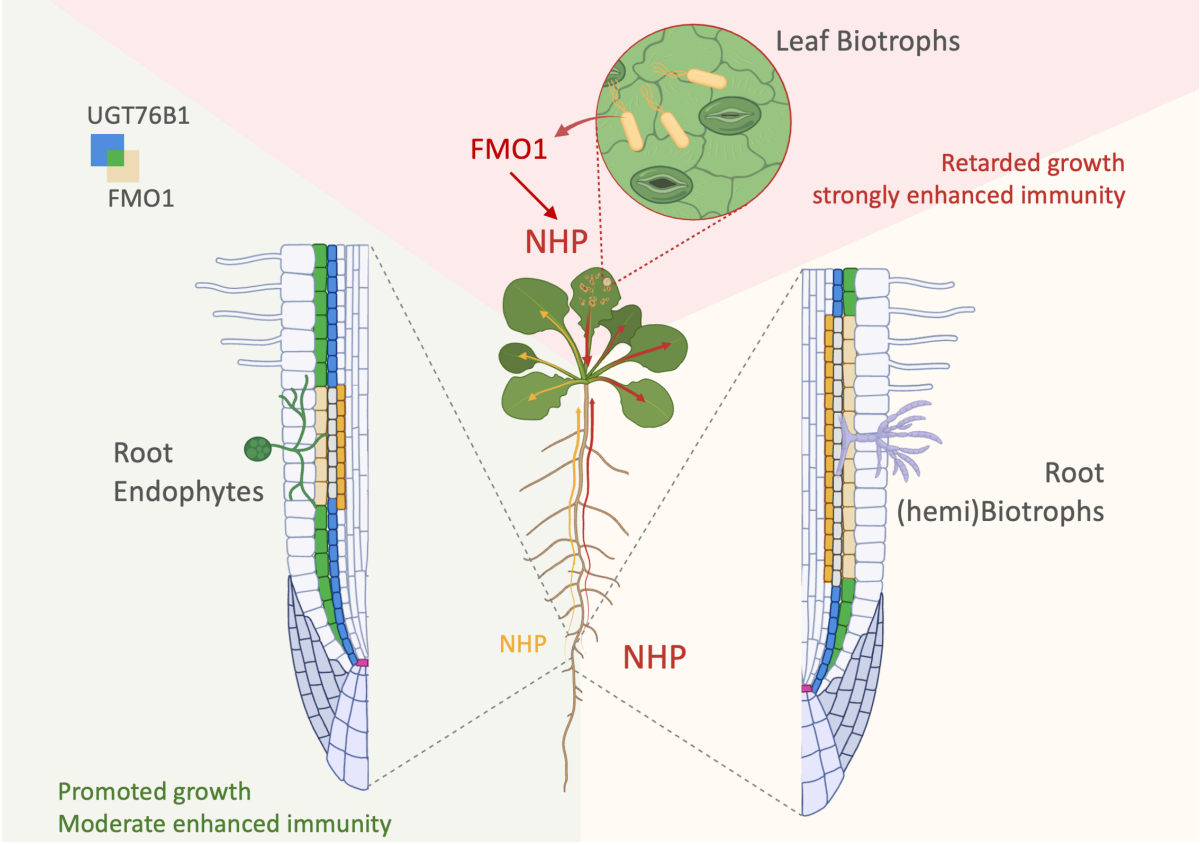

Fig. 36: Root-triggered systemic resistance. FMO1 is not expressed in leaves of naïve plants. Upon pathogen attack, FMO1 is induced and NHP is synthesized *de novo.* NHP then moves systemically to enhance immunity in distant leaves, a phenomenon known as SAR. In contrast, NHP is continuously synthesized and deactivated due to the simultaneous presence of FMO1 and UGT76B1 in roots. Endophytic fungi suppress UGT76B1 and promote FMO1 strictly at sites of root-fungi interaction. Biotrophic pathogens elicit a similar response but across a broader range around the site of interaction. These scenarios lead to different amounts of NHP released from root to shoot; a low level of translocated NHP leads to promoted growth and moderate enhanced immunity, whereas higher levels of NHP provoke retarded growth and a more strongly enhanced immunity.

Here, it is shown that numerous root-associated fungi exploit components of the leaf-to-leaf SAR pathway, albeit in a different context. While SAR in leaves is initiated by primary infection, which activates *FMO1* expression to produce the NHP signal subsequently moderated by the NHP-conjugating enzyme *UGT76B1*, *FMO1* and *UGT76B1* are constitutively active in naïve *Arabidopsis* roots to synthesize NHP and concurrently restrict its mobility through glucosylation. Upon contact with specific soil microbes, this balance shifts rapidly due to UGT76B1 suppression (via degradation) and/or *FMO1* upregulation. Thus, the leaf SAR mechanism of "switch-on and keep-in-check" is transformed in this root-triggered systemic resistance (RSR) into a "standby" mode, where *FMO1* and *UGT76B1* are simultaneously active (Fig. 36). Interestingly, both beneficial and pathogenic microbes utilize this *FMO1*/*UGT76B1* module, albeit with varying degrees of activation. It is proposed that microbial root stimuli are integrated into a unified mechanism affecting shoot growth and/or defense. This hypothesis is supported by NHP's dose-dependent effects, which not only activate defense (Schnake *et al.*, 2020) but also promote growth at low NHP concentrations (Fig. 13). Beneficial endophytes locally regulate *FMO1* and *UGT76B1* at the root-microbe interface, releasing moderate NHP amounts into the shoot to stimulate growth and moderately enhance resistance. In contrast, (hemi)biotrophic pathogens induce a broader response, extending *FMO1* and *UGT76B1* regulation beyond the interaction site. This likely leads to a larger NHP release, resulting in reduced growth and a significantly heightened resistance response (Fig. 8; 13; 15A-D).

3.1.1 Constitutive expression and regulation of UGT76B1 and FMO1

The functionality of the standby *FMO1/UGT76B1* module, which restricts NHP export from naïve roots, relies on efficient glucosylation of constitutively synthesized NHP. Interestingly, unconjugated NHP is detectable, albeit at a comparatively low level (Hartmann *et al.*, 2018; Bauer *et al.*, 2021;0.07 *vs*., *e.g*., 10 ng mg^{-1} DW 24 h after *Pst* infection in leaves; Fig. 2B). Several observations suggest that the spatial distribution of NHP, rather than its overall level in roots, is crucial. First, *FMO1* expression peaks in the cortex, whereas *UGT76B1* is strongly expressed in both the cortex and endodermis, forming a barrier to prevent NHP from reaching the vasculature. Consistent with this, cell type-specific loss of *UGT76B1* in the endodermis, but not in the cortex, fully mimics the shoot phenotype of the *ugt76b1* knockout. Additionally, *FMO1* is induced in pericycle cells by various (hemi)biotrophic and endophytic fungi (Fig. 8; 9), meaning that NHP production could occur beyond the main *UGT76B1* barrier. The importance of spatial and temporal control is further supported by differing responses to microbial interactions. Regulation of *FMO1/UGT76B1* at the contact site appears to be a general response to root colonization. The response remains localized for endophytes like

Fo47 and *Ct*, which remain between the epidermis and cortex (Hacquard *et al.*, 2016; Martínez-Soto *et al.*, 2023). However, *Fo5176* and *Ci*, which colonize the vasculature (Hacquard *et al.*, 2016; Martínez-Soto *et al.*, 2023), induce distal responses, likely due to the spread of pathogen-associated molecular patterns. Alternatively, phytotoxins produced by these (hemi)biotrophic fungi could induce *FMO1* expression (Joglekar *et al.*, 2018).

3.1.2 RSR and ISR

Over time, a dichotomy has developed between the terms SAR and ISR. These are often considered fundamentally distinct induced resistance phenotypes: leaf pathogens trigger SA/NHP-mediated SAR, while root-beneficial microbes trigger JA/ET-mediated ISR. However, recent discussions have suggested that ISR should not be limited to phenotypes systemically triggered by PGPR/PGPF and linked exclusively to JA/ET pathways (De Kesel *et al.*, 2021). Despite the antagonistic relationship between JA/ET and SA signaling, $ISR_{sensu\ stricto}$ and RSR elucidated here may also be interwoven, since some root endophytes have been reported to activate both pathways in shoots, *e.g*. *T. virens* and *T. atroviride* or the endophyte *P. indica*(Contreras-Cornejo *et al.*, 2011; Pedrotti *et al.*, 2013). *Vice versa*, different strains of one species, *P. fluorescens*, may activate JA/ET- or SA-dependent immunity (Pieterse *et al.*, 1996; van de Mortel *et al.*, 2012). These findings may well align with our observations of UGT76B1 and FMO1 regulation, *e.g.*, a still active JA signaling in *fmo1* mutants may explain the trend to repress rosette growth and to enhance resistance to *P. syringae* upon interaction with *Fo5176*, since resistance against *Fo5176* depends on both SA and JA pathways (Wang *et al.*, 2022; Fig. 15A, D).

3.1.3 Adaptive advantage of standby mode for root NHP

The rhizosphere contains a higher microbial density than the phyllosphere (Trivedi *et al.*, 2020), presenting frequent challenges that require plants to distinguish between beneficial and harmful microbes. A rapid response mechanism in roots likely provides an adaptive advantage. For example, antimicrobial coumarins are stored in roots as *O*-glucosides and quickly hydrolyzed into active aglycones upon iron deficiency or pathogen attack, releasing them into the soil to shape the microbiome (Stringlis *et al.*, 2019; Stassen *et al.*, 2021). Similarly, NHP-*O*-glucoside may serve as a storage form in roots, poised for hydrolysis and systemic release upon receiving stress signals. In interactions with (hemi)biotrophic and endophytic microbes, *FMO1* is induced in the pericycle, adjacent to the phloem (Fig. 9), rather than in its original expression tissue or directly colonized cells. Given that NHP is bidirectionally mobile, likely moving through the phloem (Fig. 3), *FMO1* activation in the pericycle allows for rapid systemic transport of NHP.

When roots perceive a stimulus, alerting the aboveground tissues to activate systemic immunity is essential. In *Arabidopsis*, root inoculation with *F. oxysporum* elevates the SA marker gene *PR1* in leaves (Lyons *et al.*, 2015). SA pre-treatment of leaves enhances resistance, as systemic activation of SA signaling can inhibit the spread of vascular pathogens (Wang *et al.*, 2022). Conversely, the *sid2* mutant, which is deficient in SA biosynthesis, shows increased susceptibility to *F. oxysporum* (Edgar *et al.*, 2006). During interactions with *Trichoderma*, SA plays a crucial role in preventing fungal invasion into the vasculature. In *sid2* mutants, *Trichoderma* becomes pathogenic, reaching aerial parts through the vascular system (Alonso-Ramírez *et al.*, 2014). Additionally, root inoculation with *Trichoderma* induces *PR1* expression in the shoot, possibly as a result of systemically enhanced immunity triggered by endophytic fungal interactions (Alonso-Ramírez *et al.*, 2014).

3.2 Physiological role of SA-GT in *Arabidopsis*

The fully combinatorial set of Columbia-based mutants allowed a comprehensive comparative analysis of UGT mutants by their levels of SA metabolites, transcriptomes, enzyme function, and response to abiotic and biotic stresses. UGT76B1, UGT74F1, and UGT74F2 are the principal SA glucosyltransferases of *Arabidopsis*, since the triple mutant no longer accumulated SA glucosides. UGT74F2 is the only SA glucose ester-forming enzyme (Bauer, 2020). They have a differential, partially overlapping cellular expression pattern covering vasculature and non-vasculature cells. The SA-*O*-glucoside forming UGT74F1 and UGT76B1 cannot replace each other, reflecting differences in their expression pattern and activity towards additional substrates. Transcriptome changes and phenotypic abiotic and biotic stress responses differentiate their link to distinct scenarios. UGT76B1 dominates immune regulation, whereas UGT74F1 and UGT74F2 are mainly related to abiotic stress responses. Nevertheless, all enzymes also show specific interactions in response to bacterial pathogens and to drought, salt, osmotic, and cold stress (Fig. 37).

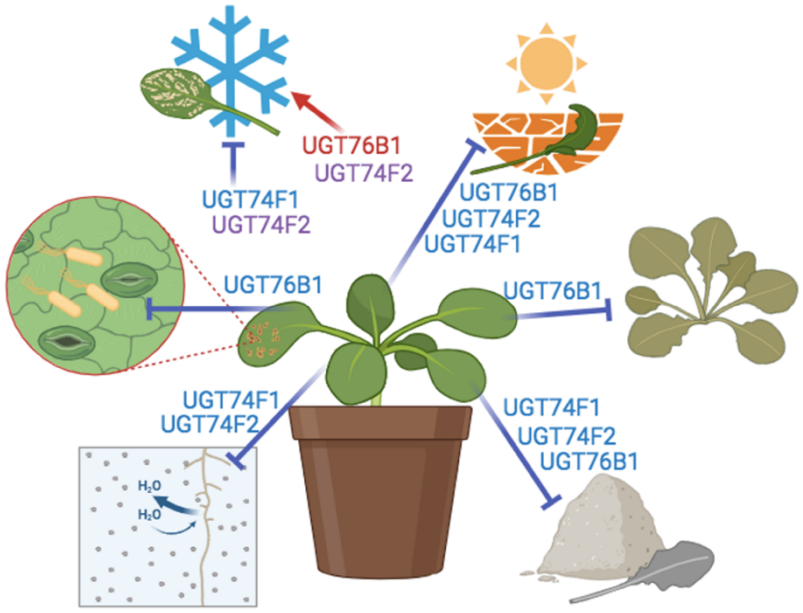

Fig. 37: Conceptual framework of the roles of the three *Arabidopsis* SA glucosyltransferases under distinct scenarios. The resilience or resistance to the depicted abiotic and biotic cues is differentially enhanced or suppressed by UGT74F1, UGT74F2, and UGT76B1. UGT76B1 stands out with its exclusive role in suppressing plant senescence and defense mechanisms. Concurrently, it collaboratively acts with UGT74F1 and UGT74F2 to mitigate plant tolerance against salt and drought stress. However, UGT76B1 exhibits a positive role in cold acclimation under cold stress, whereas UGT74F1 plays the opposite role. Notably, UGT74F2 intensifies the differential effects exhibited by UGT74F1 and UGT76B1 under cold stress conditions. UGT74F1 and UGT74F2 play a crucial role in suppressing plant tolerance against osmotic stress. Graphic depictions are based on BioRender.

3.2.1 Differential roles of SA-GTs in biotic interaction

In summary, the *ugt76b1* and *ugt74f1* mutations individually exhibited pronounced gene regulation, with their combination resulting in the most substantial changes observed across all mutants. The *ugt74f2* mutation did not yield significant alterations, whether alone or in conjunction with *ugt76b1*. However, *ugt74f2* contributed to several distinct regulatory effects in synergy with *ugt74f1*.

The mutant set under examination is comprehensive and can be distinguished by appearance. Mutants harboring the *ugt76b1* allele exhibit early senescence, elevated levels of free SA, and enhanced resistance to *Pst* (Fig. 16; 20B, D). Additional mutations in UGT74F1 or UGT74F2 do not further bolster this resistance.

While *ugt74f1* mutants have previously been reported as more susceptible to *Pst* in the *Ws* ecotype, *ugt74f2* knockdown mutants (with a Col background) demonstrated increased resistance in the same study (Boachon *et al.*, 2014). This finding is at odds with our observations. Given that differing ecotypes and incomplete knockouts can yield drastically different results, it is crucial to consider the uniform genetic background. In our comprehensive mutant set—based on this uniform background—both SA levels and signaling marker genes align with *Pst* resistance (Fig. 16; 20A, B). No significant differences were observed among *ugt74f1*, *ugt74f2*, *ugt74f1 ugt74f2* mutants and Col. This consistency may be attributed to the induction of UGT76B1 expression in *ugt74f1* and *ugt74f2* mutants by GUS staining (Fig. S4).

3.2.2 Role of SGE and SAG in resistance mechanisms

The triple mutant, which is unable to produce both SAG and SGE, exhibited resistance levels to *Pst* comparable to the *ugt76b1* single mutant, despite the latter having high levels of SAG (Fig. 1; 4B). Although some studies have proposed that SAG serves as a storage form of SA for later reuse (Chen *et al.*, 1995; Kawano *et al.*, 2004; Vaca *et al.*, 2017), direct evidence supporting this hypothesis is lacking. While exogenous application of SAG has been shown to enhance plant immunity with fewer adverse effects compared to direct SA application, the potential for endogenous SAG to be reused remains unclear (Swayambhu et al., 2021).

Notably, the additional loss of UGT74F2 and/or UGT74F1 in the *ugt76b1* mutant significantly reduced SAG and SGE levels, yet this did not further affect resistance to *Pst* (Fig. 16, 20). This suggests that neither SAG nor SGE further impacts plant immunity against *Pst* when endogenous SA levels are high. Furthermore, *ugt74f1* and *ugt74f2* single mutants showed SA levels and resistance to *Pst* similar to those of the wild type, despite their significantly reduced SAG or SGE levels. This indicates that SAG and SGE may also not substantially influence plant immunity against *Pst* when plants have basal endogenous SA level (Fig. 16, 20).

3.2.3 The roles of UGT74F1 and UGT74F2 in abiotic stress responses

Notably, upon treatment of the wild type with BTH, *UGT76B1* exhibited significant upregulation while *UGT74F1* remained unchanged (Meßner and Schäffner, unpublished data). This observation aligns with the identified role of UGT76B1 as the principal attenuator of SA signaling during pathogenic stress (Bauer *et al.*, 2021; Holmes *et al.*, 2021; Mohnike *et al.*, 2021). Conversely, *UGT74F1* and *UGT74F2* have been documented to be respectively induced during the seedling and germination stages under cold stress (Lee *et al.*, 2005; Klepikova *et al.*, 2019). With slower seedling greening observed under cold conditions and the induction of cold-related marker genes in *ugt74f1 ugt74f2* mutants (Fig. 26A, B), it is plausible that both genes operate synergistically under cold stress to modulate cold resilience.

Additionally, in the absence of UGT74F1 and UGT76B1, salt stress marker genes *SOS1/2/3* are induced, an induction not observed with the absence of UGT74F2 (Fig. 24A): this means that UGT74F1 and UGT76B1 suppress salt stress responses in naive state, and their loss may support an enhanced resistance towards salt stress. However, salt stress has been noted to stimulate the expression of UGT74F2 in leaves (Kreps *et al.*, 2002). This dynamic may explain the enhanced salt tolerance observed when two or more SA-GTs are absent (Fig. 24B).

Furthermore, all three SA-GTs exhibit significant upregulation in response to drought stress (Fig. S5; Xu *et al.*, 2023), aligning with their cumulative role under drought conditions where enhanced tolerance is accompanied by increased levels of free SA (Fig. 22B; 23A, B). It is important to note that the drought tolerance observed in SA-GT mutants correlates exclusively with SA levels. There is not any correlation between tolerances to other abiotic stresses and the levels of SAG/SGE. Consequently, the biological roles or reusability of SAG/SGE during abiotic stress responses remain unclear and warrant further investigation.

Existing literature supports the role of SA in promoting tolerance to a range of abiotic stresses in *Arabidopsis*, including salinity, osmotic stress, drought, and cold (Scott *et al.*, 2004; Jayakannan *et al.*, 2013; He *et al.*, 2014; Okuma *et al.*, 2014). In these stress scenarios, both UGT74F1 and UGT74F2 appear to act as negative regulators of SA, occasionally in conjunction with UGT76B1, aiding in maintaining homeostasis as endogenous SA levels increase. However, the specific enzymatic activities of UGT74F1 and UGT74F2 towards SA—which potentially underpin their varied roles under different abiotic stresses—warrant further exploration. Interestingly, UGT74F1 seems less responsive than UGT74F2 to various stimuli (Genevestigator plant database, https://genevestigator.com/support/data_plantbiology/). This discrepancy suggests that the constitutive expression of UGT74F1 in vasculature may primarily serve to maintain low free SA levels in these tissues, while UGT74F2 may operate

more adaptively, being inducible under abiotic stress conditions.

In conclusion, gene expression changes provoked by *ugt* mutations and phenotypic observations point towards a multifunctional and mutually modulating influence of the SA glucosyltransferases across various abiotic stressors.

3.2.4 Plant-wide expression patterns of SA-GTs

SA is ubiquitously present in both the roots and shoots of plants. Promoter-reporter analysis of the *Arabidopsis* SA biosynthesis genes *ICS1/2* reveals that SA is likely synthesized in both young and mature leaves, as well as in petioles and hypocotyls (Raskin *et al.*, 1990; Hunter *et al.*, 2013). Provided that SA is mobile via both the xylem and phloem (Maruri-López *et al.*, 2019), maintaining SA homeostasis necessitates modifications occurring throughout the entire plant.

In naïve plants, promoter::reporter lines indicate that UGT76B1 is predominantly expressed in the roots and localized within the cortex and endodermis cell layers (Fig. 17G, J). Expression in the leaves is elevated when plants are challenged by pathogens (von Saint Paul *et al.*, 2011). In contrast, UGT74F1 is found exclusively within the vascular system, specifically in the phloem companion cells, diverging from UGT76B1's expression pattern (Fig. 17B, E, H, K). UGT74F2 exhibits patchy expression in the shoot, with consistent expression in the root epidermis and cortex (Fig. 17C, F, I, L). These expression patterns align with publicly available *Arabidopsis* gene expression data and root single-cell transcript analyses (Winter *et al.*, 2007; Ryu *et al.*, 2019b). Collectively, the expression data suggest that UGT74F1 and UGT74F2, when acting together, influence most of the rosette, while collaboration with UGT76B1 ensures that SA-GTs are distributed from the surface to the center of the entire root system (Fig. 17M).

3.2.5 Exploring substrates of UGT76B1: immune regulation

While these three SA-GTs collectively modulate SA levels across the plant, each displays unique activity against different additional substrates, potentially linked to their respective spatial expressions. In complementation studies, UGT74F1 was unable to compensate for the absence of UGT76B1, even when expressed under the control of the UGT76B1 promoter and 5' UTR (Bauer, 2020; Fig. 21). This inability is likely due to UGT74F1’s lack of glycosylation activity toward NHP and ILA *in vitro* (Fig. 35). Similarly, another complementation construct, in which the UGT76B1 coding sequence was driven by the UGT74F1 regulatory element, failed to rescue the phenotypes of the *ugt76b1* mutant. This suggests that the spatial context of glucosylation by UGT76B1 is also crucial for its function (Fig. 21). Both grafting and TSKO experiments revealed that the absence of UGT76B1 in roots significantly enhances immunity

in shoots (Fig. 4, 6). Further grafting experiments using *ugt76b1 fmo1* roots confirmed that NHP acts as the key signal molecule transmitted from roots to regulate shoot defense (Fig. 5). Thus, the enhanced immunity observed in the *ugt76b1* mutant is attributable to the lack of NHP glucosylation in roots. The unmodified NHP triggers increased SA biosynthesis, leading to heightened defense responses (Fig. 4, 5, 6; Shields *et al*., 2022). This observation partially explains why the loss of UGT74F1 and/or UGT74F2 does not affect resistance to *Pst*. Free SA may undergo multiple alternative catabolic pathways, whereas the glucosylation of NHP is considered the primary mechanism for its inactivation. Consequently, the loss of UGT76B1 results in a more profound impact on plant immunity (Fig. 16, 20; Bauer *et al*., 2021; Mohnike *et al*., 2023).

3.2.6 Abiotic stress and additional substrates: UGT74F1 and UGT74F2

UGT74F1 and UGT74F2 together cover the entire rosette and likely modulate free SA levels in the shoot (Fig. 17M). Both enzymes can glycosylate AA, a precursor of tryptophan, which is a critical component in abiotic stress resilience and tolerance (Fig. 35; Quiel and Bender, 2003; Kaur *et al.*, 2015). The glycosylation of AA may attenuate the tryptophan biosynthesis pathway, as enhanced anthranilate synthase activity in maize has been linked to increased abiotic stress tolerance (Beltagy *et al*., 2019). Both rice and *Arabidopsis* exhibit stress-induced regulation of enzymes in the tryptophan biosynthesis pathway, including anthranilate synthase and tryptophan synthase (Zhao and Last, 1996; Ishihara *et al*., 2008).

The loss of UGT74F2 likely suppresses the glycosylation of stress-induced AA and its subsequent metabolite tryptophan, a precursor for essential compounds such as melatonin, glucosinolates, and indole-3-acetic acid (IAA) (Arnao and Hernández-Ruiz, 2006). Overexpression of melatonin biosynthesis genes in Arabidopsis has been shown to significantly improve salt tolerance by promoting melatonin accumulation and reducing oxidative damage (Wu *et al*., 2021). This observation suggests that the enhanced salt stress resilience observed in *ugt74f2* mutants may result from increased melatonin levels (Fig. 24). Furthermore, melatonin treatment has been reported to induce the expression of cold-related genes, such as *CBFs* and *COR15a*, which aligns with the upregulation of these genes in the *ugt74f1 ugt74f2* double mutant (Bajwa *et al.*, 2014). Additionally, several studies have demonstrated that IAA-mediated glucosinolate accumulation plays a critical role in drought tolerance in Arabidopsis (Salehin *et al*., 2019; Hornbacher *et al*., 2022). The enhanced drought tolerance in the *ugt74f2* mutant could be attributed to the suppression of AA glycosylation, which promotes the accumulation of glucosinolates.

SA has been shown to suppress the expression of *CBFs* and improve photosynthesis under cold stress in watermelon (Cheng et al., 2016). This could explain the contrasting roles of UGT76B1 and UGT74F1 under cold stress. The high endogenous SA level mutant *ugt76b1* shows downregulated *CBFs* expression, faster greening, and presumably lower resistance during germination under cold stress (Fig. 26B). In contrast, the low endogenous SA level mutant *ugt74f1 ugt74f2* displays higher *CBFs* expression, slower greening, and reduced photosynthetic ability. This difference may be attributed to their activity toward AA and another possible substrate, quercetin (Cartwright *et al*., 2008). Quercetin, a flavonol, and its derivatives have been positively correlated with freezing tolerance and cold acclimation (Schulz *et al*., 2015). The loss of both UGT74F proteins may lead to the accumulation of quercetin and its derivatives, thereby enhancing cold acclimation. Thus, the opposing phenotypes between these two SA-GT mutants likely result from their distinct specificities for different substrates.

Additionally, UGT74F2-mediated NA glycosylation may protect plant cells from NA toxicity during seed germination under salt and osmotic stress conditions (Li et al., 2015). However, NA appears to have an opposite effect in mature plants. Overexpression of nicotinamidase and exogenous application of its metabolite NA enhance drought tolerance and increase biomass in *Arabidopsis* and wheat (Ahmad *et al*., 2021; Khurshid *et al*., 2023). The enhanced tolerance of *ugt74f2*-related mutants to osmotic and drought stress may partially result from elevated NA levels in mature plants (Fig. 23, 25).

In summary, UGT76B1 processes substrates vital for plant defense and growth in addition to SA, while the substrates of UGT74F1 and UGT74F2 are either confirmed or suspected to play roles in abiotic stress responses. SA appears to serve as a central regulator of both biotic and abiotic stress resistance and tolerance, with these three SA-GTs coordinating its metabolism and function.

3.3 *In vitro* activity and specificity of three UGT enzymes

While all three UGT enzymes exhibit catalytic activity toward SA, their roles with other substrates remain largely unknown. In this study, the additional substrates of UGT76B1, namely ILA and NHP, were shown to be no substrates of either UGT74F1 or UGT74F2 (Fig. 32; 33). Likewise, UGT76B1 displayed no activity toward NA or AA. The individual and shared activities of these enzymes are summarized in Fig. 38.

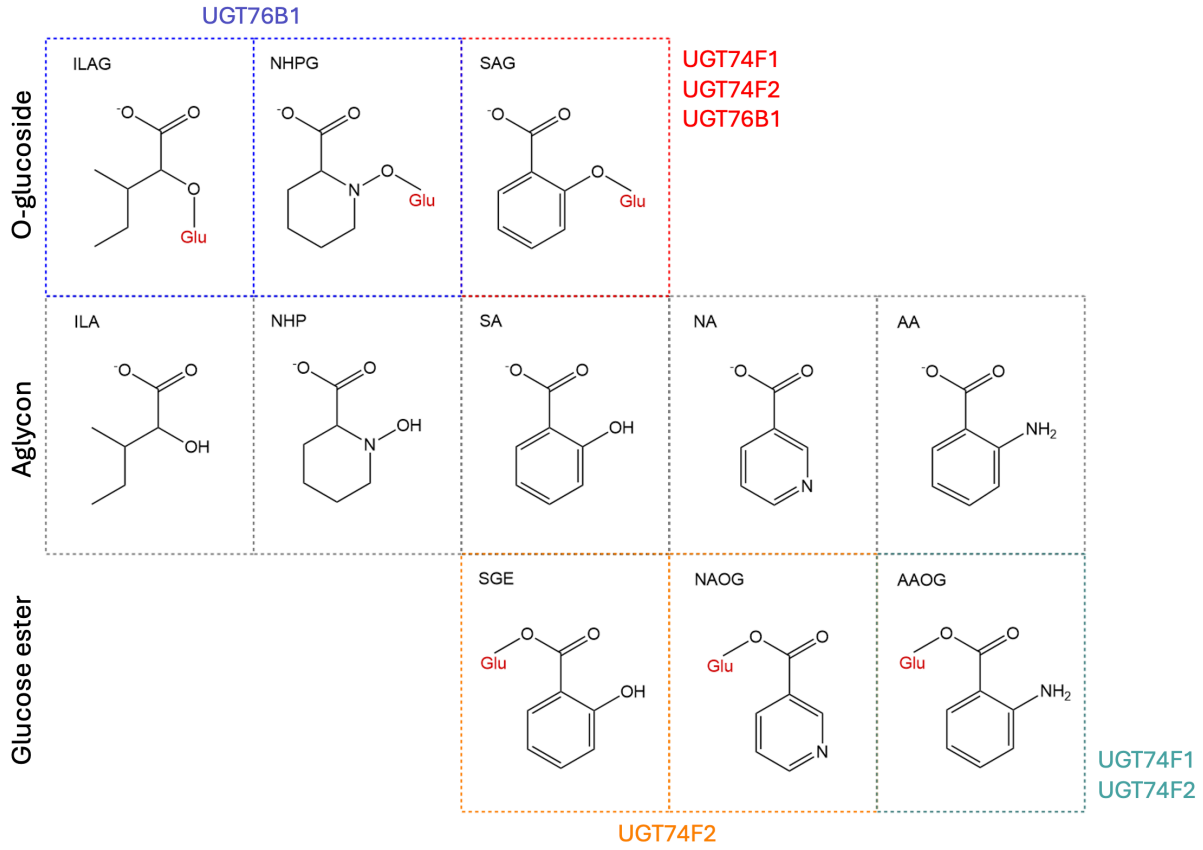

Fig. 38: Three SA-GTs and their known *in vivo* substrates and products. All three SA-GTs are known to produce SAG, and UGT74F2 produces SGE exclusively (Noutoshi *et al.*, 2012; George Thompson *et al.*, 2017). UGT76B1 has two additional hydroxy acid substrates, ILA and NHP (von Saint Paul *et al.*, 2011; Bauer *et al.,* 2021). Both UGT74F1 and UGT74F2 are active towards AA (Quiel and Bender, 2003), while UGT74F2 is active towards NA (Li *et al.*, 2015).

3.3.1 Ligand perception and catalysis

In ligand-docking simulations, all five ligands fit within the binding pockets of the three SA-GTs. Although a previous study suggested that ILA and NHP are bulkier than SA and may not fit into the binding pockets of UGT74F1 and UGT74F2 (Bauer, 2020), both UGT74F1 and UGT74F2 have been shown to catalyze larger molecules, such as the flavonoid quercetin and 1-methylindolyl-3-acetothiohydroximate, *in vitro* (Cartwright *et al.*, 2008; Grubb *et al.*, 2014). The catalytic activity of UGTs relies on a conserved catalytic triad, where modifications to any

of the triad residues result in a complete loss of SA activity in both UGT74F1 and UGT74F2 (George Thompson *et al.*, 2017). As proposed in catalytic mechanisms for UGTs, interactions between ligands and catalytic amino acids are essential for activity (Albesa-Jové and Guerin, 2016). According to the ligand docking results, the stable spatial position of a ligand determines its interaction with catalytic residues (Fig. 31-34). In the case of UGT74F2, the aromatic rings of SA, NA, and AA form Pi-Pi stacking interactions with three aromatic residues surrounding the binding pocket. This interaction stabilizes the ligands and positions them close to both UDP-Gluc and the catalytic residue His18. However, as NHP and ILA lack aromatic structures, they do not orient correctly within the binding pocket, making it unlikely for UGT74F2 to glucosylate these substrates. Although one study reported that UGT74F2 can produce an NHP glucose ester, the *in vivo* role of this activity remains to be investigated (Mohnike, 2023).

3.4 Outlook

This study investigates the distinct roles of three SA-GTs under various abiotic and biotic stresses, as well as their enzymatic activities toward different substrates. Due to their multiple enzymatic activities, the phenotypes of mutants under different stress conditions may result from the accumulation of multiple compounds. Testing the impact of single or combined application of these substrates on stress tolerance would be meaningful to elucidate their specific roles. Moreover, several intriguing GO categories were highlighted in the multiple comparisons, including *response to heat*, *response to light stimuli*, and *circadian rhythm*. These findings suggest that SA-GTs may have additional, as-yet-unidentified functions that could be explored phenotypically. The transcriptomic data provide a valuable resource for further investigation.

In the protein-ligand modeling part, the predicted enzyme activities aligned well with the results from *in vitro* experiments. Further modeling with additional substrates may be required to validate the reliability of this modeling pipeline and underlying theory. Additionally, this approach could guide enzyme mutagenesis, for example, by selectively removing activity toward specific substrates while retaining activity for others. This could be particularly interesting for UGT76B1, where removing its activity toward SA and NHP might enable the study of ILA independently. Currently, the strong impact of SA and NHP on plant phenotypes in the absence of UGT76B1 complicates the analysis of ILA's specific role.

Regarding root-shoot communication, UGT76B1 and FMO1 are coupled and exhibit sensitive regulation in response to (hemi)biotrophic and endophytic microbes, thereby influencing the shoot's defense or growth state. However, in response to most necrotrophic pathogens, only UGT76B1 appears to be responsive. Given that UGT76B1 is active toward the antimicrobial compound scopoletin (Mohnike, 2022), it is possible that UGT76B1 is additionally involved in an outward system to control the glucosylation and secretion of coumarins, operating in parallel with the inward UGT76B1-FMO1-NHP pathway for regulating systemic immunity. Additionally, conducting *in silico* simulations and *in vitro* enzyme assays for SA-GTs toward different coumarins could be worthwhile, as both UGT74F1 and UGT74F2 are also expressed in roots.

4 Material and method

4.1 Materials

4.1.1 Chemicals

The following chemicals were used for enzymatic reaction and standard for LCMS analysis: **Salicylic acid** (SA) from Roth (Germany); **N-hydroxypipcolic acid** (NHP) from MedChemExpress (US); **Isoleucic acid** (ILA, 61576-0468) from Interchim (France); **Nicotinic acid** (NA) from Duchefa Biochemie (Netherlands); **Anthranilic acid** (AA) and **uridine diphosphate glucose** (UDP-Glc) from Sigma-Aldrich; Additionally, **benzothiadiazole** (BTH, BION™) from Syngenta (Germany) was used as a salicylic acid analogue.

4.1.2 Medium

Half-strength Murashige and Skoog medium (½ MS) with vitamins (M0222.0050; Duchefa Biochemie, Netherlands; pH adjusted to 5.7), supplemented with 1% sucrose (4621.2, Roth, Germany) and 0.5% Gelrite (71010-52-1; Duchefa Biochemie, Netherlands) for solidified media. For grafting, MS medium without vitamins (M0221.0050; Duchefa Biochemie, Netherlands; pH adjusted to 5.7) was used, with the sucrose concentration adjusted as needed for different plates, and supplemented with 1% (w/v) agar (05039; Sigma-Aldrich, Germany).

LB medium: Prepared with 25 g/L Luria-Bertani (LB) (Duchefa, Netherlands) and 2 ml/L 1N NaOH; for solidified medium, 12.5 g/L agar (Duchefa, Netherlands) was added.

Nutrient-yeast extract glycerol (NYGA) agar (pH = 7): Prepared with 0.3% (w/v) Bacto yeast extract, 1.8% (w/v) Bacto agar, and 0.3% (w/v) Bacto peptone (all from BD Biosciences, US), and 2% (v/v) glycerol (Roth, Germany).

Vegetable juice sucrose (VJS) agar medium: Commercially available vegetable juice (Tomato-Vegetable Mix, Edeka, Germany) was used. For 1 liter of VJS medium, 850 ml deionized distilled water was supplemented with 150 ml vegetable juice and 0.5 g $CaCO_3$, and 40 g/L sucrose was added. The pH was adjusted to 5.8.

4.1.3 Antibiotics and herbicide

Kanamycin (working concentration: 60 µg/ml)**,** Rifampicin (100 µg/ml)**,** Spectinomycin (100 µg/ml), all from Sigma-Aldrich (Germany)**;** Gentamycin (25 µg/ml) from Roche (Germany)**.** Antibiotic stock solutions were stored at -20°C, dissolved in water except for rifampicin, which

was dissolved in DMSO. BASTA herbicide from Bayer (Hoechst, Germany) was diluted 1:800 and sprayed on rosette leaves under a laminar flow cabinet.

4.1.4 Primer list

Table 1: Primer sequences for RT-qPCR

Gene	AGI code	Forward primer sequences 5' to 3'	Reverse primer sequences 5' to 3'
UBQ5	AT3G62250	GGTGCTAAGAAGAGGAAGAAT	CTCCTTCTTCTGGTAAACGT
S16	AT5G18380 AT2G09990	TTTACGCCATCCGTCAGAGTAT	TCTGGTAACGAGAACGAGCAC
PR1	AT2G14610	GTGCCAAAGTGAGGTGTAACAA	CGTGTGTATGCATGATCACATC
PR2	AT3G57260	TGGTGTCAGATTCCGGTACA	CATCCCTGAACCTTCCTTGA
PR5	AT1G75040	ATCGGGAGATTGCAAATACG	GCGTAGCTATAGGCGTCAGG

Table 2: Primer sequences for mTFP-labelled complementation line

Cloning	Primer sequences 5' to 3'	
	Sequence	description
UGT76B1pro_GW_f	GGGGACAAGTTTGTACAAAAAAGCAG GCTcggttaaacataaaccatgt	5'-forward primer to amplify UGT76B1 promoter fragment with B1-GATEWAY extension
UGT76B1pro-mTFP-Hy_R	cctcgcccttgctcaccattttgttgtgaatttctctc	3'-reverse primer to amplify UGT76B1 promoter with mTFP overlap
UGT76B1pro-mTFP-Hy_F	gagagaaattcacaacaaaaATGgtgagcaaggg cgagg	5`-forward primer to amplify mTFP from pNIGEL19 with UGT76B1pro overlap
mTFP-UGT76B1utr-Hy_R	gttttgtttctctagtctccattcctgcacccttgtacagctc gtccatgc	3'-reverse primer to amplify mTFP with linker and UGT76B1 ATG start codon overlap
mTFP-UGT76B1utr-Hy_F	ctgtacaagggtgcaggaATGgagactagagaaac aaaacca	5'-primer to amplify the coding region of the UGT76B1 gene with linker and overlap to mTFP
UGT76B1gene_GW_R	GGGGACCACTTTGTACAAGAAAGCTG GGTctgtgatttctgctttctgat	3'-primer to amplify the UGT76B1 gene with B2 GATEWAY extension

Table 3: Primer sequences for TSKO

Cloning	Primer sequences 5' to 3'	
	Forward	Reverse
TSKO-promoter-CO2 N1/2	TTGAAGACATGGAGTAGCTTTGCTTTTTTCTT ATTAAG	TTGAAGACATATGGTATCGTTATTAACTAGG GTTCTTGA
TSKO-promoter-CASP1 N3/4	TTGAAGACATGGAGTTAAATGTGCATAAAAG TGAGTATG	TTGAAGACATATGGTTTCTCTTGCAATTGGG G
TSKO-sgRNA-mTFP N5/6	attGCTCCCAAGAGTAGCCCTCG	aaacCGAGGGCTACTCTTGGGAGC
TSKO-sgRNA-UGT76B1 N7/8	attgTTGGAGAGTTGAACTCAGTG	aaacCACTGAGTTCAACTGTCCAA

4.2 Plant material and cultivation

4.2.1 List of mutants

Several *A. thaliana* mutants or genetic crossings thereof were used in addition to wild type (accession Col, WT). Mutant lines were obtained from the *Arabidopsis* stock centers (Scholl *et al.*, 2000; Alonso *et al.*, 2003) unless otherwise indicated.

SA-GT mutant set: *ugt76b1-1* loss-of-function mutant (AT3G11340; SAIL_1171A11; von Saint Paul *et al.*, 2011). *ugt74f1-2* loss-of-function mutant was obtained by a CRISPR/Cas9-based deletion by former collegues (AT2G43840, Schäffner's Lab). *ugt74f2-2* loss-of-function mutant (AT2G43820; Quiel and Bender, 2003). *ugt74f1-3 ugt74f2-2* double mutant is generated by the same approach as *ugt74f1-2* but based on *ugt74f2-2* mutant. Other higher-order mutants were generated by genetic crossing by former collegues (Schäffner's Lab).

UGT76B1 and FMO1 fluorescent labelled transgenic line: The transgenic line *UGT76B1*$_{pro}$*:mTFP-UGT76B1* was generated to complement the *ugt76b1-1* mutant by expressing an N-terminal mTFP fusion of *UGT76B1* under the control of its native promoter. A Gibson assembly reaction (New England Biolabs, Germany) was used to fuse three fragments: (i) a 1754 bp *UGT76B1* promoter region, (ii) the mTFP coding sequence without a stop codon, and (iii) a *UGT76B1* gene segment including the ATG start codon and 505 bp of the 3'-UTR (Table. 3). This construct was recombined via pDONR221 (Invitrogen, Germany) into pAlligator2Δ35S, a modified version of pAlligator2 with the CaMV 35S promoter removed (Bensmihen *et al.*, 2004). The deletion was achieved by restriction enzyme digestion with EcoRI and HindIII, followed by blunt-ending using T4 DNA ligase and religation. The final vector was used for the Agrobacterium-mediated transformation of *ugt76b1-1* plants via the floral dip method(Clough and Bent, 1998). Segregation analysis identified two independent homozygous transgenic lines with single insertions. FMO1pro:FMO1-YFP transgenic complementation line is described by Joglekar *et al.*, 2018.

UGT76B1 TSKO line: UGT76B1 cortex- and endodermis-specific knockout lines are based on the *UGT76B1*$_{pro}$*:mTFP-UGT76B1* complementation line. Plasmids for tissue-specific genome editing were generated as previously described (Stuttmann *et al.*, 2021). Regulatory sequences of *At2g36100* (*CASP1*) and *At1g62500* (*Co2*) were amplified by PCR using oligonucleotides N1/2 and N3/4 (Extended Data Table. 4), respectively, and cloned into pAGM1251(Engler *et al.*, 2014) by BpiI restriction/ligation to yield pCK256 and pCK257. Subsequently, promoter elements were assembled with (NLS)mCherry-P2A (pCK237), zCas9i (pCK70), and rbcs-E9 (terminator, pJOG416) modules in pICH47742 to yield pCK259 and pCK260. These modules were further assembled in Level 2 acceptor pJOG292 (Ordon *et al.*, 2017) together with a BsaI-excisable *ccdB* cassette, the FAST seed fluorescence marker(Shimada *et al.*, 2010) and either a Basta (*CASP1*) or hygromycin (*Co2*) resistance cassette to yield pDGE1075 and pDGE1076, respectively. For the generation of final plant transformation vectors, oligonucleotides N5/6 and N7/8 were cloned into the sgRNA shuttle vector pDGE332 and pDGE334 (Table. 4), and the assembled sgRNA transcriptional units were mobilized into pDGE1075/1076 to yield pDGE1075-B1en and

pDGE1076-B1co. Final plasmids were transformed into *Agrobacterium tumefaciens* GV3101 pMP90 for plant transformation.

GUS reporter lines: *UGT76B1$_{pro}$:GFP-GUS* and *FMO1$_{pro}$:GUS* are described previously (Olszak *et al.*, 2006; von Saint Paul *et al.*, 2011). The promoters of *UGT74F1* (1894 bp upstream of the ATG start) and *UGT74F2* (2078 bp) are for the generation of corresponding GFP-GUS by former colleagues (Schäffner's Lab). The GUS reporter line is then introgression into different SA-GT mutant backgrounds by crossing.

Other lines used in this study: *fmo1-1* (SALK_026163; Mishina and Zeier, 2006b); *sid2 ugt76b1*, NahG *sid2 ugt76b1*, *fmo1 ugt76b1* (von Saint Paul *et al.*, 2011).

4.2.2 Conditions of plants grown on soil

Plants were cultivated in a controlled growth chamber under a 10 h light/14 h dark cycle at 22/18°C, 60/70% relative humidity, and 120 µmol m^{-2} s^{-1} light intensity (type 840 fluorescent lamps; Osram, Germany). They were grown on a mixture of peat moss-based substrate (Floragard Multiplication substrate, Germany) and quartz sand (12:1). A proportion of 6:1 was used for plant growth and monitoring in the phenotyping facility (Photon Systems Instruments).

4.2.3 Hydroponic culture and osmotic/salt stress

Hydroponic culture stock solutions were prepared, and a floating hydroponic system was established following Conn *et al.* (2013). *Arabidopsis* seeds were stratified for two days at 4°C, then transferred to a growth chamber under a 16 h light/8 h dark cycle at 22/18°C, with 60/70% relative humidity and 140 µmol m^{-2} s^{-1} light intensity. The hydroponic medium was replaced twice weekly. For salt and osmotic stress treatments, 1-week-old seedlings in hydroponic culture were supplemented with either 100 mM NaCl or 10% PEG8000. RGB and fluorescence images were taken at 2- and 3-weeks post-treatment.

4.2.4 Cold germination experiment

To test the cold resilience of *ugt* mutants, seeds were placed on half-strength MS medium with 1% sucrose. After stratification for two days at 4°C, plates were transferred to a growth chamber set to a 16 h light/8 h dark cycle at 4°C, with a light intensity of 100 µmol m^{-2} s^{-1}. Plates were removed after 4 weeks, and RGB and fluorescence images were taken.

4.2.5 Micrografting assay

The grafting protocol was adapted from a previous description (Christmann *et al.*, 2007). Seeds were sterilized and sown on half-strength MS medium without vitamins (Duchefa, The

Netherlands; 1% sucrose; 1% (w/v) bacteriological agar, Roth, Germany). After two days of stratification, plants were moved to a growth incubator (MLR 351H, Sanyo, Japan). For three days, seedlings were grown under constant light (50 µmol m^{-2} s^{-1}) at 22°C, then the light intensity was reduced to 10 µmol m^{-2} s^{-1} for two additional days to promote hypocotyl elongation. Seedlings were cut straight through the middle of the hypocotyls using a fresh razor blade, and rootstocks and scions were combined in desired combinations on half-strength MS medium with 0.5% sucrose (Fig. 39 for detailed operation illustration). The grafted seedlings were then grown vertically under constant light (10 µmol m^{-2} s^{-1}) at 27°C for one week, followed by one week at 50 µmol m^{-2} s^{-1} light under short-day conditions (10 h light at 22°C; 14 h dark at 17°C). Afterward, plants were transferred to square Petri dishes (Greiner Bio-One, Germany) containing 50 ml of half-strength MS medium without sucrose. Two weeks later, plants were examined to exclude any fusions that had developed adventitious roots. Whole rosettes were harvested for gene expression analysis. For disease assays, the plants were moved to a slurry soil and grown covered with a lid for two days to maintain high humidity. They were then cultivated under regular conditions for another two weeks before the assay.

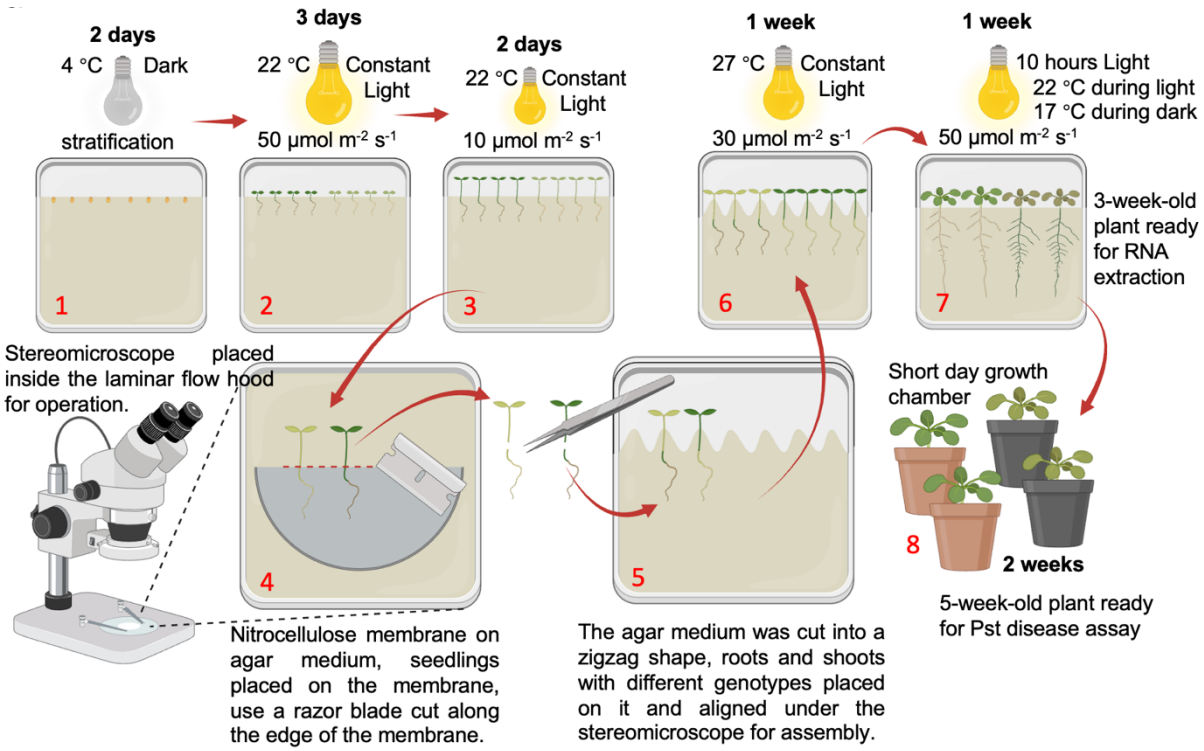

Fig. 39: Illustration of micrografting. The number in red represents the sequence of each step. Plants in different colors represent different genotypes.

4.2.6 Drought experiment

Plants for the drought experiment were grown in customized pots designed for the Photon Systems Instruments (PSI) phenotyping facility. Pots were filled with 150 ± 0.5 g of soil and

watered with 20 ml of NeemAzal®-T/S (diluted 1:1000) to control insect pests. During the seedling stage, plants were grown in a chamber with a 10 h light/14 h dark cycle at 22/18°C, 60/70% relative humidity, and 120 µmol m^{-2} s^{-1} light intensity. Lids were used to maintain moisture. Five-day-old seedlings were transferred to the PSI system, with each pot covered in blue material to mask the surrounding soil. The PSI light conditions were set to a mix of white, blue, and far-red light in a 35:5:15 ratio, averaging 120 µmol m^{-2} s^{-1}. Rosette area images were captured by the camera, and plants were watered daily at 6 a.m. by an autonomous system to maintain a pot weight of 175 g. After one week of acclimation, the watering amount was gradually reduced, allowing the pot weight to decrease by 2-3 g per day. Once the pot weight dropped to around 120 g, drought stress became visible, indicated by reduced chlorophyll fluorescence and shrinking rosette area. Rosettes were harvested at this time point for metabolomic analysis.

4.3 Molecular biology methods

4.3.1 *Arabidopsis* transformation

The floral dip method was used to transform the fluorescently labeled UGT76B1 transgenic line for the visualization of TSKO. Plants were initially grown in large round pots (approximately ten per pot) under short-day conditions until flowering, then switched to long-day conditions. A single colony of transformed *Agrobacterium tumefaciens* was inoculated in 2 ml LB medium (25 g/L LB, Duchefa, Netherlands; 2 ml/l 1N NaOH) containing antibiotics (rifampicin, 100 µg/ml, Sigma-Aldrich, Germany; gentamycin, 25 µg/ml, Roche, Germany; spectinomycin, 100 µg/ml, Sigma-Aldrich, Germany) to create a pre-culture. The bacteria were incubated overnight at 28 °C with shaking at 200 rpm. 1 ml of this pre-culture was transferred to 250 ml LB medium with the same antibiotics and grown overnight at 28 °C, 160 rpm, until reaching an OD600 of 1.5-1.6 (stationary phase). Bacterial cells were then harvested by centrifugation (10 min, 4 °C, 5,500 x g) and resuspended in 5% sucrose solution with 0.05% Silwet L-77 (Lehle Seeds, USA) to an OD600 of ~0.8. Flowering *Arabidopsis* plants were dipped in the bacterial suspension and soaked for 45 seconds, repeating the dip at least twice. The plants were then covered with plastic bags to maintain high humidity. After 24 hours, the plastic bags were removed, and the plants were grown for an additional 4-5 weeks until T0 seeds were harvested for further selection.

4.3.2 Selection of transgenic plants

The TSKO construct contains a seed coat-expressed RFP marker, while the fluorescently labeled *UGT76B1* transgenic line carries a seed coat-expressed GFP marker. The selection was based on both visible markers. T0 plants were grown, and seeds from individual T1 plants

were harvested. Under a microscope, seeds were examined to confirm a single insertion (3:1 segregation), and fluorescent seeds were selected for further cultivation. In the T2 generation, plants producing only fluorescent seeds were chosen.

For transgenic plants carrying the BASTA resistance gene, approximately two-week-old *A. thaliana* seedlings grown in soil were sprayed with BASTA solution (Phosphinothricin; Hoechst, Germany), diluted 1:800 in water. BASTA-resistant T1 plants were selected, and T2 progeny with a 3:1 segregation ratio (resistant to sensitive) after BASTA treatment were identified to confirm a single transgene insertion. These T2 plants were resown and further tested for BASTA sensitivity (leaf test) to ensure survival of sensitive individuals. Sensitive T2 plants may carry a mutation but lack the transgene, indicating a stable mutation without further CRISPR/Cas9 activity. For transgenic plants carrying the hygromycin resistance gene, selection was based on growth on half-strength MS plates containing 30 mg/L hygromycin.

4.3.3 RNA Extraction, cDNA Synthesis, and RT-qPCR

Total RNA was extracted using the protocol described by Zepeda and Verdonk (2022), with 70-100 mg of plant material per sample. RNA integrity and concentration were assessed by measuring absorbance at 260 nm and 280 nm using a Nanodrop ND-1000 spectrophotometer (Kisker-biotech, Germany) and through 1% agarose gel electrophoresis.

For cDNA synthesis, 1 µg of total RNA was reverse transcribed using the QuantiTect Reverse Transcription Kit (Qiagen, Netherlands) with removal of potential genomic DNA contamination. To verify the absence of genomic DNA, a TUBULIN9 PCR was performed using primers targeting an intron region; genomic DNA contamination was indicated by a larger PCR product.

In duplicate, real-time PCR quantification was conducted on a 7500 Real-Time PCR System (Applied Biosystems). PCR reactions were prepared in a total volume of 20 µl following the manufacturer's protocol, including 10 µl of 2x SensiMix™ SYBR Low-ROX (Bioline, USA) and 0.25 µM of each specific primer (Table 2). The cDNA samples were diluted 1:10. The cycling conditions were: 95 °C for 10 minutes (initial denaturation), followed by 40 cycles of 95 °C for 15 seconds, 55 °C for 30 seconds, and 72 °C for 45 seconds, with a final step of 95 °C for 15 seconds. A melting curve analysis was performed to ensure primer specificity.

UBQ5 and S16 were used as housekeeping genes for normalization. PR gene expression was measured as described by Alkooranee et al, (2015). Cycle values and reaction efficiency were extracted from raw data using the qPCR package (Spiess, 2018), and normalized relative quantities (NRQs) were calculated in Excel (Hellemans *et al.*, 2007). Grafting samples were analyzed according to the method described in Maksym (2018) for comparative purposes.

4.4 Microbiology assays

4.4.1 Bacterial inoculation and infection assays

Fully developed leaves from four- to five-week-old plants were gently pressure infiltrated with either 10 mM $MgCl_2$ (as a control) or suspensions of *Pst DC3000* in 10 mM $MgCl_2$. For basal resistance assays, plants inoculated with *Pst* (OD_{600} = 0.0001) were kept under the standard growth conditions for 3 days. Leaf discs from three independent plants (three discs per plant, pooled to form one biological sample) were collected at 2- and 72-hours post-inoculation, and immersed in 500 µl of 10 mM $MgCl_2$ solution containing 0.01% Silwet L77 (Momentive, USA; via Obermeier, Germany). Bacterial growth was quantified as previously described(Katagiri *et al.*, 2002). Each treatment was replicated five times, and the entire experiment was conducted independently twice.

4.4.2 Microbial culture conditions and inoculation assay

The fungal and oomycete strains used in this study are listed in Table. 5. Strains were cultured at 22°C on VJS agar medium (Osman *et al.*, 2020) (for *S. indica*, *V. longisporum*, and *P. parasitica*) or PDA medium (Sigma-Aldrich) for all other strains. For conidia harvesting, corresponding strains were grown in VJS liquid medium or PD broth (Sigma-Aldrich) at 24°C with shaking at 180 rpm. After 4 days of cultivation, the liquid cultures were filtered through cheesecloth to remove mycelium. The conidia suspension was then centrifuged at 2000 g for 10 minutes at 4°C, and the resulting pellet was washed twice with 10 mM MES buffer (pH 5.8) and resuspended in 0.05% Tween 20 solution. Conidia were counted using a hemocytometer, and the suspension was adjusted to a final concentration of 10^6 conidia ml^{-1}. For plant inoculation, 5 ml of the prepared conidia suspension was applied to the soil around the roots of 12-day-old plants (for growth measurement) and four-week-old plants (for *Pst* disease assays), taking care to avoid direct contact between the conidia and the rosette.

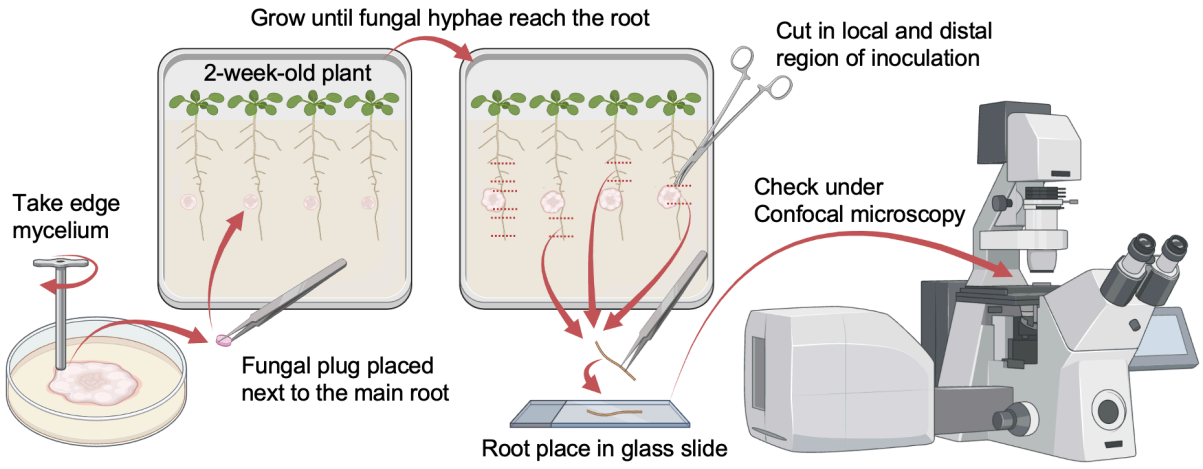

Fig. 40: Illustration of root microbe inoculation.

4.4.3 List of microorganisms

Species	Strain Designations	Source
Alternaria alternata	IMB 12090	DSMZ-German Collection of Microorganisms and Cell Cultures GmbH
Alternaria brassicicola	529	Günther Bahnweg, Helmholtz Center Munich, Germany
Aspergillus niger	Thor 2	DSMZ-German Collection of Microorganisms and Cell Cultures GmbH
Botrytis cinerea	310	DSMZ-German Collection of Microorganisms and Cell Cultures GmbH
Colletotrichum incanum	238704	Stéphane Hacquard, MPI für Züchtungsforschung Köln, Germany
Colletotrichum tofieldiae	861	Stéphane Hacquard, MPI für Züchtungsforschung Köln, Germany
Fusarium culmorum	IMB 12346	DSMZ-German Collection of Microorganisms and Cell Cultures GmbH
Fusarium graminearum	FR 26	DSMZ-German Collection of Microorganisms and Cell Cultures GmbH
Fusarium oxysporum	47	Christian Steinberg, INRAe UMR agroecologie
Fusarium oxysporum	5176	Günther Bahnweg, Helmholtz Center Munich, Germany
Laccaria bicolor	S238N	INRAe-Nancy, France
Meliniomyces bicolor	L9172K	University Tartu, Estonia
Mucor circinelloides	p8d0-3	J.Philipp Benz, TUM, Germany
Penicillium pinophilum	1960	DSMZ-German Collection of Microorganisms and Cell Cultures GmbH
Phytophthora parasitica	INRA-310	Wolfgang Dröge-Laser, Julius-Maximilians-Universität Würzburg, Germany
Sclerotinia scerotiorum	537	Günther Bahnweg, Helmholtz Center Munich, Germany
Serendipita indica	DSM 11827	Wolfgang Dröge-Laser, Julius-Maximilians-Universität Würzburg, Germany
Trichoderma hamatum	QL15d1	Monika Schmoll, Austrian Institute of Technology GmbG, Austria
Trichoderma harzianum	ES891	Monika Schmoll, Austrian Institute of Technology GmbG, Austria
Trichoderma velutinum	GL1561	Monika Schmoll, Austrian Institute of Technology GmbG, Austria
Trichoderma reesei	QM6a	Monika Schmoll, Austrian Institute of Technology GmbG, Austria
Ustilago nuda	265	Günther Bahnweg, Helmholtz Center Munich, Germany
Verticilium albo-atrum	334	Günther Bahnweg, Helmholtz Center Munich, Germany
Verticilium longisporum	Vl43	Wolfgang Dröge-Laser, Julius-Maximilians-Universität Würzburg, Germany

Table 4: Microbe strain number and source of origin.

4.5 Metabolic analysis

4.5.1 LC-MS analyses

Measurements with LC-MS were performed together with B. Lange (Institute of Biochemical Plant Pathology, Helmholtz Zentrum München). SA, SAG, SGE, NHP and NHP-*O*-Gluc were quantified using LC-MS following extraction from freeze-dried plant material(Bauer *et al.*, 2021). 5 µl of each extract was injected twice as technical replicates for the LC–MS analysis. NHP and NHP-*O*-Gluc were detected using positive ionization mode, while SA was measured in negative ionization mode. Authentic standards for SA (Sigma-Aldrich) and NHP (MedChemExpress, USA) were used for identification.

4.5.2 Glucosyltransferase activity assay with recombinant UGTs

Purification of recombinant enzymes and enzyme activity assays were conducted as described by Meßner *et al.* (2003) and von Saint Paul *et al.* (2011). Substrates with aromatic structures, including SA and AA, were analyzed using HPLC with a Diode Array Detector. Due to overlap with other compounds during HPLC elution, NA was visualized by thin-layer chromatography and fluorescent quenching on Silica gel 60 F254 plates (Merck, Germany; Li

et al., 2015) NHP and ILA were quantified using an HPLC-MS system as described by Bauer *et al.* (2021).

4.6 Expression analysis

4.6.1 Gene expression analysis by the public database

Expression patterns of the three UGT genes and *FMO1* were analyzed using publicly available data from ePlant (Waese *et al.*, 2017). The Heat Map Viewer provided an overview of the expression patterns for all three UGTs, while the Plant eFP Viewer was used to examine tissue-specific expression. Additionally, coexpression analysis between *UGT76B1* and genes involved in NHP and SA biosynthesis was obtained from ATTED-II: ath-m.c9-0 and ath-r.c5-0 (Obayashi *et al.*, 2022).

4.6.2 Histochemical localization of gene expression

Histochemical analyses of promoter::GUS reporter lines were conducted using 1 mM potassium ferrocyanide and ferricyanide(Lagarde *et al.*, 1996). *UGT76B1*pro plants were incubated for 30 minutes, while *FMO1*pro plants were stained for 12 hours. Chlorophyll was removed by destaining with 70% ethanol. Protein expression of *UGT76B1* and *FMO1* in roots was visualized using *UGT76B1*pro:mTFP-*UGT76B1* and *FMO1*pro:*FMO1*-YFP lines, respectively, with a confocal laser scanning microscope (SP8, Leica, Germany). For cell wall staining, two-week-old seedlings grown on vertical agar plates were treated with 50 µg ml^{-1} propidium iodide for 30 minutes and then rinsed twice with double-distilled water before imaging.

4.6.3 Confocal microscopy for gene expression and localization

To examine the expression patterns of *UGT76B1* and *FMO1* during interactions with various microbes, confocal microscopy was performed using a Leica SP8 microscope with a 40× water immersion objective. Fluorescence signals were captured with excitation at 458 nm for mTFP (emission window: 482-502 nm) and at 514 nm for YFP (emission window: 520-540 nm). Propidium iodide was also used, with an emission window of 626-646 nm, sharing the excitation light with either mTFP or YFP.

4.7 Protein structure prediction and ligand docking

The X-ray crystallography structure of UGT74F2 co-crystallized with SA was obtained from the Protein Data Bank (5U6M, George Thompson *et al.*, 2017). The X-ray structure of UGT76B1 was provided by R. Janowski (STB, Helmholtz Zentrum, München). Three predicted

SA-GT structures were retrieved from the AlphaFold Protein Structure Database (Jumper *et al.*, 2021). Protein-ligand induced fit docking was performed using the Schrödinger Maestro platform. For each protein-ligand pair, 50 poses were generated and clustered using the Conformer-Cluster function. The top-rated pose from each cluster was selected for Molecular Dynamics simulations, with each pose run 10 times for 10 ns. The pose with the most stable curve and lowest RMSD was chosen for protein-ligand interaction analysis (Miller *et al.*, 2021). 3D models of protein-ligand interactions were visualized using Schrödinger PyMOL software (Schrödinger and DeLano, 2020), while 2D amino acid-ligand interactions were illustrated with ChemDraw.

4.8 Statistics

Statistical analyses were conducted using R version 4.4.1 for Mac (https://www.r-project.org/). The WRS2 package, which utilizes Wilcox's WRS functions, was employed for the analysis. One-way multiple group comparisons were performed using the robust one-way analysis of variance (ANOVA) function t1way, followed by Lincon post hoc tests. Comparisons between two groups were made using Welch's two-sample t-tests.

5 Supplementary data

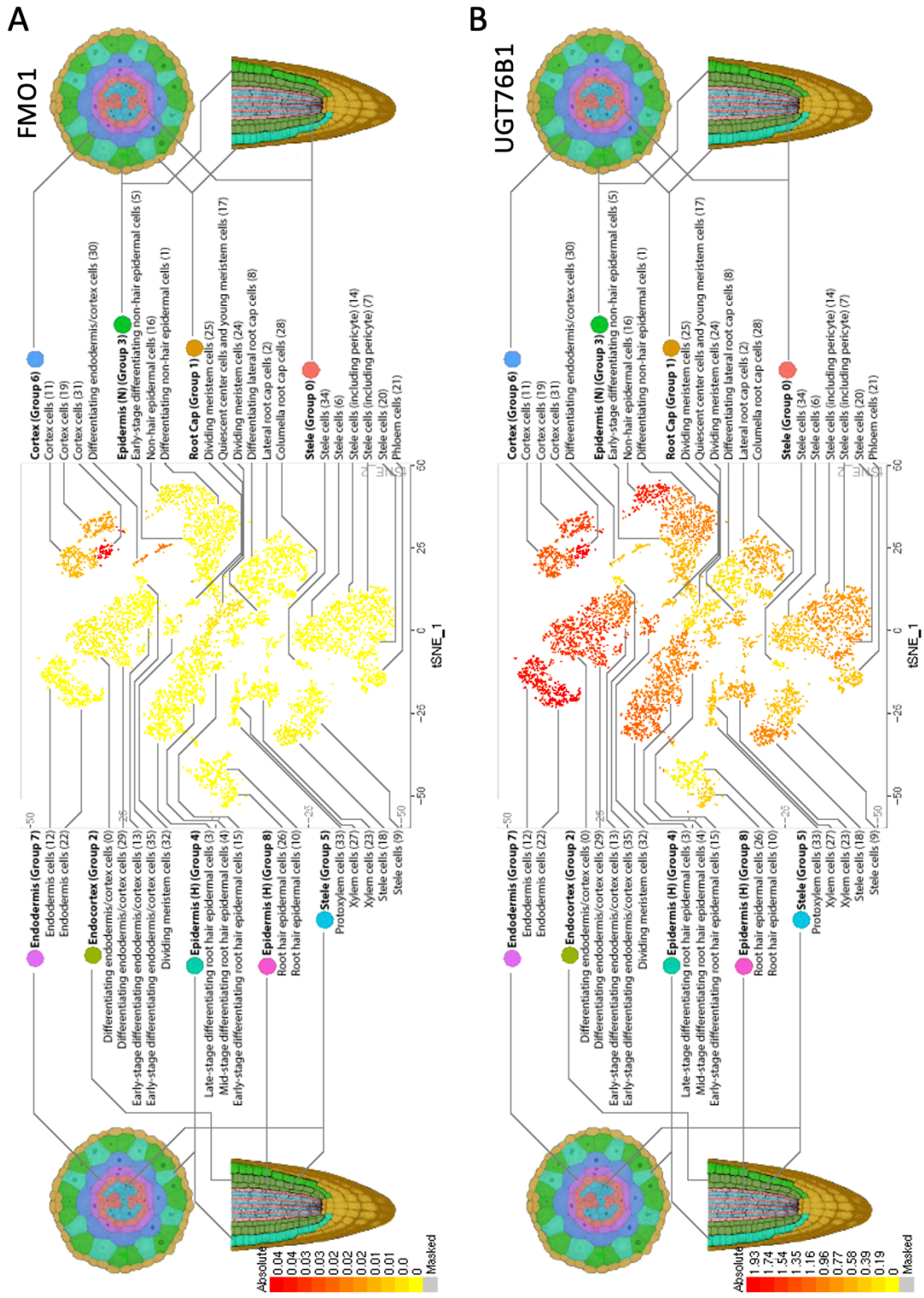

Fig. S1: Root expression profile of *FMO1* and *UGT76B1* by single cell sequencing. **A**, Expression pattern of FMO1 in the root, showing weak expression in the cortex and differentiating endodermis/cortex cells. **B**, Expression pattern of UGT76B1 in the root, with strong expression in the cortex and endodermis, and weaker expression in the epidermis and stele. The color code represents the absolute transcript levels. Images obtained from BAR, ePlant (https://bar.utoronto.ca/eplant/).

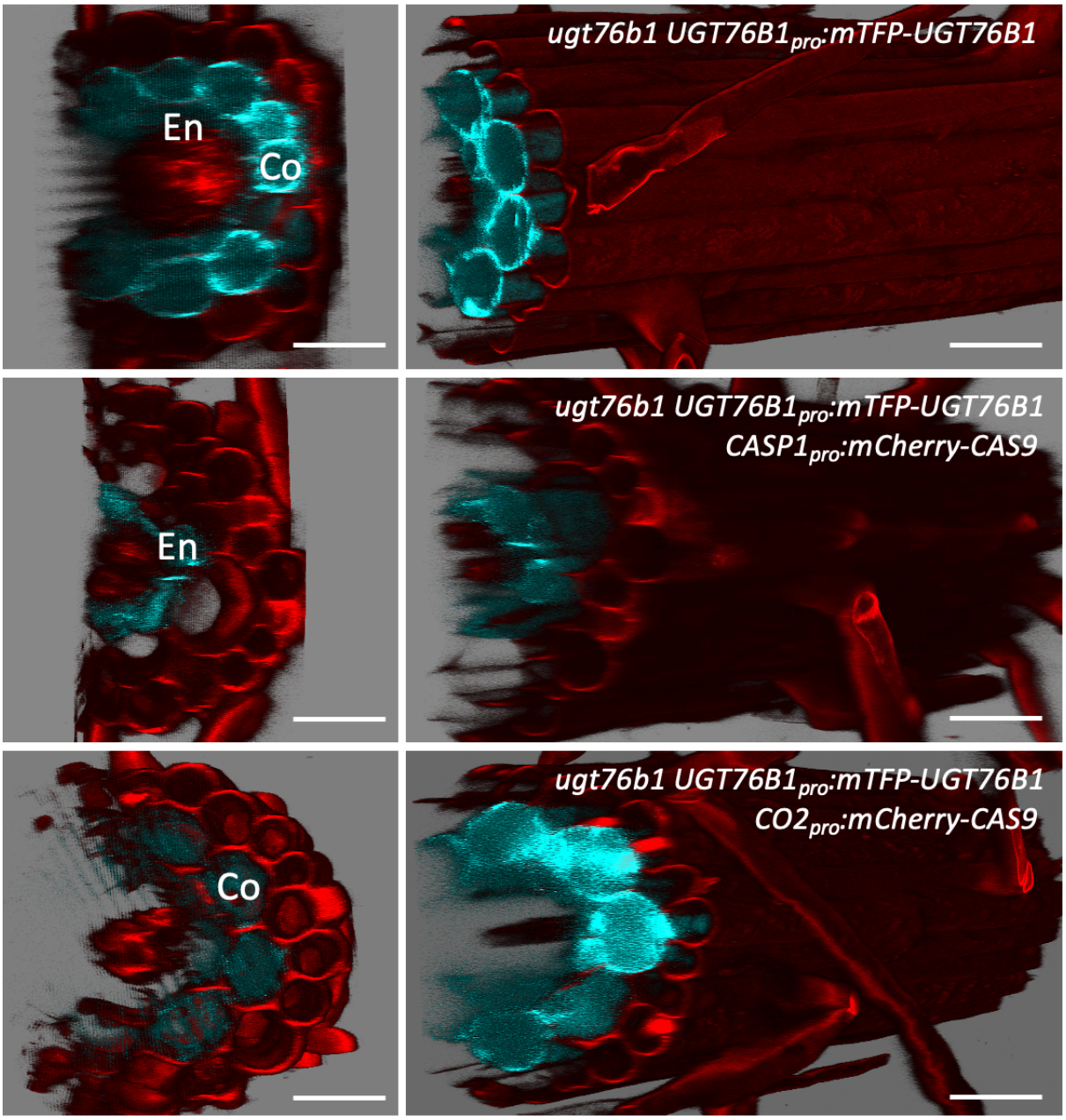

Fig. S2: Verification of tissue-specific knockout. Confocal microscopy visualization of tissue-specific knockout in 12-day-old plants grown on half-strength MS medium. The mTFP-UGT76B1 signal is shown in cyan, while the mCherry-Cas9 (red) is driven by the *CASP1* and *CO2* promoters in cortex and endodermis initial cells, respectively. The mTFP-UGT76B1 signal is absent in tissues where mCherry-Cas9 is expressed (By $CASP1_{pro}$*:mCherry-Cas9* and $CO2_{pro}$*:mCherry-Cas9* constructs). In the cortex knockout line, mCherry-Cas9 is expressed specifically in cortex initial cells, efficiently knocking out the gene, resulting in the absence of the mTFP-UGT76B1 signal in differentiated cortex cells. Bar, 30 µm.

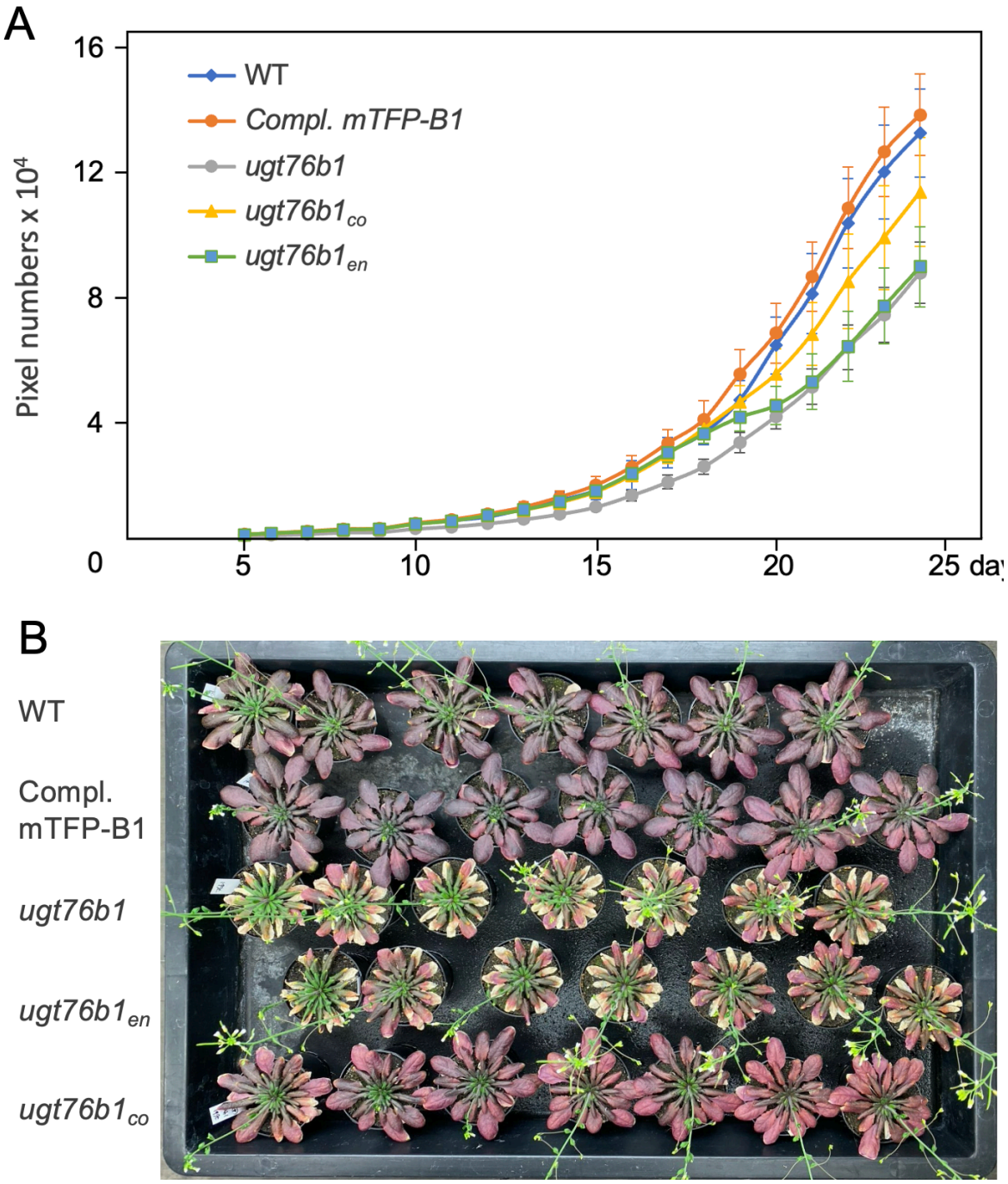

Fig. S3: Growth curve and leaf phenotypes. A, Growth monitoring of TSKO lines. Data collection began from 5-day-old plants, with leaf projection area determined by the region with active chlorophyll fluorescence by PSI system, measured daily at 6 a.m. WT and the complementation line exhibit similar leaf projection areas. *ugt76b1en* shows a growth pattern similar to the *ugt76b1* mutant, while *ugt76b1co* growth falls between that of WT and the *ugt76b1* mutant. *n* = 20, error bars represent standard deviation. **B**, Anthocyanin accumulation and early senescence induced by day length shift. Four-week-old plants grown under short-day conditions were shifted to long-day conditions for an additional week. *ugt76b1* and *ugt76b1*$_{en}$ exhibited similar early senescence phenotypes, with less visible purple color in the leaves, indicating reduced anthocyanin accumulation. *ugt76b1*$_{co}$ leaves displayed a visually lighter purple color compared to WT and the complementation line.

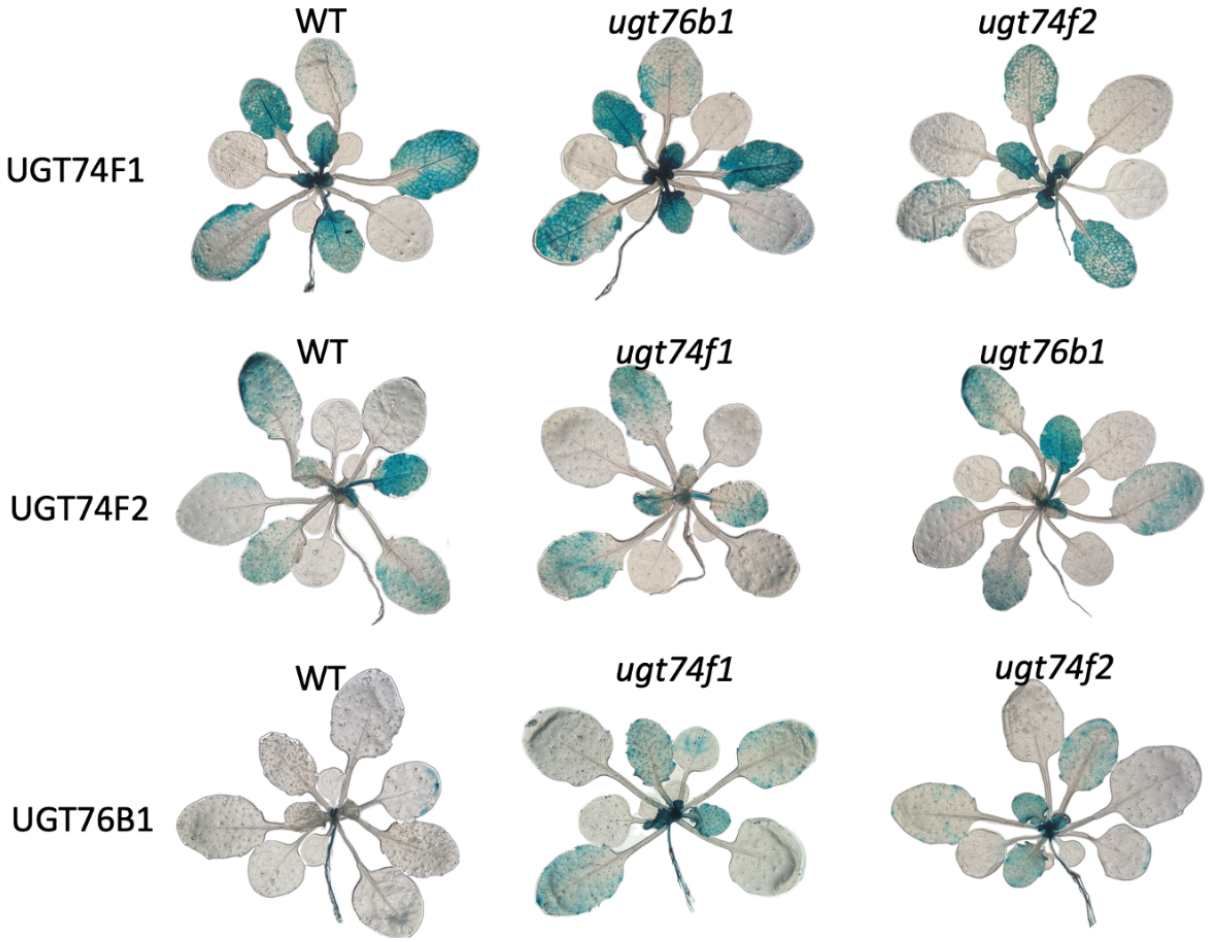

Fig. S4: Localized expression of UGT enzymes. Images of three-week-old soil grown plants after staining for GUS expression (40 min for UGT76B1, 120 min for UGT74F1, and 60 min for UGT74F2). Chlorophyll was removed by washing with 80° ethanol. The first column shows expression of *UGT76B1*, *UGT74F1* and *UGT74F2* in wild type background. The second and third columns show their expression in ugt mutant backgrounds as indicated.

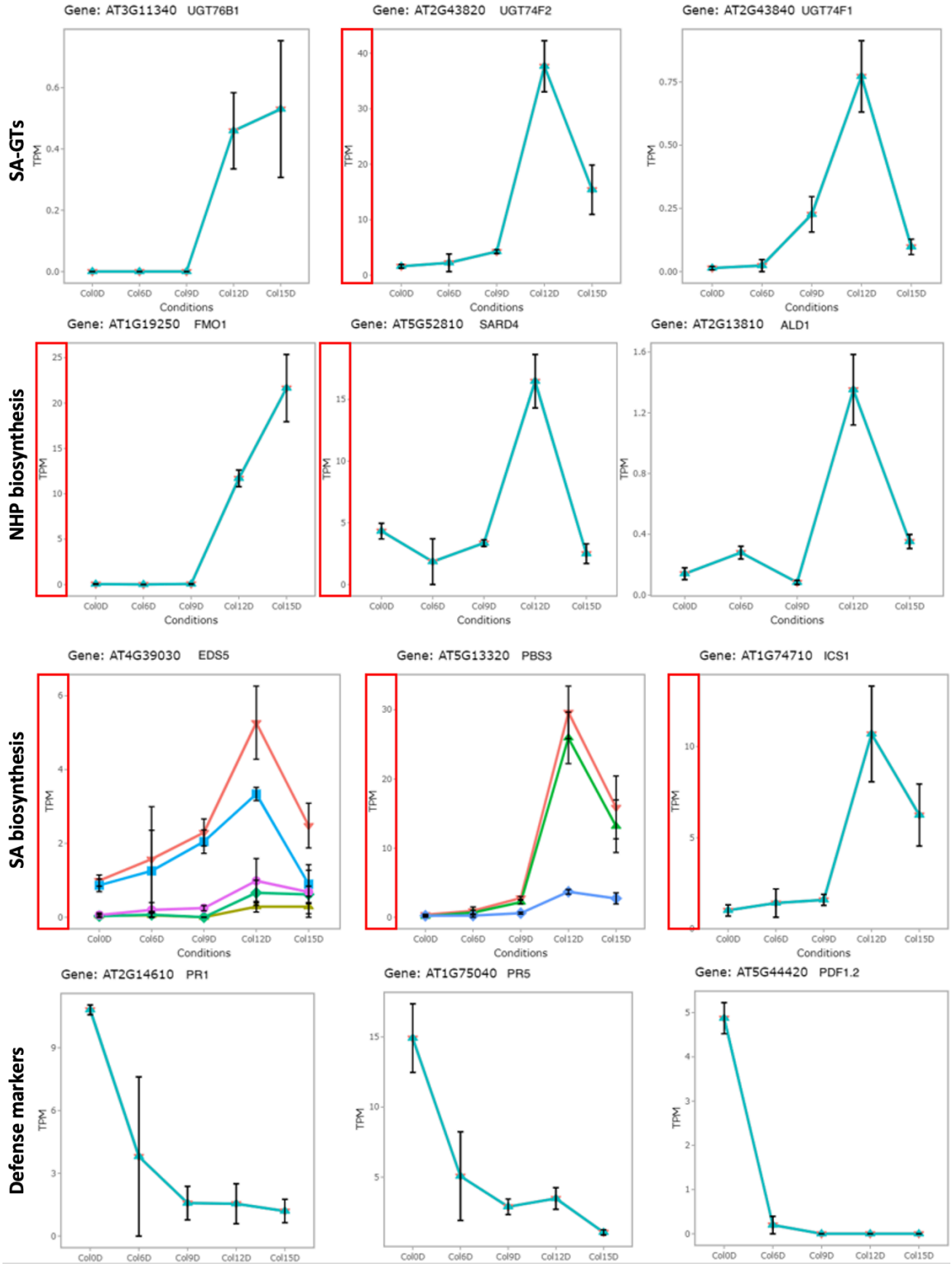

Fig. S5: Dynamic expression of SA-GTs, SA and NHP biosynthesis genes, and defense markers during drought stress. This graph presents the transcriptional changes as plants undergo drought stress, quantified as transcripts per million (TPM, Y-axis) over a period of days without watering (X-axis). Red square highlighted the high TPM changes. Each multi-curve, distinguished by color, corresponds to the different transcript of the gene, red curve stands for the sum of all transcripts. Error bars represent for the standard deviation of three biological replicates. The data is derived from RNA-seq datasets published by Xu *et al.*, 2023, and visualized using the 3D RNA-seq app available at https://3drnaseq.hutton.ac.uk/app_direct/3DRNAseq/.

6 Reference

Ahmad, Z., Bashir, K., Matsui, A., Tanaka, M., Sasaki, R., Oikawa, A., *et al.* (2021). Overexpression of nicotinamidase 3 (NIC3) gene and the exogenous application of nicotinic acid (NA) enhance drought tolerance and increase biomass in *Arabidopsis*. *Plant Mol Biol* 107, 63–84.

Albesa-Jové, D., and Guerin, M. E. (2016). The conformational plasticity of glycosyltransferases. *Curr Opin Struct Biol* 40, 23–32.

Alizadeh, H., Behboudi, K., Ahmadzadeh, M., Javan-Nikkhah, M., Zamioudis, C., Pieterse, C. M. J., *et al.* (2013). Induced systemic resistance in cucumber and *Arabidopsis thaliana* by the combination of *Trichoderma harzianum* Tr6 and *Pseudomonas sp.* Ps14. *Biological Control* 65, 14–23.

Alkooranee, J. T., Yin, Y., Aledan, T. R., Jiang, Y., Lu, G., Wu, J., *et al.* (2015). Systemic resistance to powdery mildew in *Brassica napus* (AACC) and *Raphanus alboglabra* (RRCC) by *Trichoderma harzianum* TH12. *PLoS One* 10, e0142177.

Alonso, J. M., Stepanova, A. N., Leisse, T. J., Kim, C. J., Chen, H., Shinn, P., *et al.* (2003). Genome-wide insertional mutagenesis of *Arabidopsis thaliana*. *Science* 301, 653–657.

Alonso-Ramírez, A., Poveda, J., Martín, I., Hermosa, R., Monte, E., and Nicolás, C. (2014). Salicylic acid prevents *Trichoderma harzianum* from entering the vascular system of roots. *Mol Plant Pathol* 15, 823–831.

Azooz, M. M. (2009). Salt stress mitigation by seed priming with salicylic acid in two faba bean genotypes differing in salt tolerance. *Int J Agric Biol* 11, 343–350.

Bandurska, H., and Stroi ski, A. (2005). The effect of salicylic acid on barley response to water deficit. *Acta Physiol Plant* 27, 379–386.

Bauer, S. (2020). The *Arabidopsis* glucosyltransferase UGT76B1 as a major hub in salicylic acid-related plant defence. Dissertation, Ludwig-Maximilians-Universität Munich.

Bauer, S., Mekonnen, D. W., Geist, B., Lange, B., Ghirardo, A., Zhang, W., *et al.* (2020). The isoleucic acid triad: distinct impacts on plant defense, root growth, and formation of reactive oxygen species. *J Exp Bot* 71, 4258–4270.

Bauer, S., Mekonnen, D. W., Hartmann, M., Yildiz, I., Janowski, R., Lange, B., *et al.* (2021). UGT76B1, a promiscuous hub of small molecule-based immune signaling, glucosylates N-hydroxypipecolic acid, and balances plant immunity. *Plant Cell* 33, 714–734.

Beltagy, K. M., Abdel-Rahman, M. M., Abouzied, H. M., and Madkour, S. A. (2019). Enhance maize (Zea mays L.) tolerance to abiotic stress through the genetic transformation with anthranilate synthase (ASA2 Gene) using particle bombardment. *American Journal of Bioscience and Bioengineering* 7, 28–33.

Reference

Bensmihen, S., To, A., Lambert, G., Kroj, T., Giraudat, J., and Parcy, F. (2004). Analysis of an activated ABI5 allele using a new selection method for transgenic *Arabidopsis* seeds. *FEBS Lett* 561, 127–131.

Boachon, B., Gamir, J., Pastor, V., Erb, M., Dean, J. V, Flors, V., *et al.* (2014). Role of two UDP-Glycosyltransferases from the L group of *Arabidopsis* in resistance against *Pseudomonas syringae*. *Eur J Plant Pathol* 139, 707–720.

Bowles, D., Lim, E.-K., Poppenberger, B., and Vaistij, F. E. (2006). Glycosyltransferases of lipophilic small molecules. *Annu. Rev. Plant Biol.* 57, 567–597.

Cai, J., Jozwiak, A., Holoidovsky, L., Meijler, M. M., Meir, S., Rogachev, I., *et al.* (2021). Glycosylation of N-hydroxy-pipecolic acid equilibrates between systemic acquired resistance response and plant growth. *Mol Plant* 14, 440–455.

Cao, Y., Zhang, Z.-W., Xue, L.-W., Du, J.-B., Shang, J., Xu, F., *et al.* (2009). Lack of salicylic acid in *Arabidopsis* protects plants against moderate salt stress. *Zeitschrift für Naturforschung C* 64, 231–238.

Cartwright, A. M., Lim, E.-K., Kleanthous, C., and Bowles, D. J. (2008). A kinetic analysis of regiospecific glucosylation by two glycosyltransferases of *Arabidopsis thaliana*: domain swapping to introduce new activities. *Journal of biological chemistry* 283, 15724–15731.

Chang, C.-Y., Hsieh, Y.-H., Cheng, K.-Y., Hsieh, L.-L., Cheng, T.-C., and Yao, K.-S. (2008). Effect of pH on Fenton process using estimation of hydroxyl radical with salicylic acid as trapping reagent. *Water Science and Technology* 58, 873–879.

Chen, H., and Li, X. (2017). Identification of a residue responsible for UDP-sugar donor selectivity of a dihydroxybenzoic acid glycosyltransferase from *Arabidopsis* natural accessions. *The Plant Journal* 89, 195–203.

Chen, Y.-C., Holmes, E. C., Rajniak, J., Kim, J.-G., Tang, S., Fischer, C. R., *et al.* (2018). N-hydroxy-pipecolic acid is a mobile metabolite that induces systemic disease resistance in *Arabidopsis*. *Proceedings of the National Academy of Sciences* 115, E4920–E4929.

Chen, Z., Malamy, J., Henning, J., Conrath, U., Sánchez-Casas, P., Silva, H., *et al.* (1995). Induction, modification, and transduction of the salicylic acid signal in plant defense responses. *Proceedings of the National Academy of Sciences* 92, 4134–4137.

Cheng, F., Lu, J., Gao, M., Shi, K., Kong, Q., Huang, Y., *et al.* (2016). Redox signaling and CBF-responsive pathway are involved in salicylic acid-improved photosynthesis and growth under chilling stress in watermelon. *Front Plant Sci* 7, 1519.

Chinnusamy, V., Ohta, M., Kanrar, S., Lee, B., Hong, X., Agarwal, M., *et al.* (2003). ICE1: a regulator of cold-induced transcriptome and freezing tolerance in *Arabidopsis*. *Genes Dev* 17, 1043–1054.

Christmann, A., Weiler, E. W., Steudle, E., and Grill, E. (2007). A hydraulic signal in root-to-shoot signalling of water shortage. *The Plant Journal* 52, 167–174.

Cleland, C. F., and Ajami, A. (1974). Identification of the flower-inducing factor isolated from aphid honeydew as being salicylic acid. *Plant Physiol* 54, 904–906.

Clough, S. J., and Bent, A. F. (1998). Floral dip: a simplified method for Agrobacterium-mediated transformation of *Arabidopsis thaliana*. *The plant journal* 16, 735–743.

Conn, S. J., Hocking, B., Dayod, M., Xu, B., Athman, A., Henderson, S., *et al.* (2013). Protocol: optimising hydroponic growth systems for nutritional and physiological analysis of *Arabidopsis thaliana* and other plants. *Plant Methods* 9, 1–11.

Contreras-Cornejo, H. A., Macías-Rodríguez, L., Beltrán-Peña, E., Herrera-Estrella, A., and López-Bucio, J. (2011). *Trichoderma*-induced plant immunity likely involves both hormonal-and camalexin-dependent mechanisms in *Arabidopsis thaliana* and confers resistance against necrotrophic fungi *Botrytis cinerea*. *Plant Signal Behav* 6, 1554–1563.

Cui, H., Tsuda, K., and Parker, J. E. (2015). Effector-triggered immunity: from pathogen perception to robust defense. *Annu Rev Plant Biol* 66, 487–511.

De Kesel, J., Conrath, U., Flors, V., Luna, E., Mageroy, M. H., Mauch-Mani, B., *et al.* (2021). The induced resistance lexicon: do's and don'ts. *Trends Plant Sci* 26, 685–691.

Dean, J. V, and Delaney, S. P. (2008). Metabolism of salicylic acid in wild-type, ugt74f1 and ugt74f2 glucosyltransferase mutants of *Arabidopsis thaliana*. *Physiol Plant* 132, 417–425.

Dempsey, D. A., Vlot, A. C., Wildermuth, M. C., and Klessig, D. F. (2011). Salicylic acid biosynthesis and metabolism. *The Arabidopsis book/American Society of Plant Biologists* 9.

Ding, P., and Ding, Y. (2020). Stories of salicylic acid: a plant defense hormone. *Trends Plant Sci* 25, 549–565.

Ding, Y., Sun, T., Ao, K., Peng, Y., Zhang, Y., Li, X., *et al.* (2018). Opposite roles of salicylic acid receptors NPR1 and NPR3/NPR4 in transcriptional regulation of plant immunity. *Cell* 173, 1454–1467.

Duan, L., Liu, H., Li, X., Xiao, J., and Wang, S. (2014). Multiple phytohormones and phytoalexins are involved in disease resistance to *Magnaporthe oryzae* invaded from roots in rice. *Physiol Plant* 152, 486–500.

Edgar, C. I., McGrath, K. C., Dombrecht, B., Manners, J. M., Maclean, D. C., Schenk, P. M., *et al.* (2006). Salicylic acid mediates resistance to the vascular wilt pathogen *Fusarium oxysporum* in the model host *Arabidopsis thaliana*. *Australasian Plant Pathology* 35, 581–591.

Engler, C., Youles, M., Gruetzner, R., Ehnert, T.-M., Werner, S., Jones, J. D. G., *et al.* (2014). A golden gate modular cloning toolbox for plants. *ACS Synth Biol* 3, 839–843.

Eudes, A., Mouille, G., Thevenin, J., Goyallon, A., Minic, Z., and Jouanin, L. (2008). Purification, cloning and functional characterization of an endogenous beta-glucuronidase in *Arabidopsis thaliana*. *Plant Cell Physiol* 49, 1331–1341.

Fu, Z. Q., and Dong, X. (2013). Systemic acquired resistance: turning local infection into global defense. *Annu Rev Plant Biol* 64, 839–863.

Gaffney, T., Friedrich, L., Vernooij, B., Negrotto, D., Nye, G., Uknes, S., *et al.* (1993). Requirement of salicylic acid for the induction of systemic acquired resistance. *Science (1979)* 261, 754–756.

Garcion, C., and Métraux, J.-P. (2008). Salicylic acid. *Plant Hormone Signal* 24, 229–255.

George Thompson, A. M., Iancu, C. V, Neet, K. E., Dean, J. V, and Choe, J. (2017). Differences in salicylic acid glucose conjugations by UGT74F1 and UGT74F2 from *Arabidopsis thaliana*. *Sci Rep* 7, 46629.

Grubb, C. D., Zipp, B. J., Kopycki, J., Schubert, M., Quint, M., Lim, E., *et al.* (2014). Comparative analysis of Arabidopsis UGT 74 glucosyltransferases reveals a special role of UGT74C1 in glucosinolate biosynthesis. *The Plant Journal* 79, 92–105.

Guo, B., Liu, C., Liang, Y., Li, N., and Fu, Q. (2019). Salicylic acid signals plant defence against cadmium toxicity. *Int J Mol Sci* 20, 2960.

Hacquard, S., Kracher, B., Hiruma, K., Münch, P. C., Garrido-Oter, R., Thon, M. R., *et al.* (2016). Survival trade-offs in plant roots during colonization by closely related beneficial and pathogenic fungi. *Nat Commun* 7, 11362.

Haroth, S., Feussner, K., Kelly, A. A., Zienkiewicz, K., Shaikhqasem, A., Herrfurth, C., *et al.* (2019). The glycosyltransferase UGT76E1 significantly contributes to 12-*O*-glucopyranosyl-jasmonic acid formation in wounded *Arabidopsis thaliana* leaves. *Journal of Biological Chemistry* 294, 9858–9872.

Hartmann, M., and Zeier, J. (2019). N-hydroxypipecolic acid and salicylic acid: a metabolic duo for systemic acquired resistance. *Curr Opin Plant Biol* 50, 44–57.

Hartmann, M., Zeier, T., Bernsdorff, F., Reichel-Deland, V., Kim, D., Hohmann, M., *et al.* (2018). Flavin monooxygenase-generated N-hydroxypipecolic acid is a critical element of plant systemic immunity. *Cell* 173, 456–469.

He, Q., Zhao, S., Ma, Q., Zhang, Y., Huang, L., Li, G., *et al.* (2014). Endogenous salicylic acid levels and signaling positively regulate *Arabidopsis* response to polyethylene glycol-simulated drought stress. *J Plant Growth Regul* 33, 871–880.

Hellemans, J., Mortier, G., De Paepe, A., Speleman, F., and Vandesompele, J. (2007). qBase relative quantification framework and software for management and automated analysis of real-time quantitative PCR data. *Genome Biol* 8, 1–14.

Hok, S., Danchin, E. G. J., Allasia, V., Panabières, F., Attard, A., and Keller, H. (2011). An *Arabidopsis* (malectin-like) leucine-rich repeat receptor-like kinase contributes to downy mildew disease. *Plant Cell Environ* 34, 1944–1957.

Holmes, E. C., Chen, Y.-C., Mudgett, M. B., and Sattely, E. S. (2021). *Arabidopsis* UGT76B1 glycosylates N-hydroxy-pipecolic acid and inactivates systemic acquired resistance in tomato. *Plant Cell* 33, 750–765.

Holmes, E. C., Chen, Y.-C., Sattely, E. S., and Mudgett, M. B. (2019). An engineered pathway for N-hydroxy-pipecolic acid synthesis enhances systemic acquired resistance in tomato. *Sci Signal* 12, eaay3066.

Horváth, E., Csiszár, J., Gallé, Á., Poór, P., Szepesi, Á., and Tari, I. (2015). Hardening with salicylic acid induces concentration-dependent changes in abscisic acid biosynthesis of tomato under salt stress. *J Plant Physiol* 183, 54–63.

Horváth, E., Szalai, G., and Janda, T. (2007). Induction of abiotic stress tolerance by salicylic acid signaling. *J Plant Growth Regul* 26, 290–300.

Hossain, M. M., Sultana, F., Kubota, M., and Hyakumachi, M. (2008). Differential inducible defense mechanisms against bacterial speck pathogen in *Arabidopsis thaliana* by plant-growth-promoting-fungus *Penicillium sp.* GP16-2 and its cell free filtrate. *Plant Soil* 304, 227–239.

Huang, X., Zhu, G., Liu, Q., Chen, L., Li, Y., and Hou, B. (2018). Modulation of plant salicylic acid-associated immune responses via glycosylation of dihydroxybenzoic acids. *Plant Physiol* 176, 3103–3119.

Hunter, L. J. R., Westwood, J. H., Heath, G., Macaulay, K., Smith, A. G., MacFarlane, S. A., *et al.* (2013). Regulation of RNA-dependent RNA polymerase 1 and isochorismate synthase gene expression in *Arabidopsis*. *PLoS One* 8, e66530.

Iavicoli, A., Boutet, E., Buchala, A., and Métraux, J.-P. (2003). Induced systemic resistance in *Arabidopsis thaliana* in response to root inoculation with *Pseudomonas fluorescens* CHA0. *Molecular plant-microbe interactions* 16, 851–858.

Ignatenko, A., Talanova, V., Repkina, N., and Titov, A. (2019). Exogenous salicylic acid treatment induces cold tolerance in wheat through promotion of antioxidant enzyme activity and proline accumulation. *Acta Physiol Plant* 41, 1–10.

Ishihara, A., Hashimoto, Y., Tanaka, C., Dubouzet, J. G., Nakao, T., Matsuda, F., *et al.* (2008). The tryptophan pathway is involved in the defense responses of rice against pathogenic infection via serotonin production. *The Plant Journal* 54, 481–495.

Jayakannan, M., Bose, J., Babourina, O., Rengel, Z., and Shabala, S. (2013). Salicylic acid improves salinity tolerance in *Arabidopsis* by restoring membrane potential and preventing salt-induced K+ loss via a GORK channel. *J Exp Bot* 64, 2255–2268.

Joglekar, S. (2014). Dissection of EDS1-dependent and salicylic acid-independent defence signalling pathways in *Arabidopsis thaliana*: a chemical biology approach. Dissertation, University of Cologne.

Joglekar, S., Suliman, M., Bartsch, M., Halder, V., Maintz, J., Bautor, J., *et al.* (2018). Chemical activation of EDS1/PAD4 signaling leading to pathogen resistance in *Arabidopsis*. *Plant Cell Physiol* 59, 1592–1607.

Jones, J. D. G., and Dangl, J. L. (2006). The plant immune system. *Nature* 444, 323–329.

Reference

Jumper, J., Evans, R., Pritzel, A., Green, T., Figurnov, M., Ronneberger, O., *et al.* (2021). Highly accurate protein structure prediction with AlphaFold. *Nature* 596, 583–589.

Kang, H., and Saltveit, M. E. (2002). Chilling tolerance of maize, cucumber and rice seedling leaves and roots are differentially affected by salicylic acid. *Physiol Plant* 115, 571–576.

Katagiri, F., Thilmony, R., and He, S. Y. (2002). The *Arabidopsis thaliana-Pseudomonas syringae* interaction. *The Arabidopsis Book/American Society of Plant Biologists* 1.

Kaur, H., Mukherjee, S., Baluska, F., and Bhatla, S. C. (2015). Regulatory roles of serotonin and melatonin in abiotic stress tolerance in plants. *Plant Signal Behav* 10, e1049788.

Kawano, T., Tanaka, S., Kadono, T., and Muto, S. (2004). Salicylic acid glucoside acts as a slow inducer of oxidative burst in tobacco suspension culture. *Zeitschrift für Naturforschung C* 59, 684–692.

Kleifeld, O., and Chet, I. (1992). *Trichoderma harzianum*—interaction with plants and effect on growth response. *Plant Soil* 144, 267–272.

Klein, M., and Papenbrock, J. (2008). "Sulfotransferases and their role in glucosinolate biosynthesis," in *Sulfur assimilation and abiotic stress in plants*, (Springer), 149–166.

Klepikova, A. V, Kulakovskiy, I. V, Kasianov, A. S., Logacheva, M. D., and Penin, A. A. (2019). An update to database TraVA: organ-specific cold stress response in *Arabidopsis thaliana*. *BMC Plant Biol* 19, 29–40.

Knoester, M., Pieterse, C. M. J., Bol, J. F., and Van Loon, L. C. (1999). Systemic resistance in *Arabidopsis* induced by rhizobacteria requires ethylene-dependent signaling at the site of application. *Molecular Plant-Microbe Interactions* 12, 720–727.

Kojima, H., Hossain, M. M., Kubota, M., and Hyakumachi, M. (2013). Involvement of the salicylic acid signaling pathway in the systemic resistance induced in *Arabidopsis* by plant growth-promoting fungus *Fusarium equiseti* GF19-1. *J Oleo Sci* 62, 415–426.

Korkmaz, A., Uzunlu, M., and Demirkiran, A. R. (2007). Treatment with acetyl salicylic acid protects muskmelon seedlings against drought stress. *Acta Physiol Plant* 29, 503–508.

Korolev, N., Rav David, D., and Elad, Y. (2008). The role of phytohormones in basal resistance and *Trichoderma*-induced systemic resistance to Botrytis cinerea in *Arabidopsis thaliana*. *BioControl* 53, 667–683.

Kosová, K., Prášil, I. T., Vítámvás, P., Dobrev, P., Motyka, V., Floková, K., *et al.* (2012). Complex phytohormone responses during the cold acclimation of two wheat cultivars differing in cold tolerance, winter Samanta and spring Sandra. *J Plant Physiol* 169, 567–576.

Kreps, J. A., Wu, Y., Chang, H.-S., Zhu, T., Wang, X., and Harper, J. F. (2002). Transcriptome changes for *Arabidopsis* in response to salt, osmotic, and cold stress. *Plant Physiol* 130, 2129–2141.

Krinke, O., Ruelland, E., Valentová, O., Vergnolle, C., Renou, J.-P., Taconnat, L., *et al.* (2007). Phosphatidylinositol 4-kinase activation is an early response to salicylic acid in *Arabidopsis* suspension cells. *Plant Physiol* 144, 1347–1359.

Kumar, S., Ahanger, M. A., Alshaya, H., Jan, B. L., and Yerramilli, V. (2022). Salicylic acid mitigates salt induced toxicity through the modifications of biochemical attributes and some key antioxidants in *Capsicum annuum*. *Saudi J Biol Sci* 29, 1337–1347.

Lagarde, D., Basset, M., Lepetit, M., Conejero, G., Gaymard, F., Astruc, S., *et al.* (1996). Tissue-specific expression of *Arabidopsis* AKT1 gene is consistent with a role in K+ nutrition. *The Plant Journal* 9, 195–203.

Lairson, L. L., Henrissat, B., Davies, G. J., and Withers, S. G. (2008). Glycosyltransferases: structures, functions, and mechanisms. *Annu. Rev. Biochem.* 77, 521–555.

Lebeis, S. L., Paredes, S. H., Lundberg, D. S., Breakfield, N., Gehring, J., McDonald, M., *et al.* (2015). Salicylic acid modulates colonization of the root microbiome by specific bacterial taxa. *Science (1979)* 349, 860–864.

Lee, B., Henderson, D. A., and Zhu, J.-K. (2005). The *Arabidopsis* cold-responsive transcriptome and its regulation by ICE1. *Plant Cell* 17, 3155–3175.

Lee, S., Kim, S., and Park, C. (2010). Salicylic acid promotes seed germination under high salinity by modulating antioxidant activity in *Arabidopsis*. *New Phytologist* 188, 626–637.

Lethe, M. C. L., Paris, V., Wang, X., and Chan, C. T. Y. (2024). Similarities in Structure and Function of UDP-Glycosyltransferase Homologs from Human and Plants. *Int J Mol Sci* 25, 2782.

Li, G., Peng, X., Wei, L., and Kang, G. (2013). Salicylic acid increases the contents of glutathione and ascorbate and temporally regulates the related gene expression in salt-stressed wheat seedlings. *Gene* 529, 321–325.

Li, W., Zhang, F., Chang, Y., Zhao, T., Schranz, M. E., and Wang, G. (2015). Nicotinate *O*-glucosylation is an evolutionarily metabolic trait important for seed germination under stress conditions in *Arabidopsis thaliana*. *Plant Cell* 27, 1907–1924.

Lim, E., Ashford, D. A., Hou, B., Jackson, R. G., and Bowles, D. J. (2004). *Arabidopsis* glycosyltransferases as biocatalysts in fermentation for regioselective synthesis of diverse quercetin glucosides. *Biotechnol Bioeng* 87, 623–631.

Lim, E.-K., Doucet, C. J., Li, Y., Elias, L., Worrall, D., Spencer, S. P., *et al.* (2002). The activity of *Arabidopsis* glycosyltransferases toward salicylic acid, 4-hydroxybenzoic acid, and other benzoates. *Journal of Biological Chemistry* 277, 586–592.

Liu, Z., Yan, J.-P., Li, D.-K., Luo, Q., Yan, Q., Liu, Z.-B., *et al.* (2015). UDP-glucosyltransferase71c5, a major glucosyltransferase, mediates abscisic acid homeostasis in *Arabidopsis*. *Plant Physiol* 167, 1659–1670.

Reference

Löwe, M., Jürgens, K., Zeier, T., Hartmann, M., Gruner, K., Müller, S., *et al.* (2023). N-hydroxypipecolic acid primes plants for enhanced microbial pattern-induced responses. *Front Plant Sci* 14, 1217771.

Lyons, R., Stiller, J., Powell, J., Rusu, A., Manners, J. M., and Kazan, K. (2015). *Fusarium oxysporum* triggers tissue-specific transcriptional reprogramming in *Arabidopsis thaliana*. *PLoS One* 10, e0121902.

Maksym, R. P. (2018). *Arabidopsis* small molecule glucosyltransferase UGT76B1 conjugates both ILA and SA and is essential for the root-driven control of defense marker genes in leaves. Dissertation, Ludwig-Maximilians-Universität Munich.

Martínez-Soto, D., Yu, H., Allen, K. S., and Ma, L.-J. (2023). Differential colonization of the plant vasculature between endophytic versus pathogenic *Fusarium oxysporum* strains. *Molecular Plant-Microbe Interactions* 36, 4–13.

Maruri-López, I., Aviles-Baltazar, N. Y., Buchala, A., and Serrano, M. (2019). Intra and extracellular journey of the phytohormone salicylic acid. *Front Plant Sci* 10, 423.

Maskos, Z., Rush, J. D., and Koppenol, W. H. (1990). The hydroxylation of the salicylate anion by a Fenton reaction and γ-radiolysis: a consideration of the respective mechanisms. *Free Radic Biol Med* 8, 153–162.

Mathys, J., De Cremer, K., Timmermans, P., Van Kerckhove, S., Lievens, B., Vanhaecke, M., *et al.* (2012). Genome-wide characterization of ISR induced in *Arabidopsis thaliana* by *Trichoderma hamatum* T382 against *Botrytis cinerea* infection. *Front Plant Sci* 3, 108.

Meßner, B., Thulke, O., and Schäffner, A. R. (2003). *Arabidopsis* glucosyltransferases with activities toward both endogenous and xenobiotic substrates. *Planta* 217, 138–146.

Miller, E. B., Murphy, R. B., Sindhikara, D., Borrelli, K. W., Grisewood, M. J., Ranalli, F., *et al.* (2021). Reliable and accurate solution to the induced fit docking problem for protein–ligand binding. *J Chem Theory Comput* 17, 2630–2639.

Mishina, T. E., and Zeier, J. (2006). The *Arabidopsis* flavin-dependent monooxygenase FMO1 is an essential component of biologically induced systemic acquired resistance. *Plant Physiol* 141, 1666–1675.

Mishina, T. E., and Zeier, J. (2007). Pathogen-associated molecular pattern recognition rather than development of tissue necrosis contributes to bacterial induction of systemic acquired resistance in *Arabidopsis*. *The Plant Journal* 50, 500–513.

Miura, K., and Ohta, M. (2010). SIZ1, a small ubiquitin-related modifier ligase, controls cold signaling through regulation of salicylic acid accumulation. *J Plant Physiol* 167, 555–560.

Miura, K., Okamoto, H., Okuma, E., Shiba, H., Kamada, H., Hasegawa, P. M., *et al.* (2013). SIZ1 deficiency causes reduced stomatal aperture and enhanced drought tolerance via controlling salicylic acid-induced accumulation of reactive oxygen species in *Arabidopsis*. *The Plant Journal* 73, 91–104.

Mohi-Ud-Din, M., Talukder, D., Rohman, M., Ahmed, J. U., Jagadish, S. V. K., Islam, T., *et al.* (2021). Exogenous application of methyl jasmonate and salicylic acid mitigates drought-induced oxidative damages in french bean (*Phaseolus vulgaris L.*). *Plants* 10, 2066.

Mohnike, L. (2023). Metabolism of NHP and SA. Dissertation, Georg-August-Universität Göttingen.

Mohnike, L., Rekhter, D., Huang, W., Feussner, K., Tian, H., Herrfurth, C., *et al.* (2021). The glycosyltransferase UGT76B1 modulates N-hydroxy-pipecolic acid homeostasis and plant immunity. *Plant Cell* 33, 735–749.

Mou, Z., Fan, W., and Dong, X. (2003). Inducers of plant systemic acquired resistance regulate NPR1 function through redox changes. *Cell* 113, 935–944.

Munne-Bosch, S., and Penuelas, J. (2003). Photo-and antioxidative protection, and a role for salicylic acid during drought and recovery in field-grown Phillyrea angustifolia plants. *Planta* 217, 758–766.

Nair, A., Goyal, I., Voß, E., Mrozek, P., Prajapati, S., Thurow, C., *et al.* (2021). N-hydroxypipecolic acid-induced transcription requires the salicylic acid signaling pathway at basal SA levels. *Plant Physiol* 187, 2803–2819.

Nawrath, C., Heck, S., Parinthawong, N., and Métraux, J.-P. (2002). EDS5, an essential component of salicylic acid–dependent signaling for disease resistance in *Arabidopsis*, is a member of the MATE transporter family. *Plant Cell* 14, 275–286.

Nawrath, C., and Métraux, J.-P. (1999). Salicylic acid induction–deficient mutants of *Arabidopsis* express PR-2 and PR-5 and accumulate high levels of camalexin after pathogen inoculation. *Plant Cell* 11, 1393–1404.

Nazar, R., Iqbal, N., Syeed, S., and Khan, N. A. (2011). Salicylic acid alleviates decreases in photosynthesis under salt stress by enhancing nitrogen and sulfur assimilation and antioxidant metabolism differentially in two mungbean cultivars. *J Plant Physiol* 168, 807–815.

Nazar, R., Umar, S., Khan, N. A., and Sareer, O. (2015). Salicylic acid supplementation improves photosynthesis and growth in mustard through changes in proline accumulation and ethylene formation under drought stress. *South African Journal of Botany* 98, 84–94.

Norn, S., Permin, H., Kruse, P. R., and Kruse, E. (2009). From willow bark to acetylsalicylic acid. *Dan Medicinhist Arbog* 37, 79–98.

Noutoshi, Y., Okazaki, M., Kida, T., Nishina, Y., Morishita, Y., Ogawa, T., *et al.* (2012). Novel plant immune-priming compounds identified via high-throughput chemical screening target salicylic acid glucosyltransferases in *Arabidopsis*. *Plant Cell* 24, 3795–3804.

Obayashi, T., Hibara, H., Kagaya, Y., Aoki, Y., and Kinoshita, K. (2022). ATTED-II v11: a plant gene coexpression database using a sample balancing technique by subagging of principal components. *Plant Cell Physiol* 63, 869–881.

Okamoto, M., Tsuboi, Y., Chikayama, E., Kikuchi, J., and Hirayama, T. (2009). Metabolic movement upon abscisic acid and salicylic acid combined treatments. *Plant biotechnology* 26, 551–560.

Okuma, E., Nozawa, R., Murata, Y., and Miura, K. (2014). Accumulation of endogenous salicylic acid confers drought tolerance to *Arabidopsis*. *Plant Signal Behav* 9, e28085.

Olszak, B., Malinovsky, F. G., Brodersen, P., Grell, M., Giese, H., Petersen, M., *et al.* (2006). A putative flavin-containing mono-oxygenase as a marker for certain defense and cell death pathways. *Plant science* 170, 614–623.

Ordon, J., Gantner, J., Kemna, J., Schwalgun, L., Reschke, M., Streubel, J., *et al.* (2017). Generation of chromosomal deletions in dicotyledonous plants employing a user-friendly genome editing toolkit. *The Plant Journal* 89, 155–168.

Osman, M., Stigloher, C., Mueller, M. J., and Waller, F. (2020). An improved growth medium for enhanced inoculum production of the plant growth-promoting fungus *Serendipita indica*. *Plant Methods* 16, 39.

Palma, F., López-Gómez, M., Tejera, N. A., and Lluch, C. (2013). Salicylic acid improves the salinity tolerance of *Medicago sativa* in symbiosis with *Sinorhizobium meliloti* by preventing nitrogen fixation inhibition. *Plant Science* 208, 75–82.

Park, S.-W., Kaimoyo, E., Kumar, D., Mosher, S., and Klessig, D. F. (2007). Methyl salicylate is a critical mobile signal for plant systemic acquired resistance. *Science (1979)* 318, 113–116.

Pedrotti, L., Mueller, M. J., and Waller, F. (2013). *Piriformospora indica* root colonization triggers local and systemic root responses and inhibits secondary colonization of distal roots. *PLoS One* 8, e69352.

Pieterse, C. M. J., Van Wees, S. C. M., Van Pelt, J. A., Knoester, M., Laan, R., Gerrits, H., *et al.* (1998). A novel signaling pathway controlling induced systemic resistance in *Arabidopsis*. *Plant Cell* 10, 1571–1580.

Pieterse, C. M. J., Zamioudis, C., Berendsen, R. L., Weller, D. M., Van Wees, S. C. M., and Bakker, P. A. H. M. (2014). Induced systemic resistance by beneficial microbes. *Annu Rev Phytopathol* 52, 347–375.

Pieterse, C. M., Van Wees, S. C., Hoffland, E., Van Pelt, J. A., and Van Loon, L. C. (1996). Systemic resistance in *Arabidopsis* induced by biocontrol bacteria is independent of salicylic acid accumulation and pathogenesis-related gene expression. *Plant Cell* 8, 1225–1237.

Quiel, J. A., and Bender, J. (2003). Glucose conjugation of anthranilate by the *Arabidopsis* UGT74F2 glucosyltransferase is required for tryptophan mutant blue fluorescence. *Journal of Biological Chemistry* 278, 6275–6281.

Raskin, I. (1992). Role of salicylic acid in plants. *Annu Rev Plant Biol* 43, 439–463.

Raskin, I., Skubatz, H., Tang, W., and Meeuse, B. J. D. (1990). Salicylic acid levels in thermogenic and non-thermogenic plants. *Ann Bot* 66, 369–373.

Rekhter, D., Lüdke, D., Ding, Y., Feussner, K., Zienkiewicz, K., Lipka, V., *et al.* (2019). Isochorismate-derived biosynthesis of the plant stress hormone salicylic acid. *Science (1979)* 365, 498–502.

Rivas-San Vicente, M., and Plasencia, J. (2011). Salicylic acid beyond defence: its role in plant growth and development. *J Exp Bot* 62, 3321–3338.

Ryu, C., Murphy, J. F., Mysore, K. S., and Kloepper, J. W. (2004). Plant growth-promoting rhizobacteria systemically protect *Arabidopsis thaliana* against Cucumber mosaic virus by a salicylic acid and NPR1-independent and jasmonic acid-dependent signaling pathway. *The Plant Journal* 39, 381–392.

Ryu, K. H., Huang, L., Kang, H. M., and Schiefelbein, J. (2019). Single-cell RNA sequencing resolves molecular relationships among individual plant cells. *Plant Physiol* 179, 1444–1456.

Salas-Marina, M. A., Silva-Flores, M. A., Uresti-Rivera, E. E., Castro-Longoria, E., Herrera-Estrella, A., and Casas-Flores, S. (2011). Colonization of *Arabidopsis* roots by *Trichoderma atroviride* promotes growth and enhances systemic disease resistance through jasmonic acid/ethylene and salicylic acid pathways. *Eur J Plant Pathol* 131, 15–26.

Sanabria, N., Goring, D., Nürnberger, T., and Dubery, I. (2008). Self/nonself perception and recognition mechanisms in plants: a comparison of self-incompatibility and innate immunity. *New Phytologist* 178, 503–514.

Saruhan, N., Saglam, A., and Kadioglu, A. (2012). Salicylic acid pretreatment induces drought tolerance and delays leaf rolling by inducing antioxidant systems in maize genotypes. *Acta Physiol Plant* 34, 97–106.

Sawada, H., Shim, I.-S., and Usui, K. (2006). Induction of benzoic acid 2-hydroxylase and salicylic acid biosynthesis—modulation by salt stress in rice seedlings. *Plant Science* 171, 263–270.

Schnake, A., Hartmann, M., Schreiber, S., Malik, J., Brahmann, L., Yildiz, I., *et al.* (2020). Inducible biosynthesis and immune function of the systemic acquired resistance inducer N-hydroxypipecolic acid in monocotyledonous and dicotyledonous plants. *J Exp Bot* 71, 6444–6459.

Scholl, R. L., May, S. T., and Ware, D. H. (2000). Seed and molecular resources for *Arabidopsis*. *Plant Physiol* 124, 1477–1480.

Scholten, N., Hartmann, M., Abts, S., Abts, L., Reinartz, E., Altavilla, A., *et al.* (2024). In-depth analysis of isochorismate synthase-derived metabolism in plant immunity: Identification of meta-substituted benzoates and salicyloyl-malate. *Journal of Biological Chemistry* 300.

Reference

Schrödinger, L., and DeLano, W. (2020). PyMOL.

Schulz, E., Tohge, T., Zuther, E., Fernie, A. R., and Hincha, D. K. (2015). Natural variation in flavonol and anthocyanin metabolism during cold acclimation in *Arabidopsis thaliana* accessions. *Plant Cell Environ* 38, 1658–1672.

Scott, I. M., Clarke, S. M., Wood, J. E., and Mur, L. A. J. (2004). Salicylate accumulation inhibits growth at chilling temperature in *Arabidopsis*. *Plant Physiol* 135, 1040–1049.

Senaratna, T., Touchell, D., Bunn, E., and Dixon, K. (2000). Acetyl salicylic acid (Aspirin) and salicylic acid induce multiple stress tolerance in bean and tomato plants. *Plant Growth Regul* 30, 157–161.

Shah, J., and Zeier, J. (2013). Long-distance communication and signal amplification in systemic acquired resistance. *Front Plant Sci* 4, 30.

Sherameti, I., Shahollari, B., Venus, Y., Altschmied, L., Varma, A., and Oelmuller, R. (2005). The endophytic fungus *Piriformospora indica* stimulates the expression of nitrate reductase and the starch-degrading enzyme glucan-water dikinase in tobacco and *Arabidopsis* roots through a homeodomain transcription factor that binds to a conserved motif in. *Journal of Biological Chemistry* 280, 26241–26247.

Shimada, T. L., Shimada, T., and Hara-Nishimura, I. (2010). A rapid and non-destructive screenable marker, FAST, for identifying transformed seeds of *Arabidopsis thaliana*. *The Plant Journal* 61, 519–528.

Silverman, P., Seskar, M., Kanter, D., Schweizer, P., Metraux, J.-P., and Raskin, I. (1995). Salicylic acid in rice (biosynthesis, conjugation, and possible role). *Plant Physiol* 108, 633–639.

Singh, A., Lim, G., and Kachroo, P. (2017). Transport of chemical signals in systemic acquired resistance. *J Integr Plant Biol* 59, 336–344.

Song, J. T. (2006). Induction of a salicylic acid glucosyltransferase, AtSGT1, is an early disease response in *Arabidopsis thaliana*. *Mol Cells* 22, 233–238.

Song, J. T., Koo, Y. J., Seo, H. S., Kim, M. C., Do Choi, Y., and Kim, J. H. (2008). Overexpression of AtSGT1, an *Arabidopsis* salicylic acid glucosyltransferase, leads to increased susceptibility to *Pseudomonas syringae*. *Phytochemistry* 69, 1128–1134.

Staskawicz, B. J. (2001). Genetics of plant-pathogen interactions specifying plant disease resistance. *Plant Physiol* 125, 73–76.

Stassen, M. J. J., Hsu, S.-H., Pieterse, C. M. J., and Stringlis, I. A. (2021). Coumarin communication along the microbiome–root–shoot axis. *Trends Plant Sci* 26, 169–183.

Stein, E., Molitor, A., Kogel, K.-H., and Waller, F. (2008). Systemic resistance in *Arabidopsis* conferred by the mycorrhizal fungus *Piriformospora indica* requires jasmonic acid signaling and the cytoplasmic function of NPR1. *Plant Cell Physiol* 49, 1747–1751.

Strasser, R. (2016). Plant protein glycosylation. *Glycobiology* 26, 926–939.

Stringlis, I. A., De Jonge, R., and Pieterse, C. M. J. (2019). The age of coumarins in plant–microbe interactions. *Plant Cell Physiol* 60, 1405–1419.

Stuttmann, J., Barthel, K., Martin, P., Ordon, J., Erickson, J. L., Herr, R., *et al.* (2021). Highly efficient multiplex editing: one-shot generation of 8× *Nicotiana benthamiana* and 12× *Arabidopsis* mutants. *The Plant Journal* 106, 8–22.

Swayambhu, G., Raghavan, I., Ravi, B. G., Pfeifer, B. A., and Wang, Z. Q. (2021). Salicylate Glucoside as a Nontoxic Plant Protectant Alternative to Salicylic Acid. *ACS Agricultural Science & Technology* 1, 515–521.

Tanaka, K., Hayashi, K., Natsume, M., Kamiya, Y., Sakakibara, H., Kawaide, H., *et al.* (2014). UGT74D1 catalyzes the glucosylation of 2-oxindole-3-acetic acid in the auxin metabolic pathway in *Arabidopsis*. *Plant Cell Physiol* 55, 218–228.

Taşgın, E., Atıcı, Ö., Nalbantoğlu, B., and Popova, L. P. (2006). Effects of salicylic acid and cold treatments on protein levels and on the activities of antioxidant enzymes in the apoplast of winter wheat leaves. *Phytochemistry* 67, 710–715.

Tjamos, S. E., Flemetakis, E., Paplomatas, E. J., and Katinakis, P. (2005). Induction of resistance to *Verticillium dahliae* in *Arabidopsis thaliana* by the biocontrol agent K-165 and pathogenesis-related proteins gene expression. *Molecular Plant-Microbe Interactions* 18, 555–561.

Tognetti, V. B., Van Aken, O., Morreel, K., Vandenbroucke, K., Van De Cotte, B., De Clercq, I., *et al.* (2010). Perturbation of indole-3-butyric acid homeostasis by the UDP-glucosyltransferase UGT74E2 modulates *Arabidopsis* architecture and water stress tolerance. *Plant Cell* 22, 2660–2679.

Torrens-Spence, M. P., Bobokalonova, A., Carballo, V., Glinkerman, C. M., Pluskal, T., Shen, A., *et al.* (2019). PBS3 and EPS1 complete salicylic acid biosynthesis from isochorismate in *Arabidopsis*. *Mol Plant* 12, 1577–1586.

Trivedi, P., Leach, J. E., Tringe, S. G., Sa, T., and Singh, B. K. (2020). Plant–microbiome interactions: from community assembly to plant health. *Nat Rev Microbiol* 18, 607–621.

Tsutsui, T., Kato, W., Asada, Y., Sako, K., Sato, T., Sonoda, Y., *et al.* (2009). DEAR1, a transcriptional repressor of DREB protein that mediates plant defense and freezing stress responses in *Arabidopsis*. *J Plant Res* 122, 633–643.

Vaca, E., Behrens, C., Theccanat, T., Choe, J., and Dean, J. V (2017). Mechanistic differences in the uptake of salicylic acid glucose conjugates by vacuolar membrane-enriched vesicles isolated from *Arabidopsis thaliana*. *Physiol Plant* 161, 322–338.

van de Mortel, J. E., de Vos, R. C. H., Dekkers, E., Pineda, A., Guillod, L., Bouwmeester, K., *et al.* (2012). Metabolic and transcriptomic changes induced in *Arabidopsis* by the rhizobacterium *Pseudomonas fluorescens* SS101. *Plant Physiol* 160, 2173–2188.

Reference

Van Peer, R., Niemann, G. J., and Schippers, B. (1991). Induced resistance and phytoalexin accumulation in biological control of *Fusarium* wilt of carnation by *Pseudomonas sp.* strain WCS 417 r. *Phytopathology* 81, 728–734.

Venegas-Molina, J., Proietti, S., Pollier, J., Orozco-Freire, W., Ramirez-Villacis, D., and Leon-Reyes, A. (2020). Induced tolerance to abiotic and biotic stresses of broccoli and *Arabidopsis* after treatment with elicitor molecules. *Sci Rep* 10, 10319.

Vlot, A. C., Klessig, D. F., and Park, S.-W. (2008). Systemic acquired resistance: the elusive signal (s). *Curr Opin Plant Biol* 11, 436–442.

Vlot, A. C., Sales, J. H., Lenk, M., Bauer, K., Brambilla, A., Sommer, A., *et al.* (2021). Systemic propagation of immunity in plants. *New Phytologist* 229, 1234–1250.

von Saint Paul, V., Zhang, W., Kanawati, B., Geist, B., Faus-Keßler, T., Schmitt-Kopplin, P., *et al.* (2011). The *Arabidopsis* glucosyltransferase UGT76B1 conjugates isoleucic acid and modulates plant defense and senescence. *Plant Cell* 23, 4124–4145.

Waese, J., Fan, J., Pasha, A., Yu, H., Fucile, G., Shi, R., *et al.* (2017). ePlant: visualizing and exploring multiple levels of data for hypothesis generation in plant biology. *Plant Cell* 29, 1806–1821.

Wan, S.-B., Tian, L., Tian, R.-R., Pan, Q.-H., Zhan, J.-C., Wen, P.-F., *et al.* (2009). Involvement of phospholipase D in the low temperature acclimation-induced thermotolerance in grape berry. *Plant Physiology and Biochemistry* 47, 504–510.

Wang, G., and Pichersky, E. (2007). Nicotinamidase participates in the salvage pathway of NAD biosynthesis in *Arabidopsis*. *The Plant Journal* 49, 1020–1029.

Wang, J., and Hou, B. (2009). Glycosyltransferases: key players involved in the modification of plant secondary metabolites. *Frontiers of Biology in China* 4, 39–46.

Wang, J., Ma, X.-M., Kojima, M., Sakakibara, H., and Hou, B.-K. (2013). Glucosyltransferase UGT76C1 finely modulates cytokinin responses via cytokinin *N*-glucosylation in *Arabidopsis thaliana*. *Plant Physiology and Biochemistry* 65, 9–16.

Wang, L., Calabria, J., Chen, H.-W., and Somssich, M. (2022). The *Arabidopsis thaliana*–*Fusarium oxysporum* strain 5176 pathosystem: an overview. *J Exp Bot* 73, 6052–6067.

Wang, X. (2009). Structure, mechanism and engineering of plant natural product glycosyltransferases. *FEBS Lett* 583, 3303–3309.

Wassie, M., Zhang, W., Zhang, Q., Ji, K., Cao, L., and Chen, L. (2020). Exogenous salicylic acid ameliorates heat stress-induced damages and improves growth and photosynthetic efficiency in alfalfa (*Medicago sativa L.*). *Ecotoxicol Environ Saf* 191, 110206.

Weller, D. M., Mavrodi, D. V, van Pelt, J. A., Pieterse, C. M. J., van Loon, L. C., and Bakker, P. A. H. M. (2012). Induced systemic resistance in *Arabidopsis thaliana* against *Pseudomonas syringae* pv. tomato by 2, 4-diacetylphloroglucinol-producing *Pseudomonas fluorescens*. *Phytopathology* 102, 403–412.

Wendehenne, D., Gao, Q., Kachroo, A., and Kachroo, P. (2014). Free radical-mediated systemic immunity in plants. *Curr Opin Plant Biol* 20, 127–134.

Wildermuth, M. C., Dewdney, J., Wu, G., and Ausubel, F. M. (2001). Isochorismate synthase is required to synthesize salicylic acid for plant defence. *Nature* 414, 562–565.

Winter, D., Vinegar, B., Nahal, H., Ammar, R., Wilson, G. V, and Provart, N. J. (2007). An "Electronic Fluorescent Pictograph" browser for exploring and analyzing large-scale biological data sets. *PLoS One* 2, e718.

Wu, J., Zhu, W., and Zhao, Q. (2023). Salicylic acid biosynthesis is not from phenylalanine in *Arabidopsis*. *J Integr Plant Biol* 65, 881–887.

Wu, Y., Zhang, D., Chu, J. Y., Boyle, P., Wang, Y., Brindle, I. D., *et al.* (2012). The *Arabidopsis* NPR1 protein is a receptor for the plant defense hormone salicylic acid. *Cell Rep* 1, 639–647.

Xu, D., Tang, Q., Xu, P., Schäffner, A. R., Leister, D., and Kleine, T. (2023). Response of the organellar and nuclear (post) transcriptomes of *Arabidopsis* to drought. *Front Plant Sci* 14, 1220928.

Yildiz, I., Mantz, M., Hartmann, M., Zeier, T., Kessel, J., Thurow, C., *et al.* (2021). The mobile SAR signal N-hydroxypipecolic acid induces NPR1-dependent transcriptional reprogramming and immune priming. *Plant Physiol* 186, 1679–1705.

Yin, R., Han, K., Heller, W., Albert, A., Dobrev, P. I., Zažímalová, E., *et al.* (2014). Kaempferol 3-O-rhamnoside-7-O-rhamnoside is an endogenous flavonol inhibitor of polar auxin transport in *Arabidopsis* shoots. *New Phytologist* 201, 466–475.

Yonekura-Sakakibara, K., and Hanada, K. (2011). An evolutionary view of functional diversity in family 1 glycosyltransferases. *The Plant Journal* 66, 182–193.

Yoshioka, Y., Ichikawa, H., Naznin, H. A., Kogure, A., and Hyakumachi, M. (2012). Systemic resistance induced in *Arabidopsis thaliana* by *Trichoderma asperellum* SKT-1, a microbial pesticide of seedborne diseases of rice. *Pest Manag Sci* 68, 60–66.

Yuan, M., Jiang, Z., Bi, G., Nomura, K., Liu, M., Wang, Y., *et al.* (2021). Pattern-recognition receptors are required for NLR-mediated plant immunity. *Nature* 592, 105–109.

Zeilmaker, T., Ludwig, N. R., Elberse, J., Seidl, M. F., Berke, L., Van Doorn, A., *et al.* (2015). DOWNY MILDEW RESISTANT 6 and DMR 6-LIKE OXYGENASE 1 are partially redundant but distinct suppressors of immunity in *Arabidopsis*. *The Plant Journal* 81, 210–222.

Zepeda, B., and Verdonk, J. C. (2022). RNA extraction from plant tissue with homemade acid guanidinium thiocyanate phenol chloroform (AGPC). *Curr Protoc* 2, e351.

Zhang, K., Halitschke, R., Yin, C., Liu, C.-J., and Gan, S.-S. (2013). Salicylic acid 3-hydroxylase regulates *Arabidopsis* leaf longevity by mediating salicylic acid catabolism. *Proceedings of the National Academy of Sciences* 110, 14807–14812.

Reference

Zhang, Y., Zhao, L., Zhao, J., Li, Y., Wang, J., Guo, R., *et al.* (2017). S5H/DMR6 encodes a salicylic acid 5-hydroxylase that fine-tunes salicylic acid homeostasis. *Plant Physiol* 175, 1082–1093.

Zhao, J., and Last, R. L. (1996). Coordinate regulation of the tryptophan biosynthetic pathway and indolic phytoalexin accumulation in *Arabidopsis*. *Plant Cell* 8, 2235–2244.

Zhu, Y., Yang, H., Mang, H.-G., and Hua, J. (2011). Induction of BAP1 by a moderate decrease in temperature is mediated by ICE1 in *Arabidopsis*. *Plant Physiol* 155, 580–588.

7 Acknowledgement

I extend my heartfelt gratitude to everyone who contributed to the success of my research, providing invaluable support, encouragement, and guidance throughout this journey. This thesis would not have been possible without the help of many remarkable individuals:

First and foremost, I would like to thank my direct supervisor, PD. Dr. Anton Schäffner, for his concern and guidance throughout more than four years. His advice and insights greatly broadened my research perspective, and he consistently worked to ensure I had access to the materials and experimental guidance necessary for my research to progress smoothly.

I am also grateful to my thesis committee members. Prof. Dr. Jürgen Zeier reviewed this work and manuscript and provided essential feedback and guidance, while Prof. Dr. Jörg Durner and Prof. Dr. Klaus Förstemann offered invaluable feedback during each Thesis Advisory Committee meeting.

Special thanks to Prof. Dr. Jörg-Peter Schnitzler for hosting me after institutional changes and for his encouraging words and valuable input at institute meetings.

I am deeply thankful to Birgit Lange for her technical support and assistance with my experiments, as well as to Ting Zhu for her help and for sharing her perspectives. I also appreciate the support of former colleagues Dr. Elisabeth Georgii, Dr. Thayssa Rabelo Schley, and Dr. Komal Jhala. Additionally, I am grateful to Dr. Johannes Stuttmann, Dr. Dirk Becker, Dr. Robert Janowski and Prasath Balaji Sivaprakasam Padmanaban for their assistance and insightful discussions on experimental materials and techniques.

I am sincerely grateful to all members of the BIOP and EUS teams for their companionship over the past four years. Their support has been a source of encouragement both professionally and personally.

I especially want to thank the LMU-CSC Scholarship Program. Without its financial and logistical support, it would have been impossible for me to pursue my studies in Germany and meet so many wonderful people.

Finally, I owe profound thanks to my parents (XuePing Zhang, 张雪萍; RongLiang Xu, 徐荣亮) for their constant encouragement and unconditional support, and above all, to my wife, Dr. Qian Tang (唐倩). Together, we have supported each other in life and collaborated in research. Many of my ideas would not have been possible without her assistance.